APR 10 1964

SC-DC-64-344

Final Report

Sandia Corporation Purchase Order No. 16-8672

MASTER

ELECTRICAL AND THERMAL MEASUREMENTS ON FE-AFE PHASE TRANSITIONS IN LEAD HAFNATE TITANATE COMPOSITIONS

LEGAL NOTICE

This report was prepared as an account of Government sponsored work. Neither the United States, nor the Commission, nor any person acting on behalf of the Commission:

A. Makes any warranty or representation, expressed or implied, with respect to the accuracy, completeness, or usefulness of the information contained in this report, or that the use of any information, apparatus, method, or process disclosed in this report may not infringe privately owned rights; or

B. Assumes any liabilities with respect to the use of, or for damages resulting from the use of any information, apparatus, method, or process disclosed in this report.

As used in the above, "person acting on behalf of the Commission" includes any employee or contractor of the Commission, or employee of such contractor, to the extent that such employee or contractor of the Commission, or employee of such contractor prepares, disseminates, or provides access to, any information pursuant to his employment or contract with the Commission, or his employment with such contractor.

J. W. Northrip

G. A. Baum

E. E. Kohnke

Physics Department Solid State Laboratory

Facsimile Price $ 13.50

Microfilm Price $ 6.14

Available from the
Office of Technical Services
Department of Commerce
Washington 25, D. C.

October, 1963

RESEARCH FOUNDATION
OKLAHOMA STATE UNIVERSITY

DISCLAIMER

This report was prepared as an account of work sponsored by an agency of the United States Government. Neither the United States Government nor any agency Thereof, nor any of their employees, makes any warranty, express or implied, or assumes any legal liability or responsibility for the accuracy, completeness, or usefulness of any information, apparatus, product, or process disclosed, or represents that its use would not infringe privately owned rights. Reference herein to any specific commercial product, process, or service by trade name, trademark, manufacturer, or otherwise does not necessarily constitute or imply its endorsement, recommendation, or favoring by the United States Government or any agency thereof. The views and opinions of authors expressed herein do not necessarily state or reflect those of the United States Government or any agency thereof.

DISCLAIMER

Portions of this document may be illegible in electronic image products. Images are produced from the best available original document.

THIS PAGE

WAS INTENTIONALLY

LEFT BLANK

SC-DC-64-344

PREFACE

This is a final report on the study of ferroelectric-antiferroelectric transitions in lead perovskites conducted at Oklahoma State University during 1962-63 under Sandia Corporation Purchase Order No. 16-8672. Certain of the electrical data presented have already been published in an interim report dated December, 1962. Major advisor for the project was Dr. E. E. Kohnke with Mr. John W. Northrip acting as project leader and Mr. Gary A. Baum as technical assistant.

The report consists of two parts. Section A describes the electrical and thermal work carried out within the scope of the above mentioned Purchase Order. It will provide the basis of a Ph.D. dissertation for Mr. Northrip. Section B is the result of some extra measurements using the available experimental equipment and Sandia specimens. These were performed by Mr. Baum to satisfy M.S. thesis requirements and were considered of sufficient interest to be included.

The work described herein has been carried out using the facilities of the Physics Department Solid State Laboratory and has been administered by the Research Foundation, Oklahoma State University.

SECTION A

ELECTRICAL AND THERMAL MEASUREMENTS

ABSTRACT

Investigations have been carried out to determine the characteristics of ferroelectric and antiferroelectric transitions in lead perovskites. Materials studied include solid solutions of lead zirconate titanate, lead zirconate titanate stannate, and lead hafnate titanate. These solid solutions were chosen because compositions among them possess a ferroelectric-to-antiferroelectric transition with rising temperature while others display an antiferroelectric-to-ferroelectric transition under the same conditions.

Dielectric constant and loss were determined as functions of temperature and applied electric field, with an emphasis being placed on the use of loss conductance rather than tan δ as a method of examining the loss mechanisms in these materials. By this technique, the variation of transition temperature with external electric field was determined. The decrease of peak dielectric constant with external field characteristic of dielectric saturation was found to be especially prominent in transitions involving a ferroelectric phase. Hysteresis measurements were made primarily in an effort to separate the antiferroelectric double loop behavior from the normal ferroelectric loops near transitions. It was found that parts of some samples retained ferroelectric character many degrees above the normal transition temperature. Measurements of specific heat as a function of temperature were used to determine the relative free energies and entropies of the phases.

From the results of these studies it appears that the reversal of transition direction mentioned above results from very slight shifts in the relative magnitudes of the free energy and the entropy of the ferroelectric and antiferroelectric phases of these materials, rather than from some wide change in their structural or chemical character.

TABLE OF CONTENTS

Chapter		Page
I.	INTRODUCTION	1
II.	CRYSTALLOGRAPHY AND CHEMISTRY OF PEROVSKITES	6
	Lead Perovskite Materials	10
III.	THERMODYNAMICS OF PHASE TRANSITIONS IN FERROELECTRICS AND ANTIFERROELECTRICS	17
	Thermodynamics of Phase Transitions	17
	Applications of the Above Considerations to Ferroelectric and Antiferroelectric Transitions	24
IV.	DIELECTRIC MEASUREMENTS	31
	Dielectric Susceptibilities	31
	Dielectric Loss	34
	Measurement Equipment	36
	Experimental Samples	38
	Measurement Procedures and Calculating Techniques	39
	Results	40
V.	POLARIZATION MEASUREMENTS	57
	Experimental Equipment	60
	Calculation Techniques	60
	Experimental Results	63
VI.	THERMAL MEASUREMENTS	68
	Description of Equipment	69
	Description of Samples	71
	Measurement Techniques	74
	Experimental Results	84
VII.	RESULTS OF RELATED WORK	97
	Clevite Work on $Pb_{0.99}Nb_{0.02}(Zr_{0.68}Ti_{0.07}Sn_{0.25})_{0.98}O_3$	97
	Clevite Lead Zirconate Titanate Stannate Compositional Studies	102
	Sandia Studies on Lead Hafnate Titanate Compositions	103

Chapter Page

VIII. CONCLUSIONS 106

Free Energy Relationships in $Pb_{0.99}Nb_{0.02}(Zr_{0.68}Ti_{0.07}Sn_{0.25})_{0.98}O_3$ 106

Results for the Lead Hafnate Titanate Samples . . . 114

Qualitative Theory of FE-AFE Transitions in Lead Perovskites 116

Resume of Experimental Techniques 118

BIBLIOGRAPHY 121

LIST OF TABLES

Table		Page
I.	Tolerance Factors for Principal Perovskite A^{+2} B^{+4} O_3 Ferroelectrics	8
II.	Phase Boundary Relationships	30
III.	Dimensions of Samples Used in Dielectric Measurements	39
IV.	Data from Preliminary Thermal Measurements	88
V.	Heat of Transition Data	96

LIST OF FIGURES

Figure		Page
1.	Representation of a Ferroelectric (a) and Antiferroelectric (b) Dipole Array	10
2.	Compositional Phase Diagram for $Pb(Zr_{1-x}Ti_x)O_3$ (After Sawaguchi (S4))	13
3.	Compositional Phase Diagram for $Pb(Zr_{0.70-x}Ti_xSn_{0.30})O_3$ (After Jaffe (J3))	14
4.	Compositional Phase Diagram for $Pb(Hf_{1-x}Ti_x)O_3$ + 1 wt. % Nb_2O_5 (After Hall (H2))	16
5.	U and G vs. T for p = 0, E = 0	20
6.	Variation of Free Energy with Polarization for a Ferroelectric Material	32
7.	Polarization vs. Bias Voltage Showing Nonlinear Saturation Effect	33
8.	Block Diagram of Dielectric Measurement Apparatus	37
9.	Dielectric Data for PZST	41
10.	Phase Diagram of PZST as a Function of Field and Temperature	43
11.	Dielectric Constant at the Transition vs. Field for PZST	45
12.	Behavior of PZST Above the Curie Temperature as a Function of Applied Electric Field	46
13.	Dielectric Constant vs. Field for Sample 95HN2	48
14.	Dielectric Constant vs. Field for Sample 96HN2	49
15.	Dielectric Constant vs. Field for Sample 97HN2	50
16.	Dielectric Constant vs. Field for Sample 98HN4	51
17.	Dielectric Constant vs. Field for Sample 100HN2	52
18.	Curie Temperature vs. Bias Field for Lead Hafnate Titanate Compositions	53

Figure | Page

19. Peak Dielectric Constant vs. Bias Field for Lead Hafnate Titanate Compositions 54

20. Tentative Temperature-Field Phase Diagram for 96HN2 56

21. Double Hysteresis Loop Observed During Field-Enforced AFE-FE Transition 59

22. Sawyer-Tower Circuit for 60 cps Hysteresis Loops 61

23. Circuit for Slow-Loop Hysteresis Measurements 62

24. Hysteresis Parameters for the 95/5 Lead Hafnate Titanate Composition 64

25. Hysteresis Parameters for the 96/4 Lead Hafnate Titanate Composition 65

26. Hysteresis Loops and Portions of Double Hysteresis Loops Showing Field-Enforced Ferroelectric Phase in the 96/4 Lead Hafnate Titanate Composition (Temperature Decreasing) 67

27. Calorimeter Design 70

28. Construction of Sample Assembly 72

29. Determination of Loss Factor in Preliminary Measurements 77

30. Exponential Cooling Curve for Quartz Check Sample 78

31. Block Diagram of Automated Thermal Measurement Apparatus 82

32. Amplifier Schematic for Automated System (All Capacitances in mfd) 83

33. Input Power and Rate of Change of Temperature as Function of Temperature for PZST 85

34. Exponential Cooling for Lead Hafnate Titanate Samples . . . 86

35. Measurement of Thermal Loss Factor for Lead Hafnate Titanate Samples 87

36. Specific Heat vs. Temperature for $Pb(Hf_{0.95}Ti_{0.05})O_3$ + 1 wt. % Nb_2O_5 89

37. Specific Heat vs. Temperature for $Pb(Hf_{0.96}Ti_{0.04})O_3$ + 1 wt. % Nb_2O_5 90

38. Specific Heat vs. Temperature for $Pb(Hf_{0.97}Ti_{0.03})O_3$ + 1 wt. % Nb_2O_5 91

Figure | Page

39. Specific Heat vs. Temperature for $Pb(Hf_{0.98}Ti_{0.02})O_3$ + 1 wt. % Nb_2O_5 92

40. Specific Heat vs. Temperature for $PbHfO_3$ + 1 wt. % Nb_2O_5 93

41. Specific Heat vs. Temperature for PZST 94

42. Excess Power vs. Time Plot Used to Calculate Curie Transition Energy for PZST 95

43. Polarization vs. Temperature and Pressure for PZST (After Berlincourt (B3)) 99

44. Electric Field-Pressure Phase Diagram for PZST (After Berlincourt (B4)) 100

45. Electric Field-Temperature Phase Diagram for PZST (After Berlincourt (B4)) 101

46. Comparison of Transitions Observed with Increasing Temperature and Increasing Field for PZST 109

47. C_p/T for PZST Sample 113

48. Free Energy vs. Temperature for PZST (Relative to FE Phase at 100°C) 113

49. Relative Free Energies of the Various Phases for a PZST Sample at Zero Field 115

50. Relative Free Energies of the Various Phases for a PZST Sample with External Field of 5 KV/cm 115

CHAPTER I

INTRODUCTION

Although the study of ferroelectricity is of relatively recent origin, it is a field which has shown phenomenal growth. The unique properties of these materials (high dielectric constant, strong electromechanical coupling, charge storage capabilities, etc.) have led to a large amount of published work ranging from materials research and fundamental theory to device applications. Several good reviews of this work have already been published (K1, M1, I1, J2, S1) so no comprehensive review of past literature will be attempted here.

From a crystallographic viewpoint, certain materials are characterized by the presence of a spontaneous electric dipole within the unit cell. That is, the center of negative charge does not coincide with the center of positive charge at zero electric field. Since the magnitudes of these internal dipoles change with temperature, giving rise to detectable surface charges, the materials have come to be called "pyroelectrics". In 1917, during studies of the dielectric and piezoelectric anomalies of Rochelle salt, Anderson (A1), and Cady (C1) discovered that its spontaneous internal polarization could be reversed by the application of an electric field at certain temperatures. This gave rise to hysteresis loops similar to those observed in ferromagnetism and thus the phenomenon was given the name "ferroelectricity". This correspondence, however, is sometimes misleading since ferromagnetism

occurs principally at the electronic level while ferroelectricity is basically an ionic phenomenon. It is interesting to note that in much European literature the term used is "seignettelectricity" from the French term for Rochelle salt (Seignette salt).

Thus, a ferroelectric is a material exhibiting a reversible spontaneous electrical dipole within each unit cell. The existence of this polarization at the macroscopic level is usually masked by surface charges and is revealed by applying an electric field to reverse the dipoles, causing a current to flow in the external circuit. The interaction of this internal polarization with the ionic positions in the crystal lattice gives rise to the striking electrical, mechanical, optical, and thermal effects associated with ferroelectricity.

During the course of ferroelectric investigations another class of materials was found in which the basic cell exhibited a spontaneous dipole but with neighboring dipoles antiparallel. In such materials there is no macroscopic polarization but many of the other phenomena characterizing ferroelectricity are present. In correspondence to their ferromagnetic analogues these materials are called antiferroelectrics.

Most ferroelectric and antiferroelectric materials have been grouped into four chemical classes:

1. Rochelle salt and its isomorphous salts. These materials are characterized by having both an upper and a lower temperature limit to the ferroelectric region and are piezoelectric in the non-ferroelectric state. Present theories attribute their ferroelectric properties to orientations involving the hydroxyl groups in this complex structure.

2. Potassium dihydrogen phosphate and isomorphous compounds. These materials exhibit their ferroelectric properties only at temperatures well below zero Centigrade. Their behavior is attributed to an orientation of the phosphate radicals by the hydrogen bonds. Ammonium dihydrogen phosphate was one of the first studied antiferroelectric materials.
3. The perovskite compounds. These materials have so far been the most important group from an application viewpoint since they exhibit strong ferroelectric properties at room temperature, have high polarizations, and are mechanically stable. Their ferroelectric properties are attributed to slight perturbations of the basic cubic perovskite structure. More will be said about this class of compounds in the next chapter.
4. Miscellaneous structures. This includes many compounds, usually of a complex layered structure, which cannot be conveniently grouped under a single structure. In general, these compounds have low polarizations with a corresponding decrease in the anomalies observed in all properties.

Almost all ferroelectric materials exhibit a phase transition into a more symmetric phase at some temperature. This more symmetric phase is no longer ferroelectric; it exhibits normal dielectric behavior with the exception that the dielectric constant decreases with rising temperature. Because of this decrease, this upper phase has been called "paraelectric". It should be pointed out, however, that the internal behavior of the paraelectric phase does not differ from that of a dielectric in the same way that a paramagnetic material differs from a diamagnetic one.

The temperature at which the ferroelectric or antiferroelectric phase becomes paraelectric is known as the Curie temperature. This phase transition has been studied quite thoroughly in many materials. It has been found in some materials to be first order, in some second order, and in at least one case a "higher than second order" transition was reported (G1). The transition is most easily detected by the pronounced peak of dielectric constant occurring at that temperature or by the discontinuous release of polarization charge if the transition is of first order. All other properties connected with the spontaneous internal polarization (piezoelectric behavior, optical birefringence, etc.) also undergo drastic changes at this temperature.

Besides the Curie transition there are other phase transitions which may occur within a ferroelectric or antiferroelectric material. These transitions involve minor shifts within the lattice and usually cause a shift in the direction of internal polarization (the ferroelectric axis). These again are accompanied by anomalies in all the properties connected with polarization but usually to a much lesser degree than in the Curie transition. Some of these changes will be discussed more fully in the next chapter, which deals with the behavior of materials having the perovskite structure.

A few materials exhibit phase transitions in which they change from the ferroelectric to the antiferroelectric state. This phenomenon was first observed in sodium niobate (C2), which is antiferroelectric between -60°C and -200°C and ferroelectric below -200°C. Within the last few years it has been found that several lead perovskite solid solutions also exhibit this behavior. It is these materials which are of interest here.

It is the purpose of this research to study some of the thermodynamic characteristics of the ferroelectric and antiferroelectric phases in these lead perovskites. A survey of the chemical and crystallographic characteristics of the perovskite structure has been made with special emphasis on the role of ionic properties in the determination of ferroelectric behavior. A review of the thermodynamics of ferroelectrics and antiferroelectrics is given and a proposal outlined for the relationships between the various phases which would lead to the observed phase diagrams for ferroelectric and antiferroelectric phases.

Much of this study has been devoted to the refinement and interpretation of the experimental techniques used in studying the various phase transitions. Measurements have been made of dielectric constant and loss as functions of both temperature and electric field. An important finding of this work has been the development of the "loss conductance" as a more sensitive and accurate indicator of material characteristics than the more conventional loss tangent or dissipation factor. Polarization measurements have been made in the vicinity of the ferroelectric-antiferroelectric transitions in an effort to explain some of the anomalous hysteresis loops observed in this region. A calorimetric study has been made to determine the specific heat and heats of transition of these materials in order to approximate the temperature dependence of the free energies of the various phases.

Finally a correlation of this work with other work on perovskite solid solutions has been made in an effort to determine some of the patterns of behavior in this important family of materials.

CHAPTER II

CRYSTALLOGRAPHY AND CHEMISTRY OF PEROVSKITES

The perovskite family of materials has played a very important role in the history of ferroelectricity. Because of their large polarizations and high electromechanical coupling coefficients, these materials have become the most commercially useful of all ferroelectric materials. Barium titanate, the first ferroelectric perovskite discovered, has been the subject of a vast amount of research which had led to much of our basic knowledge about ferroelectrics in general. The fact that many of the perovskites are soluble with one another has led to a whole range of solid solutions which allow a variation of the ferroelectric properties to fit the convenience of the user. It is in this realm of solid solutions that this study is most interested.

The basic perovskite lattice is of simple cubic structure having the composition ABO_3. The structural unit cell can be pictured as a cube having A atoms at the corner, a B atom in the body center position, and oxygen atoms in the face centers.

In making a transformation into a ferroelectric or antiferroelectric phase, the basic perovskite cube must become slightly distorted. A one dimensional distortion of the cube leaves the lattice in the tetragonal symmetry. If this distortion is a lengthening of a cube edge, the material becomes ferroelectric; if it represents a compression, the material becomes antiferroelectric. A two dimensional shear of the cube

leads to the orthorhombic phase in which the polarization axis lies along a face diagonal. If the original cube is given a three dimensional shear, the symmetry becomes rhombohedral with the polarization axis being one of the body diagonals.

The use of ceramic samples of perovskite materials leads to certain interesting crystallographic results. In the absence of electric fields or orienting stresses, the sample is nearly isotropic because of the random polarization of the ceramic grains. The application of an electric field to a sample in the ferroelectric phase, however, aligns many of the ferroelectric domains ("poles" the sample) and produces a distinct anisotropy. This poled sample represents a symmetry characterized by an infinite-fold rotational axis; i.e., the material is isotropic in the plane perpendicular to the axis of rotation. This is true regardless of the actual crystalline symmetry characterizing the ferroelectric state.

To fit the cubic pattern of the perovskite structure, the A atoms must have a coordination number of twelve and the B atoms a coordination number of six. From the viewpoint of valence the sum of the A-valence and the B-valence must be six giving rise to both $A^{+1} B^{+5} O_3$ and $A^{+2} B^{+4} O_3$ compounds.

The concept of ionic size plays an important part in the determination of the ferroelectric properties of perovskite compounds. If the ions fit ideally into the unit cube described above, it can be seen that the sum of the A-ion diameter and an oxygen diameter makes up a face diagonal of the cube, while the sum of a B-ion diameter and an oxygen diameter makes up a cube edge. For this reason, perfect packing of the ions requires the following relation to hold:

$$R_A + R_O = \sqrt{2}\,(R_B + R_O)$$

Since the perovskite structure is observed in a large number of compounds, this relation cannot hold ideally for all of them. It is precisely this deviation from perfect packing which allows a slightly distorted cubic structure possessing spontaneous polarization within the unit cell to exist as a stable configuration. The deviations from ideal packing are usually described in terms of a tolerance factor, t, defined as follows:

$$t = \frac{R_A + R_O}{\sqrt{2}\,(R_B + R_O)}$$

A value of t greater than one signifies that the B ion is small enough to "rattle around" within the ionic framework of the A and O ions. A value of t less than one indicates that the B ion is large enough to deform the basic BO_6 octahedra of the structure. In a first approximation therefore, high values of t have been associated with ferroelectricity and low values with antiferroelectricity. The tolerance factors for the principal ferroelectric and antiferroelectric compounds are given in Table I, obtained from Megaw (M2).

TABLE I

TOLERANCE FACTORS FOR PRINCIPAL PEROVSKITE $A^{+2}\ B^{+4}\ O_3$ FERROELECTRICS

	B Ion			
A Ion	Ti (0.64)	Zr (0.77)	Hf (0.76)	Sn (0.74)
Ca (1.16)	0.89	0.84	0.84	0.85
Sr (1.37)	0.97	0.91	0.91	0.92
Ba (1.52)	1.02	0.96	0.96	0.97
Pb (1.32)	0.98	0.93	0.93	*0.92

* not produced as a stable perovskite compound

The ferroelectric properties of these materials cannot be explained completely on the basis of ionic size. Although the tolerance factor for lead titanate is less than one, this compound exhibits the strongest ferroelectric properties observed to this time. For this reason, attention must be directed to other properties of the ions, such as their polarizability. Roth, in his classification of ABO_3 compounds (R1), discusses the effect of the polarizability of the A ion on the structural properties of the compound formed. He finds that for A ions of low polarizability (>0.60 $\mathring{A}^3$) a cubic or pseudocubic structure is stable over the whole range of B radii. For Pb^{+2}, on the other hand, which has a polarizability of 0.90 $\mathring{A}^3$, ferroelectric and antiferroelectric structures occur for all B radii in the range between 0.65 $\mathring{A}$ and 0.85 $\mathring{A}$.

This dependence of ferroelectric properties on polarizability also shows up in the x-ray structural studies of the ion displacements in $BaTiO_3$ and $PbTiO_3$ (S2). In $BaTiO_3$, the phase change from cubic to tetragonal involves a shift of the Ba^{+2} ion of 0.05 $\mathring{A}$ with reference to the oxygen lattice. In $PbTiO_3$ this shift is 0.47 $\mathring{A}$. Thus the increase of polarizability of the lead ion allows ionic motion an order of magnitude greater than that observed in $BaTiO_3$.

A third factor which enters into the formation of ferroelectric structures in perovskite compounds is the concept of directional or covalent bonding. Megaw (M2) has pointed out that any covalent character in the bonding of the ions leads to a minimal energy for certain bond directions which can influence the ability of the material to undergo certain types of distortions.

From the viewpoint of electrostatics, the phenomenon of ferroelectricity represents a cooperative interaction involving the orientation

of a dipole in the field caused by surrounding dipoles. If dipoles are arranged in a one-dimensional array as shown in Figure 1 (a) below, the minimum energy is found when they are aligned in a parallel manner. This then represents a ferroelectric array. If they are placed side by side as in Figure 1 (b), the minimum energy is represented by an anti-parallel (antiferroelectric) arrangement. In a two or three dimensional array, the relative strengths of these two interactions determines whether the material exhibits ferroelectric or antiferroelectric behavior.

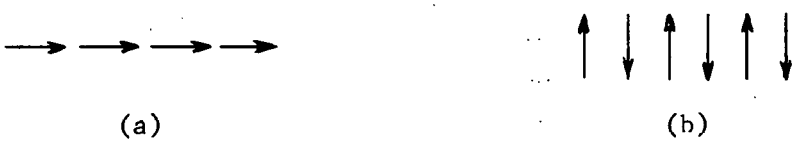

Figure 1. Representation of a Ferroelectric (a) and Anti-ferroelectric (b) Dipole Array.

The interaction between the dipoles and the internal field must be strong enough to override all factors which tend to disorient or destroy them in order to produce a stable ferroelectric or antiferroelectric phase. Thus it can be seen that ferroelectricity represents a balancing of strong mechanical and electrical interactions in the production of a stable distorted structure possessing spontaneous internal polarization.

Lead Perovskite Materials

The materials of greatest interest in this study are the solid solutions lead zirconate titanate, lead zirconate titanate stannate, and lead hafnate titanate. These compose a system of perovskite materials having a common A ion with the variation in properties being attributed to the varying characteristics of the B ions. Some of these characteristics are given in the following paragraphs.

The Ti^{+4} ion is the smallest of the perovskite B ions considered, with a Goldschmidt radius of 0.64 Å. The electronegativity of this element is 2.27, meaning that its bonds with oxygen tend to be about equally ionic and covalent. Because of its ionic size, the presence of Ti^{+4} in solid solutions tends to favor the ferroelectric state. In fact, lead perovskite solid solutions containing more than twelve per cent of this ion tend to be ferroelectric under all conditions.

Zirconium possesses about the same electronegativity as titanium but has a radius of 0.77 Å. The consequent increase in the tolerance factor induced by the presence of this ion in lead perovskites tends to favor antiferroelectricity in its solid solutions.

The Hf^{+4} ion, although much heavier than the Zr^{+4} ion is almost the same size, having a radius equal to 0.76 Å. However, it is somewhat less electronegative (2.1) which according to the criteria of Sanderson (S3) and Wells (W1) leads to a more ionic character in its bonds with oxygen and to a somewhat smaller polarizability. This means that within the framework of the perovskite lattice the hafnium ion carries a slightly larger charge than the zirconium ion but is not quite as susceptible to the distortions of its electron clouds. This ion still behaves very similarly to the Zr^{+4} ion with relation to its antiferroelectric character.

The Sn^{+4} ion behaves quite differently from the other three ions discussed here because of its basically different electron configuration. The four valence electrons in the tin atom represent two s-electrons and two p-electrons from the same shell, while for the others they are two s-electrons and two d-electrons from the next smaller shell. Thus while the ionic radius of this ion (0.74) is nearly the same as that of the

zirconium or hafnium ion, it does not show the tendency to induce antiferroelectricity nearly so strongly as these ions. The electronegativity of tin is 3.10 leading to a much stronger covalent character in its oxygen bonds and a greater susceptibility to ionic deformation.

The compounds and solid solutions involving the above ions have been the subject of many studies. These have in general attested to the strong ferroelectric character of lead titanate and the antiferroelectric tendencies of lead zirconate and lead hafnate. Certain studies, however, revealed deviations from the expected similarities in the characteristics of the zirconate and hafnate solutions, especially in the very low titanate regions.

In his work on lead zirconate titanate, Sawaguchi (S4) developed the phase diagram for the low titanate region given in Figure 2. It can be seen from this figure that for solid solutions containing from 3 to 6% titanium, the material undergoes an antiferroelectric to ferroelectric transition on heating. That is, the room temperature phase of these compositions is antiferroelectric, but they also exhibit a high temperature ferroelectric phase before reaching the Curie temperature.

In a later study, Jaffe, Roth, and Marzullo (J3) developed a similar diagram for lead zirconate titanate containing 30% lead stannate (Figure 3). They found that the addition of the stannate not only increased the compositional region exhibiting antiferroelectric behavior, but also reversed the slope of the phase boundary separating the ferroelectric and antiferroelectric phases. Thus for compositions containing between 7 and 12% titanium, the room temperature phase is ferroelectric and transforms into an antiferroelectric phase on increasing temperature before reaching the Curie transition temperature. Later work at Sandia

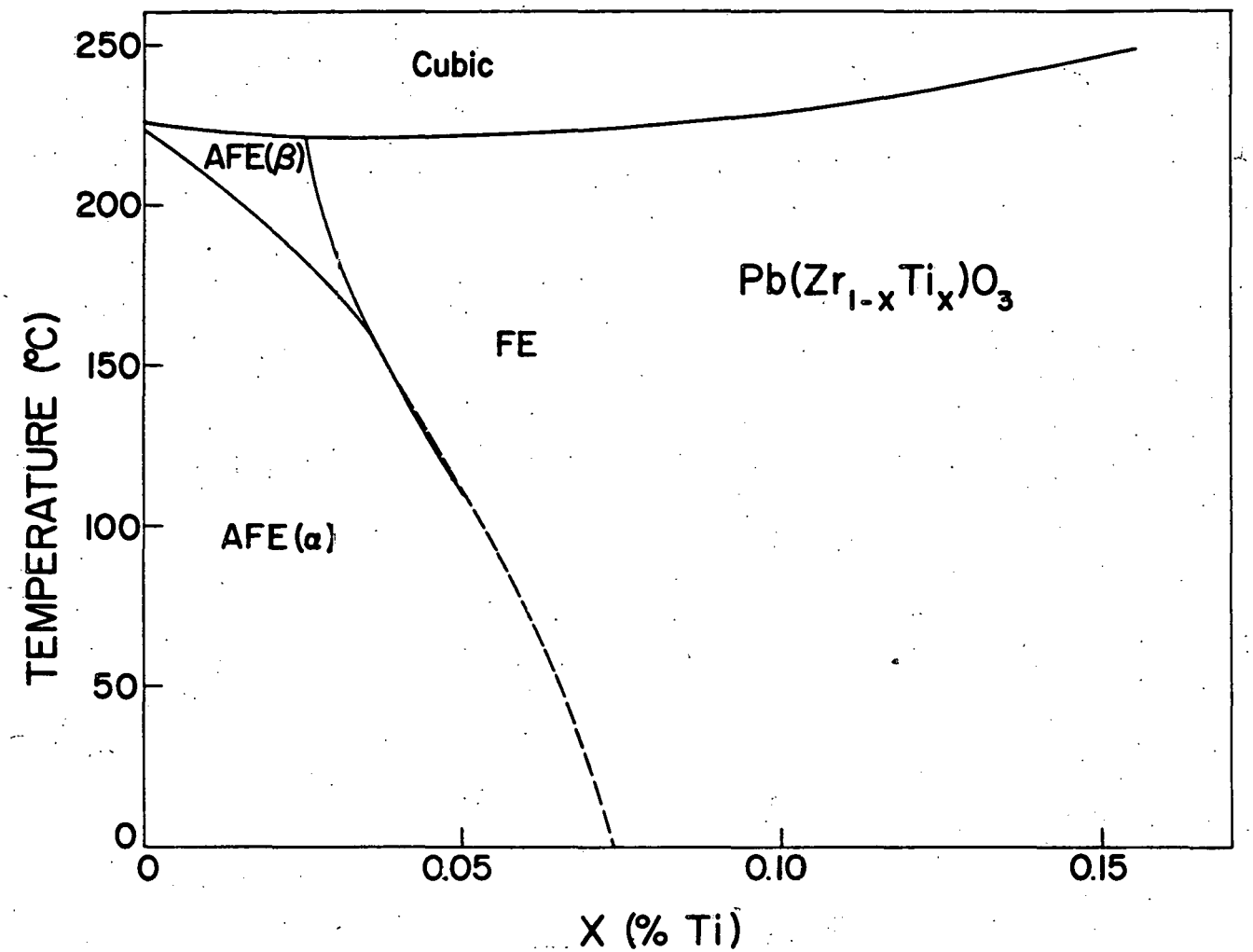

Figure 2. Compositional Phase Diagram for $Pb(Zr_{1-x}Ti_x)O_3$ (After Sawaguchi (S4)).

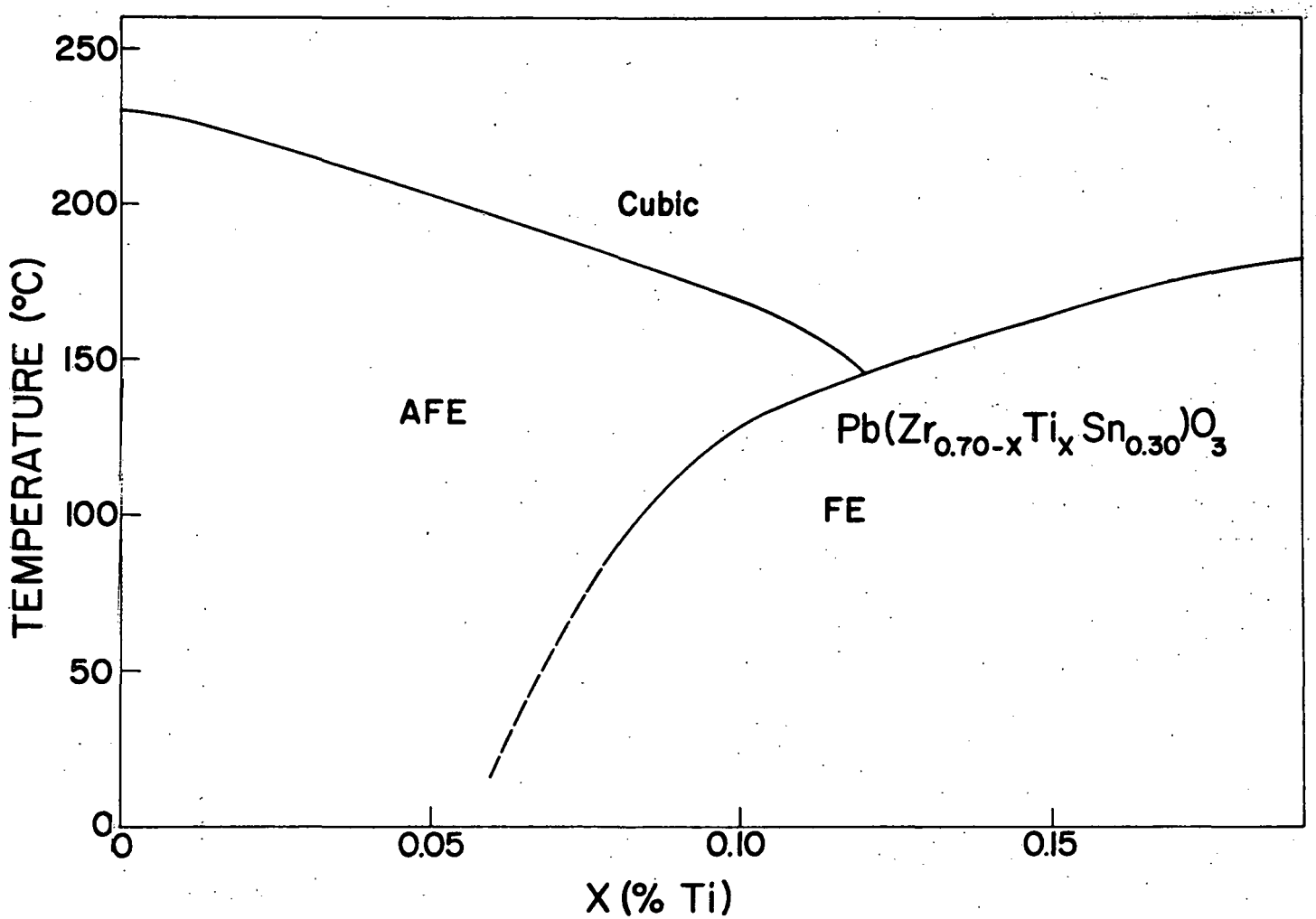

Figure 3. Compositional Phase Diagram for $Pb(Zr_{0.70-x}Ti_xSn_{0.30})O_3$ (After Jaffe (J3)).

Corporation and Clevite Research Laboratories revealed that this behavior was also exhibited by solid solutions containing smaller percentages of stannate.

Early work on lead hafnate by Shirane and Pepinsky (S5) indicated that this material behaved much like lead zirconate. This was to be expected from the similarities in the character of the ions. However, later work at Sandia Corporation by Hall (H1) showed that solid solutions of lead hafnate and lead titanate showed the ferroelectric to antiferroelectric phase relationship characterisitic of the lead zirconate titanate stannate solutions (Figure 4).

This leads to a situation in which temperature dependence of the phase stability of lead zirconate can be reversed either by adding lead stannate to the solution or by substituting the extremely similar hafnium ion for the zirconium ion. The present study on some of the thermodynamic characteristics of the transitions was initiated in an effort to examine the factors responsible for this behavior.

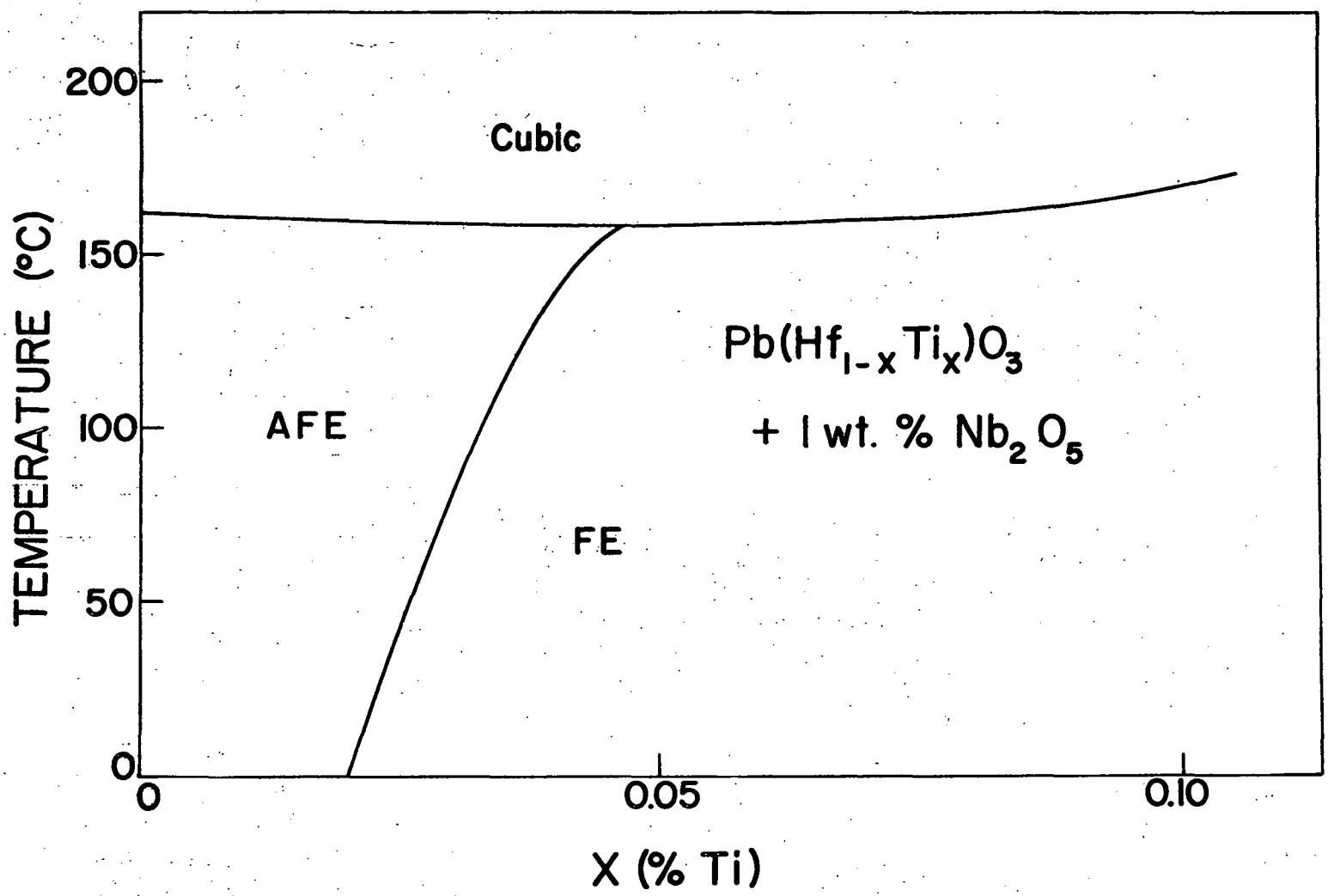

Figure 4. Compositional Phase Diagram for $Pb(Hf_{1-x}Ti_x)O_3$ + 1 wt. % Nb_2O_5 (After Hall (H1)).

CHAPTER III

THERMODYNAMICS OF PHASE TRANSITIONS IN FERROELECTRICS AND ANTIFERROELECTRICS

The purpose of this chapter is to outline some of the basic thermodynamic considerations which are of importance in discussing phase transitions in ferroelectric and antiferroelectric materials. This will be done by first considering the relationships common to all phase transitions together with some of the factors which determine transition rates. Then the thermodynamic properties of ferroelectrics and antiferroelectrics will be related with an emphasis on the factors which govern the relative stability of the various phases observed in the lead perovskites. Finally, a discussion of the application of the Gibbs phase rule to these systems will be given, together with a description of the information which may be obtained from the various types of phase diagrams.

Thermodynamics of Phase Transitions

Phase transitions in materials are usually discussed in terms of the Gibbs free energy. For convenient illustration one takes a simple homogeneous, isotropic medium where considering energy exchanges between the system and its surroundings to arise from changes of temperature, pressure, or electrical potential difference, this free energy is given by,

$$G = U - TS + PV - vQ$$

U = internal energy

T = temperature

S = entropy

p = pressure

V = volume

v = voltage

Q = dipolar charge

This may also be represented for polarizable materials in terms of energy densities by the relation:

$$G' = U' - TS' + p - EP$$

where the primes represent densities of the symbolized quantities and

E = applied electric field

P = polarization (charge per unit area or dipole moment per unit volume).

Using these definitions, the common thermodynamic relations for variation of free energy may be derived:

$$\left(\frac{\partial G}{\partial T}\right)_{p,v} = -S$$

$$\left(\frac{\partial G}{\partial p}\right)_{T,v} = V$$

$$\left(\frac{\partial G}{\partial v}\right)_{T,p} = -Q.$$

A transition occurring with a discontinuity in one of the above quantities is called a first order transition. A transition in which all of the above quantities are continuous, but where one of their derivatives (the second derivative of free energy with respect to an intensive parameter) is discontinuous, is called a second order transition. Higher order transitions may be defined similarly.

The type of phase relationship which is of most interest to this study is known as polymorphism. Polymorphism is the existence of several crystalline modifications of the same substance. Phase transitions

between polymorphic modifications represent the simplest crystalline reactions since they involve no macroscopic motion of ions. The polymorphic structure which has the lowest free energy under a given set of conditions will be the most stable structure. All of the other forms will tend to transform into this structure, although there may be energy barriers which cause the reaction to go extremely slowly.

At absolute zero, zero pressure, and zero electric field, the relative stability is determined primarily by the structure energies of the various polymorphic forms. It should be noted that this is not the total lattice energy but may be represented as the difference between the energy of the given structure and that of a minimum energy optimum packing configuration. There will be one of the polymorphic forms which represents a minimum structural energy and this will be the most stable form of the material in the absence of intensive variables.

As the temperature increases the temperature-entropy product becomes the dominant term in the free energy equation. Although the internal energy increases with temperature, the magnitude of the change is ordinarily much smaller than that of the temperature-entropy product. Thus the free energy becomes a monotonically decreasing function of temperature. If the entropy of the form most stable at absolute zero is greater than the entropy of other forms at all temperatures, this form will always be the most stable and no transitions will occur. However, if this is not the case, there may exist a situation in which for $U_2 > U_1$, $U_2 - TS_2 = U_1 - TS_1$. This is illustrated in Figure 5.

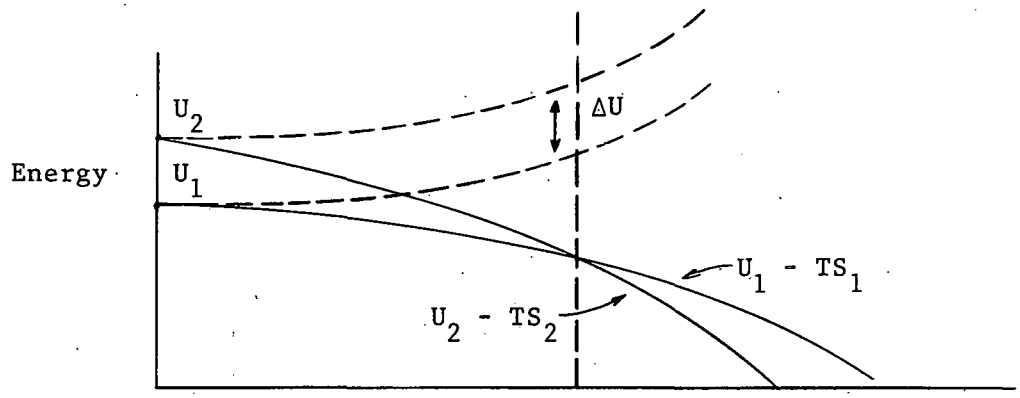

Figure 5. U and G vs. T for p = 0, E = 0.

Under these conditions there will be a transition from phase 1 to phase 2. Since this transition is accompanied by a discontinuous change in entropy as shown by the slopes of the free energy curves, it is of first order and involves a positive heat of transformation. That this quantity is always positive for transformations occurring on rising temperature can be seen from the relation:

$$U_2 - U_1 = TS_2 - TS_1 = T(S_2 - S_1).$$

The temperature is a positive quantity and S_2 must be greater than S_1 in order for the curves to cross, so both factors on the right hand side of the equation are positive. Thus a polymorphic transition on rising temperature must be accompanied by an absorption of heat. If more than two structures are possible for the given material, there may be temperature regions in which each is stable.

Under ordinary conditions an increase in the electric field applied to a material produces a monotonic decrease in free energy in the same manner as an increase in temperature. In this case the extensive variable of interest is the dipolar charge on the sample or the polarization of the material. For materials having no spontaneous polarization, the polarization

due to the application of the field is given by

$$P(E) = \int_0^E \frac{dP}{dE}\, dE \equiv \int_0^E \epsilon_0 \chi(E) dE.$$

Thus materials having high susceptibility will, other factors being equal, be more stable at high fields than materials of low susceptibility. In ferroelectric materials the spontaneous polarization adds to this effect immensely, assuming the polarization to be aligned with the field. If the spontaneous polarization is oriented antiparallel to the external field however, the effect is to increase the free energy rather than to decrease it. For materials possessing spontaneous polarizations and very high coercive fields, it is possible that the free energy could actually be increased appreciably by the application of an electric field.

On the other hand, the influence of an increase of pressure on the free energy is opposite to that of temperature and electric field, due to the positive sign of the pressure volume product in the free energy equation. Thus an increase of pressure produces an increase of free energy and the most stable structures at high pressures will be those of minimum volume.

The experimental determination of the relative free energies of several phases in a polymorphic system is greatly hindered by the wide variation in transformation rate observed in such systems. In general, there exists an energy barrier between two phases which have equal free energies and an activation energy is required to cause the transformation to take place. Because of the relative immobility of ions within a solid lattice, this may lead to an extremely slow rate of transition in cases where drastic rearrangements are necessary to form the new phase. For

this reason, these transformations often exhibit large hysteresis and quite often a phase may exist as a stable configuration for long periods of time at temperatures where it no longer represents the minimum free energy in a polymorphic family.

Buerger (B1) has given a crystallographic classification of phase transitions in solids according to the types of microscopic bonding changes necessary to form the new phase. He places all polymorphic transitions into four groups:

I. Transformations of secondary coordination. These represent, in general, changes in the weak bonded or non-nearest neighbor configurations. In this type of transformation the strong bonded (contacting atom) configurations remain undisturbed and merely shift their spatial relationships to one another. A good example of this type of transformation is the ferroelectric transition in potassium dihydrogen phosphate, in which the phosphate tetrahedra change orientation, causing minor changes in the length of the hydrogen bonds. This type of transition is relatively rapid and will take place at quite low temperatures unless the rearrangement requires an actual reconstruction of the secondary bonds.

II. Transformations of disorder. This class includes changes in rotational disorder (such as the α - β quartz transformation) and transformations of substitutional disorder (such as those occurring in alloys). In general, the first of these proceed rapidly while the last are quite sluggish and take place only at high temperatures.

III. Transformations of first coordination. These transformations represent a change in the bond structure of nearest neighbors and distortions of the strongly bonded structural configurations. If the change is merely a dilatation of the strongly bonded group (the case in perovskite

transitions) the transition may proceed rather rapidly. However, even the simplest first coordination transitions usually become rather sluggish at low temperatures. If the transformation requires a bond rearrangement among nearest neighbors, the rate of change is exceedingly slow, allowing seemingly stable structures to exist under conditions where they are not energetically favorable.

IV. Transformations of bond type. In these transformations the polymorphic structures possess entirely different bonding characteristics. This is exemplified in the diamond and graphite configurations of carbon. Transformations of this type usually proceed rather slowly and are often difficult to initiate. It is quite possible that the ferroelectric transformations in perovskites fall partially into this class. In structures such as the perovskites, the ratio of ionic to covalent character in the oxygen to metal bonds is a function of bond length. Thus, the distortions of the basic cubic lattice may cause a partial change of bond type.

The use of ceramic or powdered materials may also affect the transition rates appreciably. If the transition is controlled by the nucleation rate, i.e. if the new phase spreads rapidly throughout the lattice once it is nucleated, the transition rate is usually somewhat slower in finely divided material. However, if the rate is controlled by the ability of the new phase to grow throughout the lattice after being nucleated at a surface, ceramics and powders transform much more readily than large single crystals.

Applications of the Above Considerations to Ferroelectric and Antiferroelectric Transitions

In the special case of polymorphic systems involving ferroelectric (FE) or antiferroelectric (AFE) phases, certain relationships are introduced into the above free energy picture. The presence of a large spontaneous polarization in the FE phase allows the electric contribution to play a more dominant role in the transition behavior than is normal in polymorphic transitions. The application of an electric field lowers the free energy curve of the FE phase much more than that of either the AFE or cubic (PE) phases. This causes a shift in transition temperatures in such a manner as to increase the temperature range over which the FE phase is stable, e.g., Ferroelectric Curie temperatures are raised by the application of an electric field. The only exception to this rule might be in the case of small fields applied in the opposite direction to the polarization of the FE sample. Since the field and polarization vectors are antiparallel in this case, the free energy of the phase would be raised instead of lowered. However, this leads to an instability in that the decrease of free energy obtained by switching is greater than that obtained by a transformation into a new phase. Thus it would seem that usually switching should occur first and the ultimate change in transition temperature should be nearly independent of the field direction.

In the transitions from AFE to a PE phase, the application of an electric field tends to favor the PE phase. As will be discussed in the section on dielectric measurements, the polarizability of the lattice in the cubic phase is greater than that in the antiferroelectric phase. Thus from the free energy equation, the application of an electric field

lowers the PE free energy more than the AFE. This is verified by the observation that Antiferroelectric Curie temperatures are lowered by the application of an electric field.

In the perovskite structure a transition from PE to FE is accompanied by an increase in volume, while a transition from PE to AFE results in a decrease of volume. Thus the application of a hydrostatic pressure (which increases the free energy of each phase by an amount proportional to the phase volume) leads to a favoring of the AFE phase over the PE and FE phases, and a favoring of the PE phase over the FE phase.

The variation of the free energies of the different phases with temperature depends on the relationships between the various factors which determine the entropy of the system. Since there is negligible macroscopic ionic motion associated with the phase transformations in perovskite solid solutions, the configurational entropies of the three phases are approximately equal. The entropy differences between the phases must then be accounted for by either an order-disorder transformation or by differences in the phase vibrational entropies. In the potassium dihydrogen phosphate family of ferroelectric materials, the constancy of the entropy change at the Curie transition throughout the family indicates that the dominant mechanism is the order-disorder one (K1). In perovskites, on the other hand, the entropy change at the transition varies widely from material to material, suggesting that in this family the vibrational entropy is dominant.

Following the reasoning of Buerger (B1), it can be seen that the cubic phase represents the highest entropy of the possible phases of a perovskite structure. As an unpoled ferroelectric approaches the Curie temperature the thermal vibrations and expansion of the lattice lower the

coercive force to the point that domains have a certain probability of becoming thermally switched. At the transition this switching takes place rapidly enough that the time average of each ionic position becomes the same as the position in the cubic state. This is the same as saying that the ferroelectrically active ions oscillate about positions which are equivalent to their positions in the cubic phase. Thus the cubic phase may be regarded as a disordered equivalent of the polar phase and therefore the phase of highest entropy. This is borne out by the fact that the cubic phase is always the most stable phase at high temperatures.

The entropy relationship between the FE and AFE phases is more difficult to determine from basic principles. Although the AFE phase shows no net polarization, it can be considered as being composed of two sublattices possessing equal and opposite spontaneous polarizations. Thus, in perovskites, both the FE and the AFE phases represent a polar distortion of the original nonpolar lattice. The differences of the entropy associated with these phases then result from small differences in bond structure and in the vibrational configurations of their lattices. It is to be expected that these phases will have nearly equal entropies for many compositions. Thus the reversal of direction of the phase transition with temperature which was discussed in the previous chapter does not result from a drastic change in the energy relations in either phase, but rather from a small change which allows a slight entropy dominance of one phase to become an entropy dominance of the other. Further remarks on this subject will be included in the final chapter, which gives some of the conclusions which can be reached from experimental results.

Application of Gibbs Phase Rule Concepts to this System

The Gibbs phase rule may be stated in generalized form as

$$F = C - P + N$$

where

F = number of degrees of freedom of system

C = number of chemical components

P = number of phases present

N = number of intensive variables.

The number of degrees of freedom represents the number of variables which may be changed independently without causing the appearance or disappearance of a new phase. This equation does not specify a definite relationship between phases, but rather is used to correlate data from experimental studies.

The phase relationships for a given system are usually given in the form of graphs called phase diagrams. In these plots, which use compositional relations and intensive parameters as variables, each phase extends over that set of points specifying the conditions under which it is most stable. In general, the number of dimensions, D, required by such a plot is given by

$$D = C + N - 1.$$

Thus the phase relation in a two component system under fixed external conditions may be specified on a straight line, while those for a three component system under fixed external conditions require a plane (the common triangular compositional phase diagrams). A plane is also required to plot the relations in a two component system as a function of one external variable (temperature, pressure, etc.). To show the phase

relationships in a solid solution family such as the lead zirconate titanate stannates as a function of temperature, pressure and electric field would require a five dimensional phase diagram.

In a phase diagram of D dimensions a single phase will be stable in a [D] dimensional region, transition conditions between two phases will be represented by [D - 1] dimensional phase boundary, and equilibrium between three phases can occur only over a [D - 2] dimensional region. For example, in a two dimensional phase diagram a single phase is represented by an area, the boundary between two phases by a line, and the coexistence of three phases by a single point. This agrees with the Gibbs phase rule which specifies that for C + N = 3 (the necessary condition for a two-dimensional phase diagram) a single phase has two degrees of freedom, a pair of phases has only one degree of freedom, and three phases can exist together under only an isolated set of conditions.

In working with systems involving ferroelectric solid solutions, the chemist or ceramist is, in general, interested in the variation of properties with composition. Phase diagrams used by ceramists generally depict either relationships involving composition alone or relationships between composition and one intensive variable, usually temperature. The physicist or engineer, on the other hand, is usually interested in the characteristics of a single sample, which represents a single composition because of the low internal mobility of the ions. Phase diagrams of interest to the physicist depict the relationship between phases as two intensive parameters are varied (transition temperature vs. electric field, etc.).

The derivation of specific thermodynamic data from phase diagrams involving composition as a variable is complicated by the fact that a

change of composition affects not only the internal energies of the various phases, but also the other extensive parameters (entropy, molar volume, polarization). Thus the slopes of the boundaries between phases as functions of composition are not easily interpreted in terms of the parameters involved in the free energy equations.

In phase diagrams involving two or more intensive variables, the slopes of the phase boundaries can be used to determine the relationships between the corresponding extensive parameters. For first order transitions such as those observed in this study this is given by a generalized Clausius-Clapeyron equation:

$$\left(\frac{\partial X_i}{\partial X_j}\right) = -\frac{\Delta x_j}{\Delta x_i}$$

where X_i, X_j . . . represent intensive variables (generalized forces), $(\partial X_i/\partial X_j)$ represents the slope of the phase boundary with all other intensive variables held constant, and Δx_i, Δx_j . . . represent the discontinuous changes in the corresponding extensive variables at the transition.

The various types of phase diagrams and the information to be obtained from each are given in Table II. Using these relationships and the measurements of polarization, cell volume, and specific heat of the material, a free energy diagram explaining the phase relationship as a function of the intensive parameters can be developed.

TABLE II

PHASE BOUNDARY RELATIONSHIPS

Type of Phase Diagram	Intensive Parameter Boundary Slopes	Extensive Parameter Relationship (1st order Transition)
Transition temperature vs. pressure	$\left(\frac{\partial T}{\partial p}\right)_E$	$\frac{\Delta V}{\Delta S} \equiv \frac{T\Delta V}{H}$ *
Transition temperature vs. electric field	$\left(\frac{\partial T}{\partial E}\right)_p$	$-\frac{V\Delta P}{\Delta S} \equiv -\frac{\Delta P}{\Delta S'}$
Transition pressure vs. electric field	$\left(\frac{\partial p}{\partial E}\right)_T$	$\frac{V\Delta P}{\Delta V} \equiv \frac{\Delta P}{\Delta V/V}$

* H = Latent heat of transition.

CHAPTER IV

DIELECTRIC MEASUREMENTS

Measurements of the dielectric susceptibility and loss have played an important role throughout the study of ferroelectrics. It was the extremely high values of susceptibility which first caused interest in these materials and which later led to many of their important applications. The variation of susceptibility with temperature has long been the prime tool for precise determination of transition temperatures.

Dielectric Susceptibilities

In ferroelectric materials, the dielectric constant ($k = \epsilon_o^{-1}\ dD/dE$) and dielectric susceptibility ($\chi = \epsilon_o^{-1}\ dP/dE$) become approximately the same. Since these two factors are related by

$$k = \chi + 1$$

and have magnitudes varying from a few hundred to a few thousand, there is little error introduced by using them interchangeably. In general, measurements determine k while most theories deal with χ. In discussing the dielectric susceptibility of a ferroelectric material, however, it is necessary to differentiate between the changes of polarization due to switching and the "true" small signal polarization changes.

The abnormally high dielectric constants of ferroelectric and antiferroelectric materials are due to the freedom of certain ions within the pseudocubic lattice structure to move under the influence of small

fields. This leads to large ionic contributions to the susceptibility and also to the extreme variations of dielectric constant with those parameters which affect lattice spacings and orientations.

Using curves representing the variation of free energy as a function of polarization (related to ionic position) such as those in Figure 6 below, the behavior of the dielectric susceptibility in the vicinity of the Curie temperature can be explained.

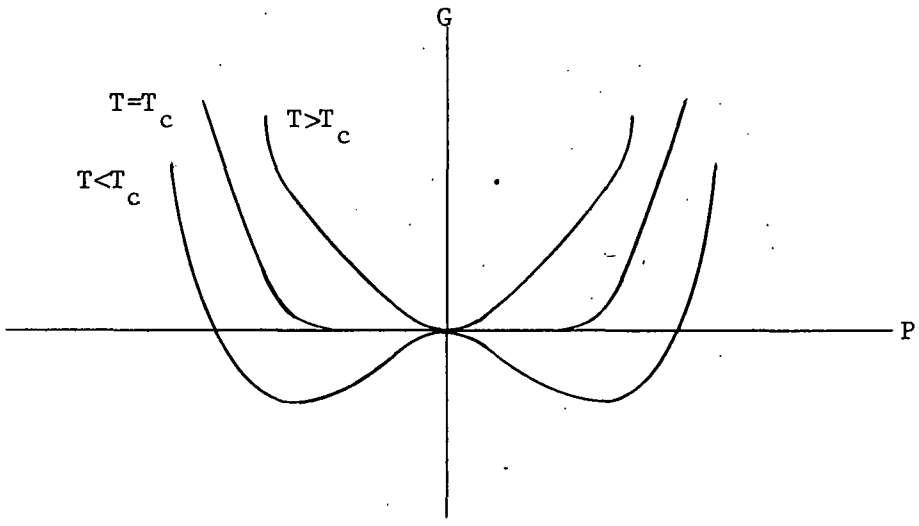

Figure 6. Variation of Free Energy with Polarization for a Ferroelectric Material.

The curves represent a symmetric variation of the free energy about zero polarization with a simple minimum, an extended minimum and a double minimum. The application of a linear external field to the material superimposes a slope on each of these curves, causing a shift in the position of the minimum. This is equivalent to saying that the ionic motion caused by the application of the external field is highly dependent on the exact shape of the minimum for the temperature concerned. For temperatures below the Curie temperature ($T<T_c$), the material is ferroelectric and the susceptibility is determined by the ability of the ion to move about within one of the symmetric minima. A shift from

one minimum to the other within this temperature region represents switching rather than small signal dielectric behavior. At the Curie temperature ($T = T_c$), the free energy curve is flat at the bottom allowing large ionic shifts with very small fields and thus extremely high dielectric susceptibilities. Above the Curie temperature ($T>T_c$), the free energy exhibits a simple minimum but the ions are still relatively free to move to both sides of this minimum under the influence of a small field. This is the reason the susceptibility in the paraelectric state is higher near the Curie temperature than that of the ferroelectric state.

For antiferroelectric materials, the curves are similar, except that the minima below the Curie temperature are not symmetric. That is, the mechanical constraints in this phase cause one direction of ion shift to be highly favored over the other. This leads to a more restricted ionic motion under the influence of a small external field and thus to lower susceptibilities.

The nonlinearity of dielectric susceptibility may be measured by making small signal capacitance measurements while superimposing a constant biasing voltage on the sample. In the figure below, which is representative of polarization vs. field for a material above the Curie

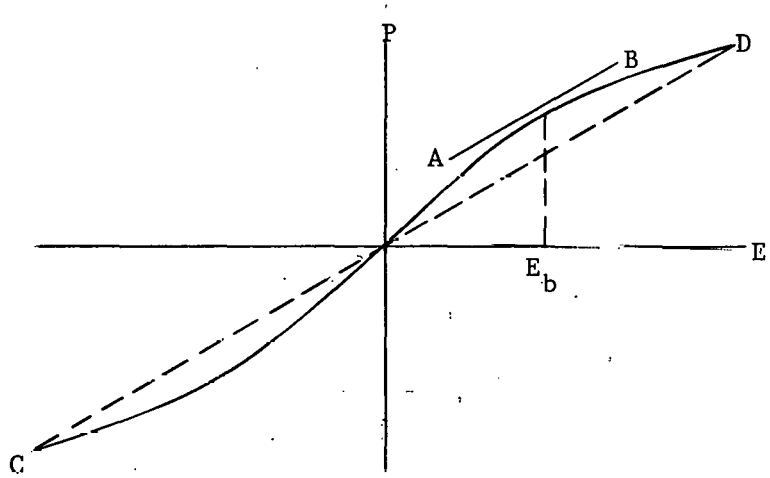

Figure 7. Polarization vs. Bias Voltage Showing Nonlinear Saturation Effect.

temperature, the slope of the line segment AB (the tangent to the curve at $E = E_b$) represents the dielectric susceptibility of the material at a given bias as determined by small signal measurements. This is in sharp contrast to the results of large signal dielectric contant measurements which require much larger bias voltages to achieve the same slope, as is indicated by the line segment CD. Using small signal measurements, the effect of dielectric saturation then becomes apparent as a decrease in the measured susceptibility with an increase in the bias voltage. This saturation is quite significant near a ferroelectric Curie point.

Measurements of the dielectric susceptibility in the paraelectric region as a function of temperature show that it varies according to the Curie-Weiss Law,

$$X = \frac{C}{T - T_o}$$

where C = Curie constant

and T_o = Curie-Weiss temperature.

For materials in the FE phase, the Curie-Weiss temperature is usually only a few degrees different from the Curie temperature, while for antiferroelectric materials this difference may be much greater, sometimes more than fifty degrees.

Dielectric Loss

Most publications of dielectric measurements on ferroelectric materials have reported dielectric loss measurements in terms of tan δ, the ratio of the loss current to the capacitive current. Variations of loss thus reported are caused not only by changes in loss mechanism but also by changes in sample capacitance. This leads to no problems for studies

such as those concerned with internal friction on quartz since loss variations of interest occur under conditions where the sample capacitance is constant. In ferroelectrics, on the other hand, many regions of interest are accompanied not only by changes of loss mechanism but also by extraordinary changes of sample capacitance. Thus the loss tangent will be a poor indicator of actual loss values and may at times become misleading. For example, near the Curie temperature of a ferroelectric one would expect rather high dielectric losses since the material is easily influenced by small electric field gradients. However, the exceptionally high dielectric constants in this region lead to very low values of tan δ. For this reason, it would seem more valid to report ferroelectric data in terms of a dielectric constant and an "equivalent conductance". From the definition of tan δ this equivalent conductance can be obtained by the equation

$$g = 2\pi fc \tan \delta$$

g = equivalent conductance

f = measuring frequency

c = total capacitance.

The term "equivalent" is used here to indicate the contributions of all mechanisms for converting electrical energy to thermal energy, i.e., Joule heating, domain wall motion, irreversible losses in phase transformations, etc. Since all of these mechanisms do not have the same dependence on sample geometry, it seems more satisfactory to speak of the "conductance of a sample" rather than the "conductivity of a material".

This viewpoint is also helpful in experiments where measuring system components contribute currents which are not small compared to the capacitive and loss currents of the sample. Since the measuring system

and sample are equivalently in parallel, their respective capacitances and conductances are additive, while the relationship between the true loss tangent of the sample and the measured loss tangent is more complicated.

Measurement Equipment

Dielectric measurements for this study were made with a General Radio Model 716C capacitance bridge. This was driven by a General Radio Model 1302-A Oscillator. Null detection was accomplished with a General Radio Model 1231 filter and amplifier with an oscilloscope as the final null detection device. All measurements were made with a driving frequency of one kilocycle and a peak-to-peak voltage of one volt. Using this system capacitances were measureable with a sensitivity of about $\pm$ 1$\mu\mu$F, and tan δ with a sensitivity of $\pm$ 0.0002.

The sample was maintained in an oil bath containing Dow Corning 200 silicone oil and equipped with an immersion heater and magnetic stirrer. Temperature measurements were made by means of thermometers placed at the sample position. A general laboratory thermometer was used for the lower temperature regions, while one with an expanded scale was used above 140°C for more accurate determination of the transition temperatures. With this bath measurements could be made in the temperature region 20 - 230°C with the rate of change of temperature ranging from 3 C$^{\circ}$ per minute at low temperatures to as low as 0.2 C$^{\circ}$ per minute near transition points.

In order to measure dielectric constant and loss as a function of both temperature and electric field, a system was designed which would allow dc voltages up to two kilovolts to be placed on the sample while making dielectric measurements. This system is shown in Figure 8. The dc

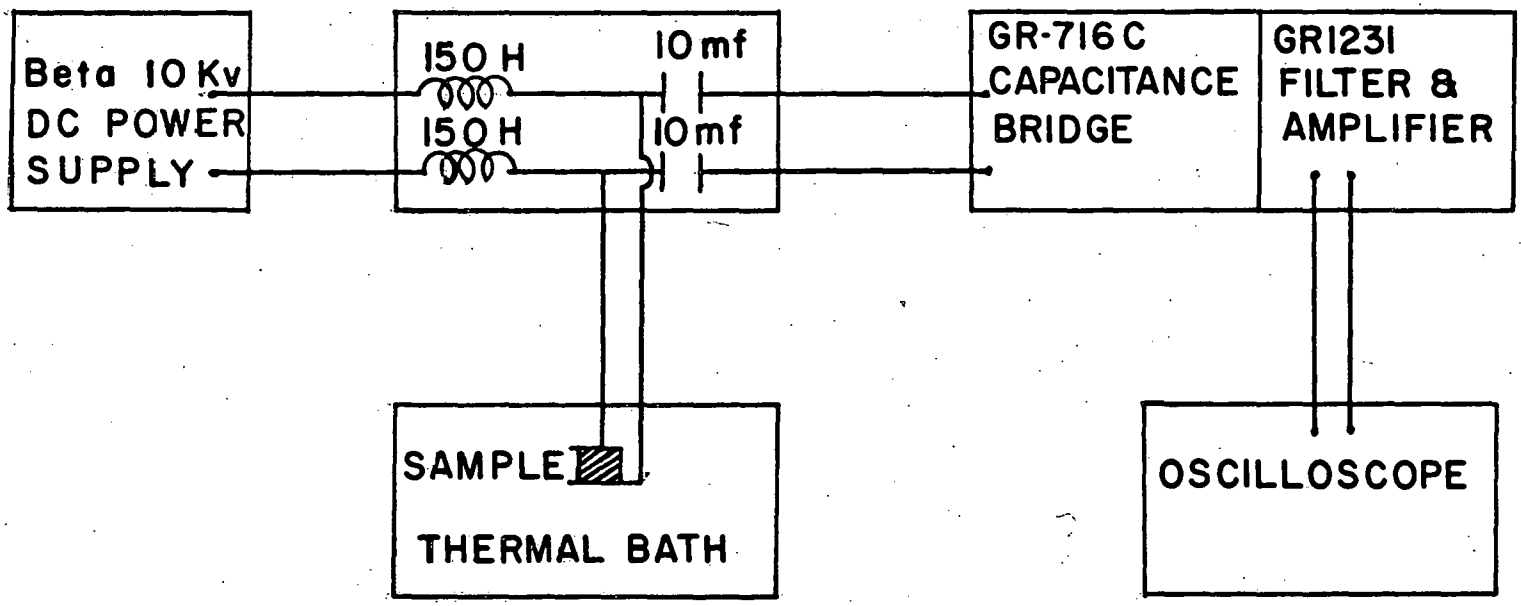

Figure 3. Block Diagram of Dielectric Measurement Apparatus.

voltage was supplied by a Beta 10 kilovolt power supply which was isolated from the sample by two 150 henry chokes. These provided a separating impedance of 1.9 megohms as compared with a maximum sample impedance of about 0.3 megohms at the measuring frequency of one kilocycle. At the same time they allowed the dc voltages to be placed on the sample with negligible loss. The biasing voltages were separated from the capacitance bridge by two 10 microfarad, 2 kilovolt oil filled capacitors. These provided dc separation with negligible measuring signal loss. The measuring system introduced stray capacitances of the order of 1000$\mu\mu$F into the results which could be measured before introducing the sample and then subtracted from the sample readings.

Experimental Samples

The samples used in this study were furnished by Sandia Corporation in the form of small ceramic discs of lead zirconate titanate stannate and lead hafnate titanate. The compositions had all been made with a small amount of Nb_2O_5 additive to aid in firing and to reduce conductivity. The samples were sintered at approximately 1400° C and were furnished with fired silver electrodes. As a first step in the present investigations, the samples were heated to 500° C for approximately two hours and allowed to cool in the absence of an electric field in order to reduce the effects of past treatment. In measurements at bias voltages, the measurements at low bias were always made before those at higher bias so that any poling of the sample could be attributed to the bias used in the measurement being made. The actual dimensions of the principal samples used in the dielectric studies are given in Table III.

TABLE III

DIMENSIONS OF SAMPLES USED IN DIELECTRIC MEASUREMENTS

Sample	Diameter (mm)	Thickness (mm)	Density (gm/cm^3)
PZST6	16.09	1.74	7.74
95HN2	13.95	2.65	8.93
96HN2	14.17	2.09	9.00
97HN2	13.92	2.22	9.04
98HN4	14.12	0.88	8.94
100HN2	14.18	1.75	8.99

Measurement Procedures and Calculating Techniques

1. Measurement of the system capacitance and loss tangent were taken with the sample removed. System loss was converted into conductance by the equation given earlier.

2. The sample was placed in the system and the electrical bias to be used for the run placed on it.

3. Measurements of the capacitance and loss tangent of the sample were obtained from room temperature to about thirty degrees above the Curie temperature during both the heating and cooling portions of the run.

4. The sample dielectric constant at each temperature was calculated using the equation:

$$k = \frac{t\ (\text{Total capacitance} - \text{System capacitance})}{\epsilon_o A}$$

where t = sample thickness

and A = electrode area.

5. The sample conductance was calculated at each temperature using the relation:

$$g = 2\pi f\ (\tan \delta)(\text{total capacitance}) - g(\text{system})$$

Because of the large number of measurements made, it was found convenient to use the IBM 650 as the principal means of data reduction.

Results

Lead Zirconate Titanate Stannate

The first samples studied were those of $Pb(Zr_{0.68}\ Ti_{0.07}\ Sn_{0.25})O_3$. A tentative phase diagram for this material was worked out during the summer of 1961 at Sandia Corporation and it was found to show both FE and AFE phases over large temperature ranges. The present measurements served two purposes: first, to check out the present measuring system and procedures, and second, to refine the phase diagram for the composition.

Figure 9 shows typical curves of the dielectric constant and loss which were exhibited by these samples. The dielectric constant curve indicates the nature of the three transitions of interest. The Curie transition, which exhibits about 3 C^{o} temperature hysteresis with rising and falling temperatures, is characterized by the highest peak of dielectric constant. At temperatures above this transition there is a decrease of the dielectric constant following the Curie-Weiss Law.

The FE-AFE transition, which occurs on rising temperature in this material, is accompanied by a small peak in the dielectric constant curve and an extremely large one in the conductance curve. The AFE-FE transition is shown on decreasing temperature by a sudden drop in dielectric constant to values corresponding to those observed with increasing temperature. This is accompanied again by a peak in the conductance curve.

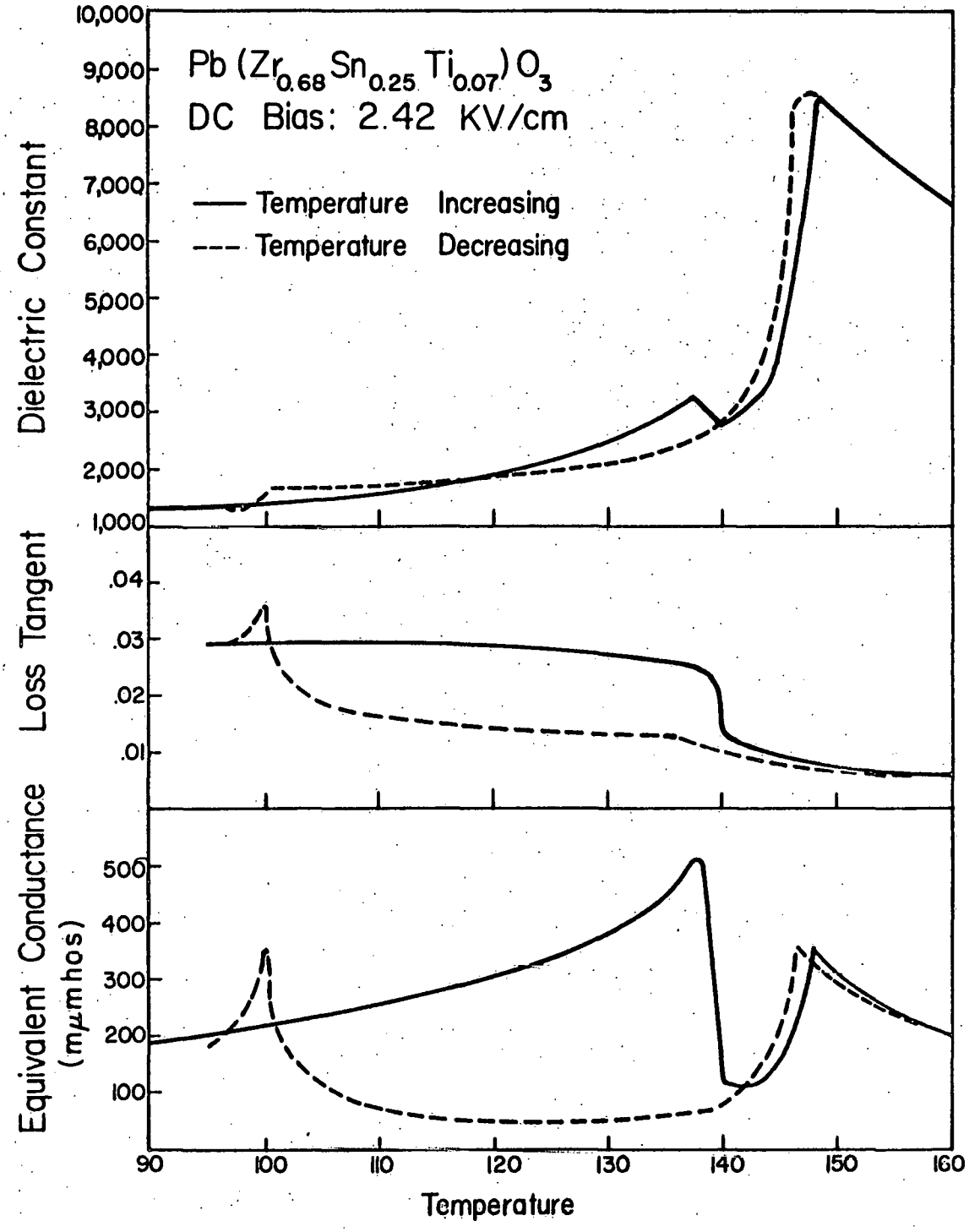

Figure 9. Dielectric Data for PZST.

These curves show the advantage of equivalent conductance as a measure of dielectric loss over the traditional tan δ. For this material, the loss maximum at the Curie transition is completely lost in the tan δ curve. The relative magnitudes of the loss currents at the various transitions are also given their proper perspective in the conductance measurements. Thus, the FE-AFE transition, where mechanical losses would be expected to be greatest, exhibits the highest maximum in loss conductance.

Figure 10 shows the phase diagram for this material as a function of temperature and electric field. This diagram indicates that for low fields the AFE region is stable over a 24 degree range on heating and a range of about 55 degrees on cooling. This large hysteresis is indicative of the fact that the free energies of the FE and AFE phases show virtually the same temperature dependence in the region of interest. As the electric field is increased, the AFE phase becomes less energetically competitive and finally is lost altogether. Thus we see that there are three regions of interest given by this phase diagram:

a) Low fields - those for which the AFE phase exists over an appreciable range of rising temperatures.

b) Moderate fields - those for which the FE-AFE transition approaches the Curie transition rather slowly and the AFE phase is "squeezed out".

c) High fields - those for which the AFE phase is missing.

It is also interesting to note that the temperature at which polarization disappears (the FE-AFE transition temperature for low and moderate fields and the Curie temperature for high fields) apparently has continuous slope at the point where the AFE phase disappears.

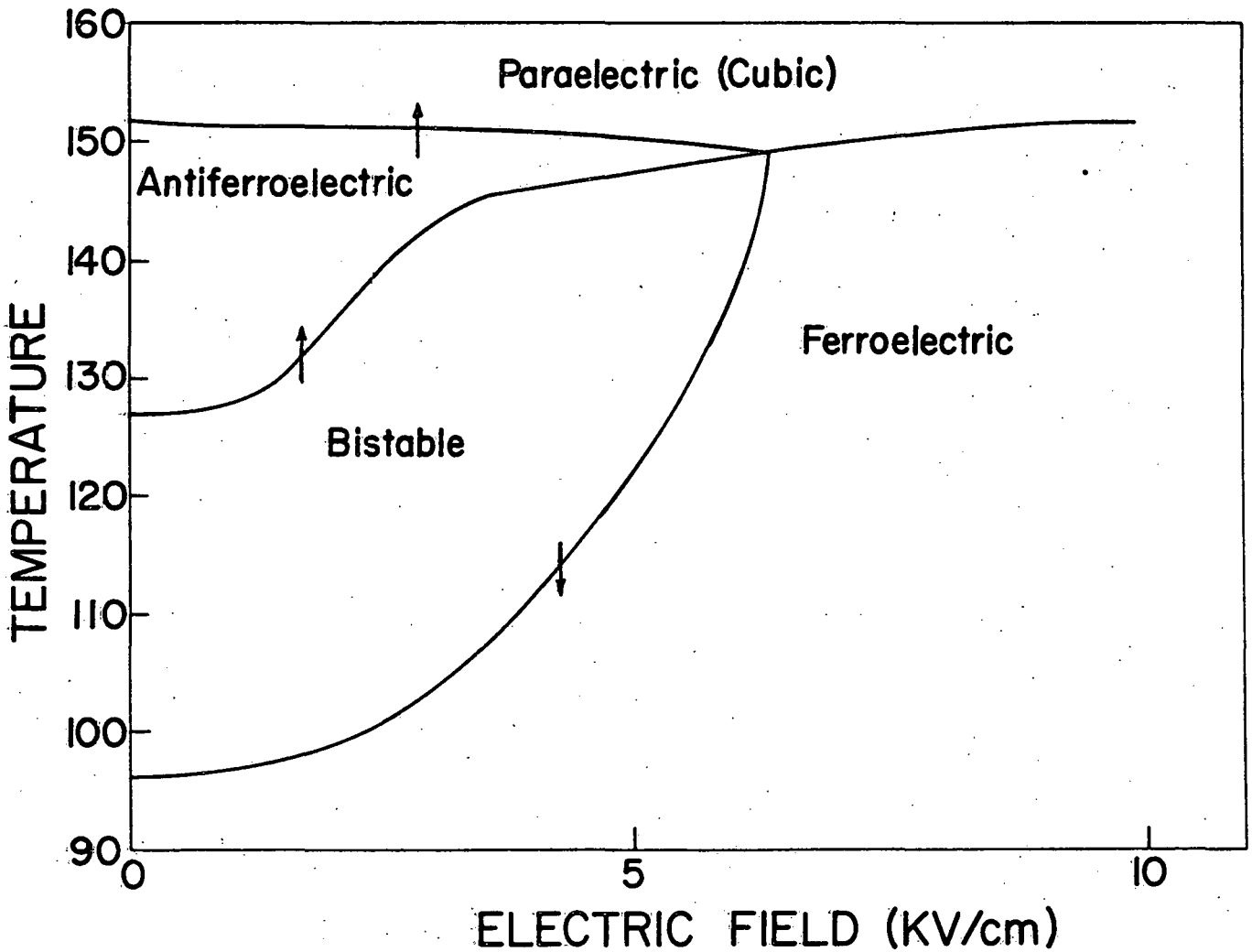

Figure 10. Phase Diagram of PZST as a Function of Field and Temperature.

Figure 11 shows the dielectric constant at the transition as a function of bias. Instead of the normal decrease of the transition dielectric constant for large fields explained by saturation effects, here there is actually an increase. This would seem to require an explanation based on the intrusion of some ferroelectric character into this transition, due to the nearly equal free energies of all three phases in this region. For fields above that at which the AFE phase disappears, normal saturation behavior is again evident.

Figure 12 indicates the behavior of this material in the paraelectric region. This is shown as a dependence of the Curie constant and Curie-Weiss temperature on the applied electrical bias. The Curie constant decreases quite rapidly with increasing bias while the Curie-Weiss temperature increases as the electric field causes the material to assume a dominance of ferroelectric characteristics.

Lead Hafnate Titanate

Measurements were also made on the series of lead hafnate titanate samples furnished by Sandia Corporation. These materials gave results which were not as sharply defined as those obtained with the lead zirconate titanate stannate samples. This was primarily due to the extreme dependence of the FE-AFE nature of these materials on their composition. The samples having a hafnate/titanate ratio of 95/5 were ferroelectric at all temperatures. The 96/4 samples exhibited an FE-AFE transition at low field but this transition was relatively near the Curie point and was not nearly so sharp as in the lead zirconate titanate stannate samples. The 97/3 samples were antiferroelectric under nearly all conditions. Some ferroelectric nature could be imparted to this material by

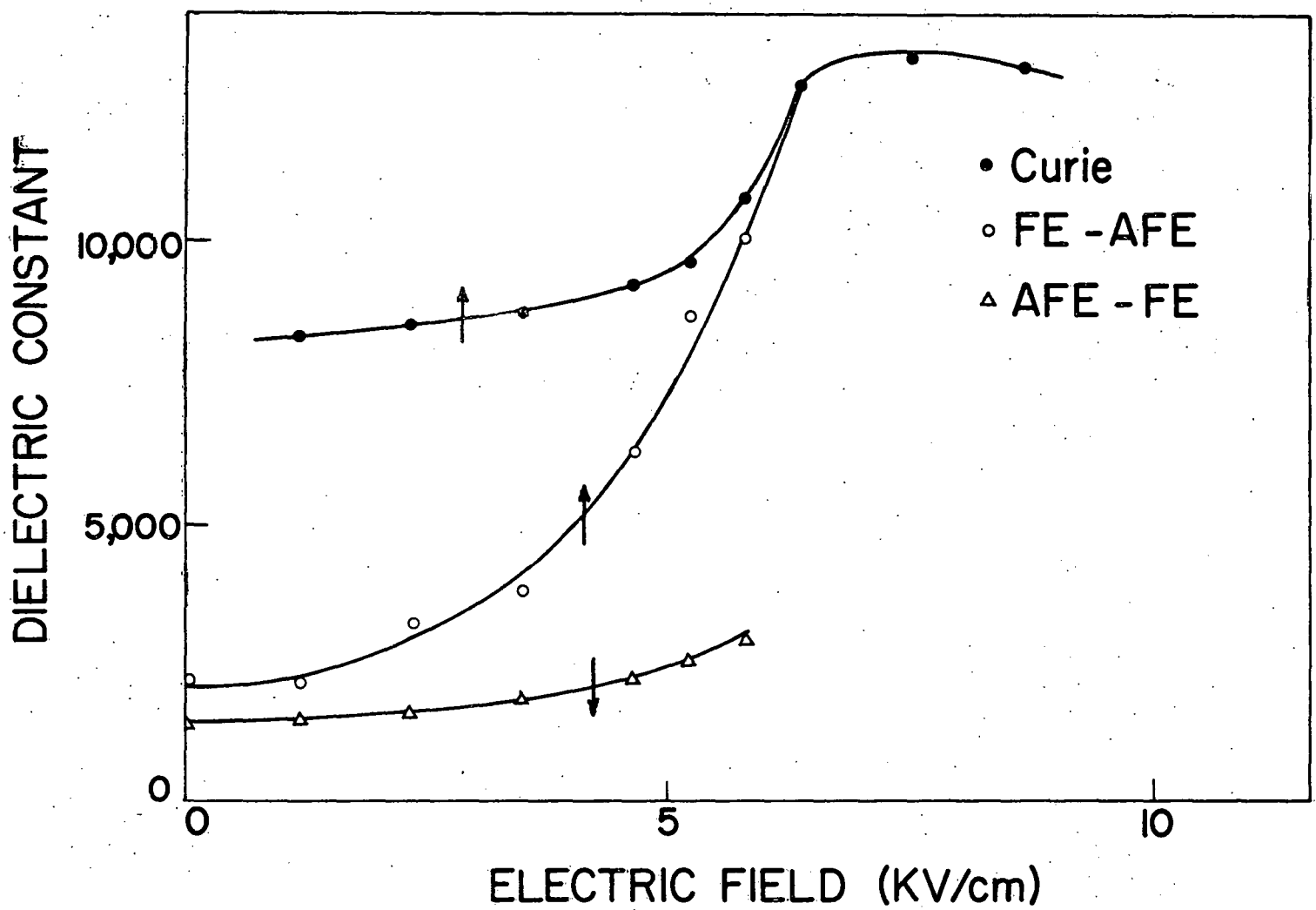

Figure 11. Dielectric Constant at the Transition vs. Field for PZST.

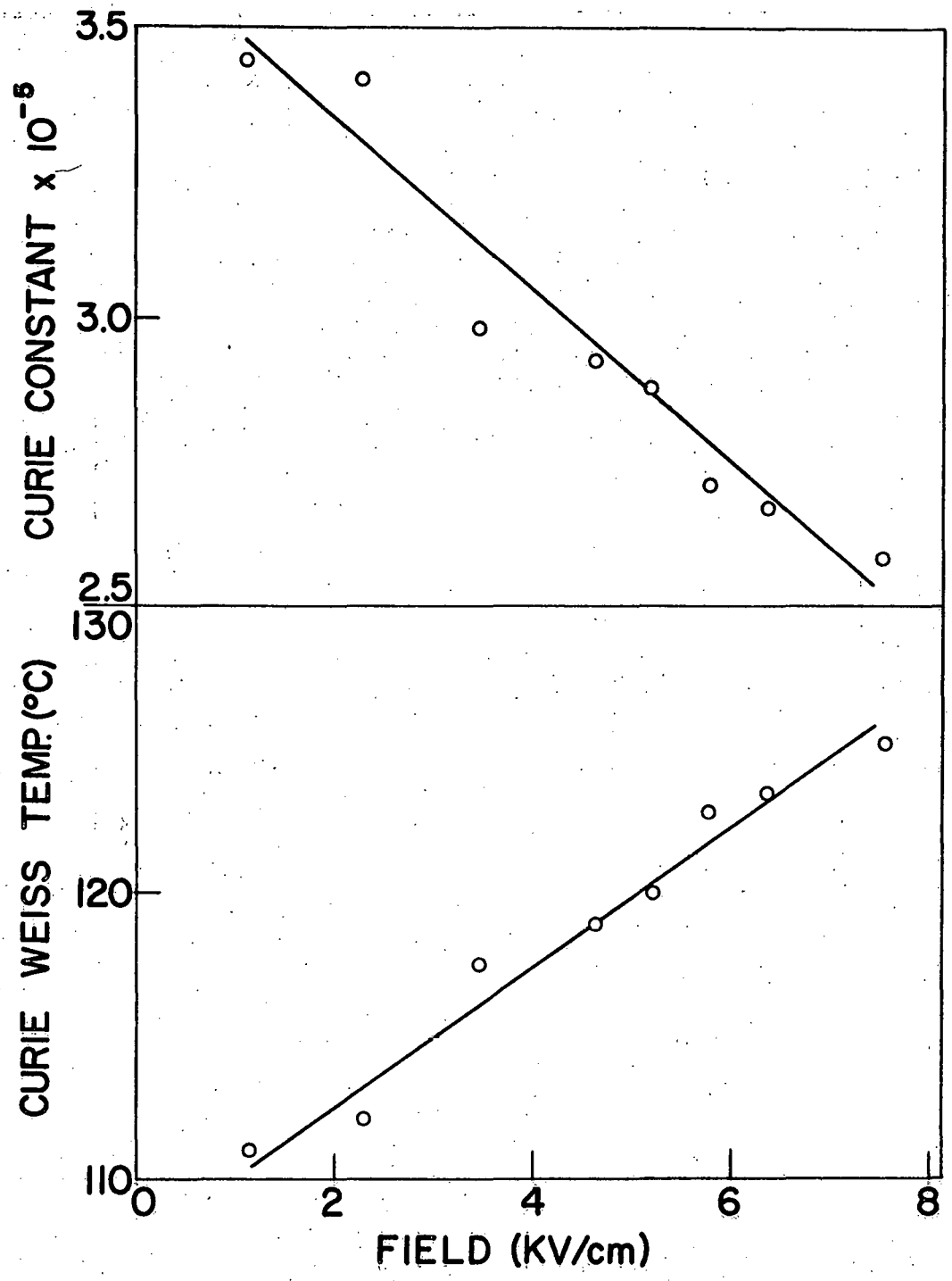

Figure 12. Behavior of PZST Above the Curie Temperature as a Function of Applied Electric Field.

the application of strong fields at room temperature but the FE-AFE transitions observed following this procedure were extremely sluggish, extending from 75° C to 95° C at all observed biases. The samples containing hafnate/titanate ratios greater than 97/3 were antiferroelectric under all observed conditions.

Figure 13, 14, 15, 16, and 17 show the behavior of these materials. It can be seen that with increasing bias field the peaks become quite broad for the samples exhibiting ferroelectric behavior. Figure 18 indicates the variation of Curie temperature with bias field for these compositions. Transitions from ferroelectric to paraelectric are characterized by an increase in the Curie temperature with bias field. For the 96/4 and 97/3 samples, antiferroelectric to paraelectric transitions cause a corresponding decrease in transition temperature with field. The results for the 98/2 and 100/0 samples were quite interesting in that virtually no bias field dependence of transition temperature was observed; the transitions occurred within one degree for each sample regardless of the bias field.

The effects of dielectric saturation, which are readily apparent in the dielectric constant curves, are compiled in Figure 19. This decrease of peak dielectric constant with increasing field is quite strong for the 95/5 samples (30% decrease between zero and five kilovolts per centimeter), becoming less dominant as the materials become more antiferroelectric and peak dielectric constants at zero bias become smaller. The increase of peak dielectric constant which accompanied the disappearance of the AFE phase in the PSZT samples was not noticed in the 96/4 composition, but this was probably due to the lack of sharpness in the FE-AFE and Curie transitions and the consequent blending of their effects. The

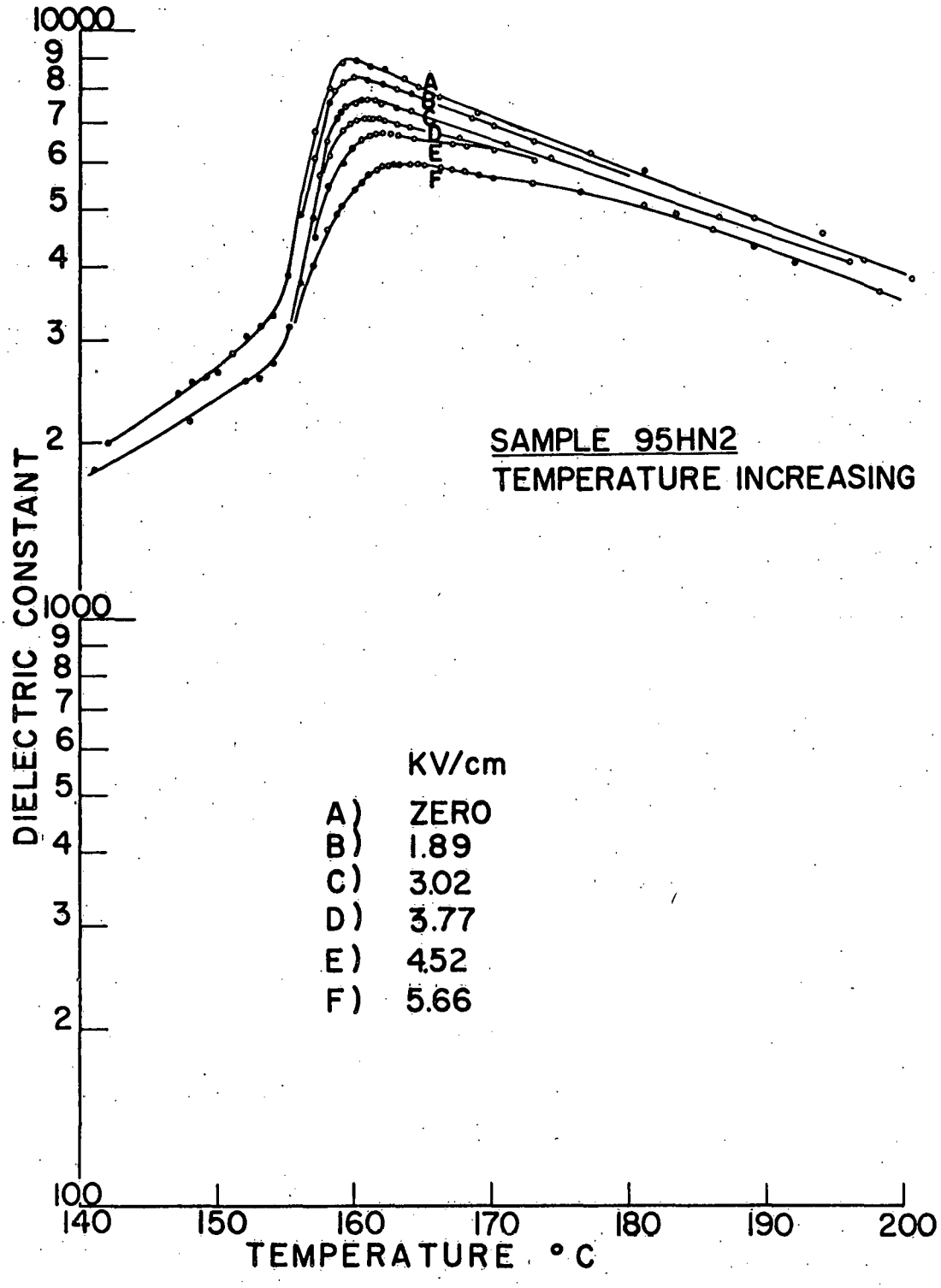

Figure 13. Dielectric Constant vs. Field for Sample 95HN2.

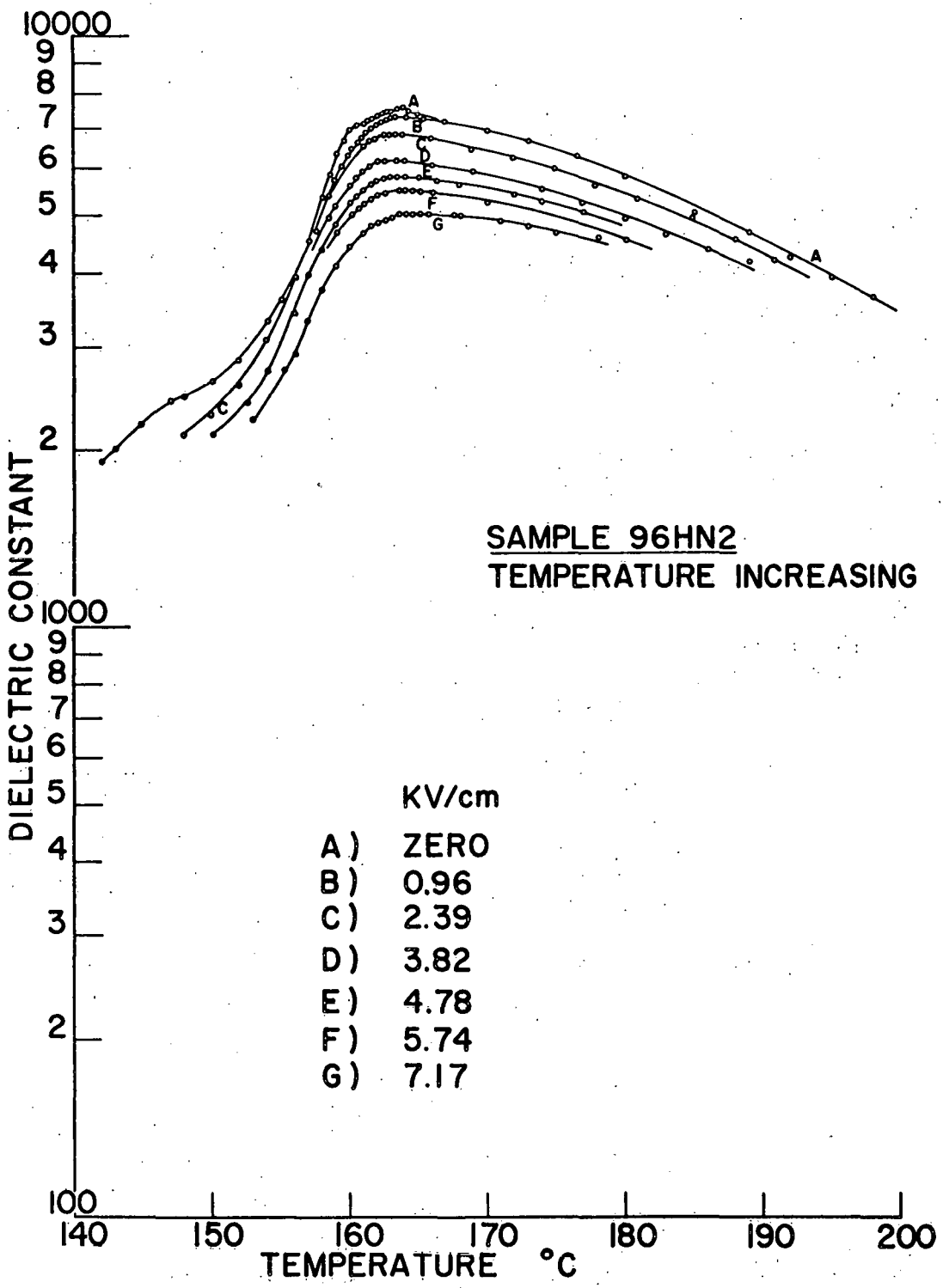

Figure 14. Dielectric Constant vs. Field for Sample 96HN2.

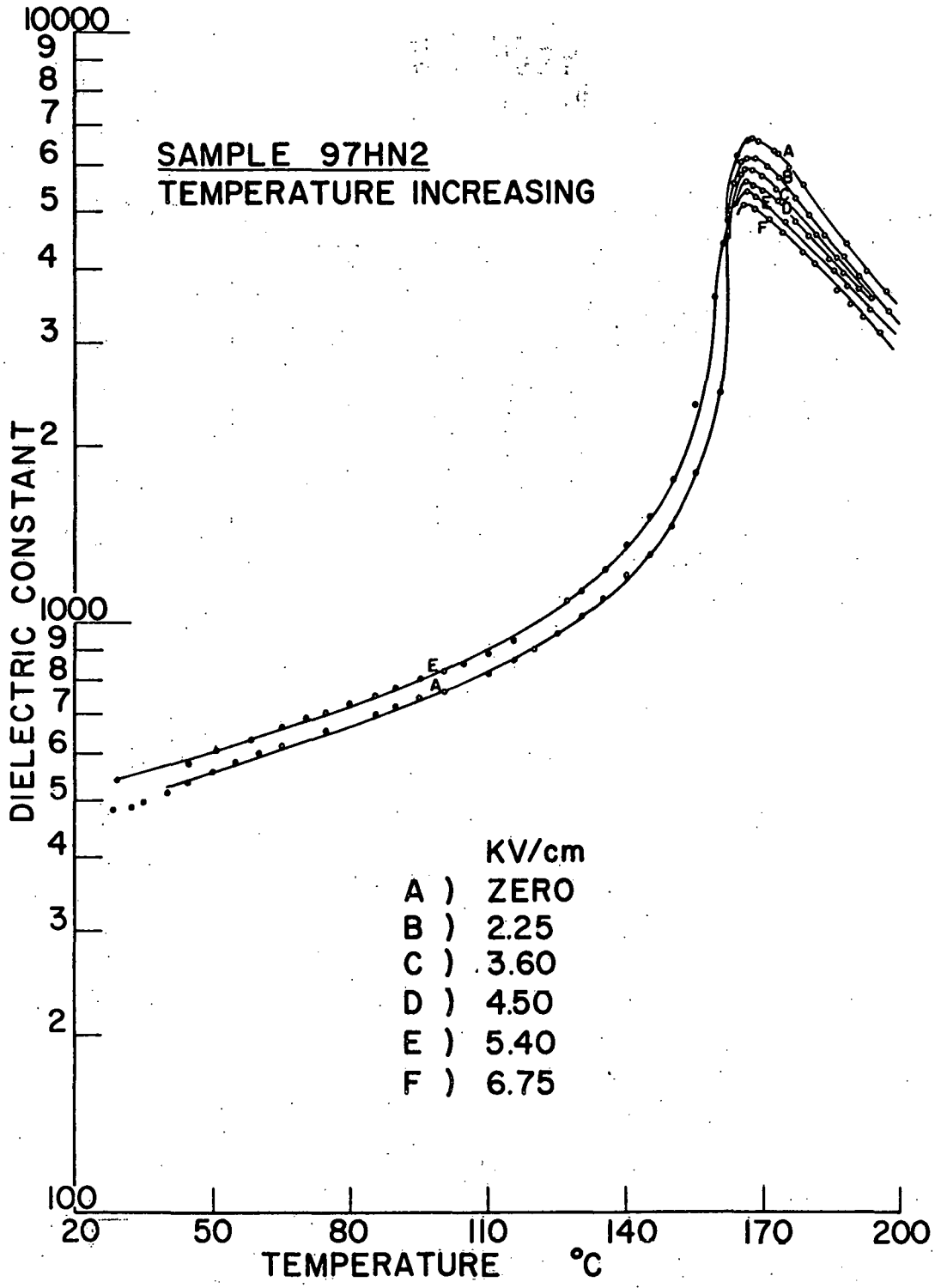

Figure 15. Dielectric Constant vs. Field for Sample 97HN2.

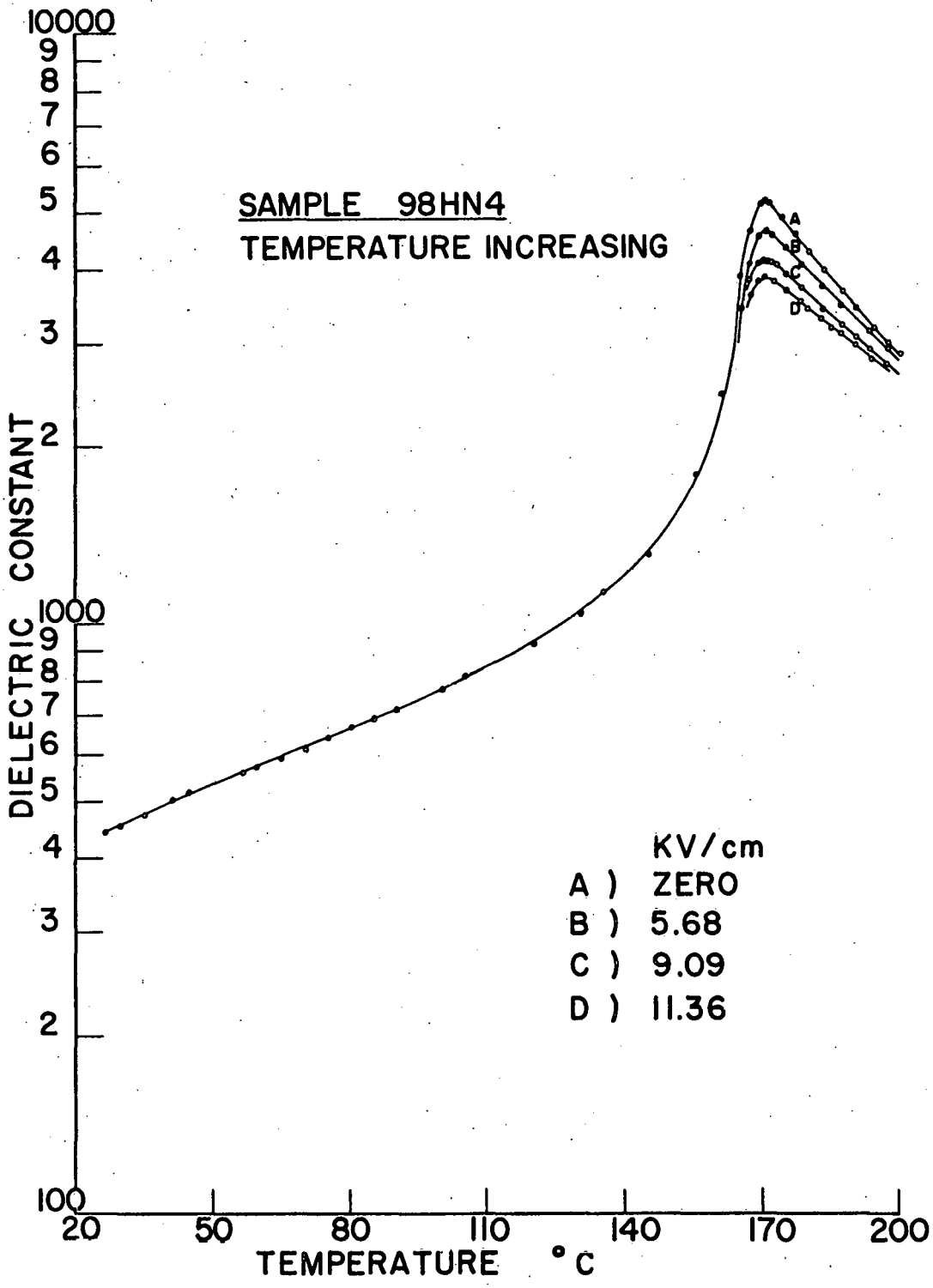

Figure 16. Dielectric Constant vs. Field for Sample 98HN4.

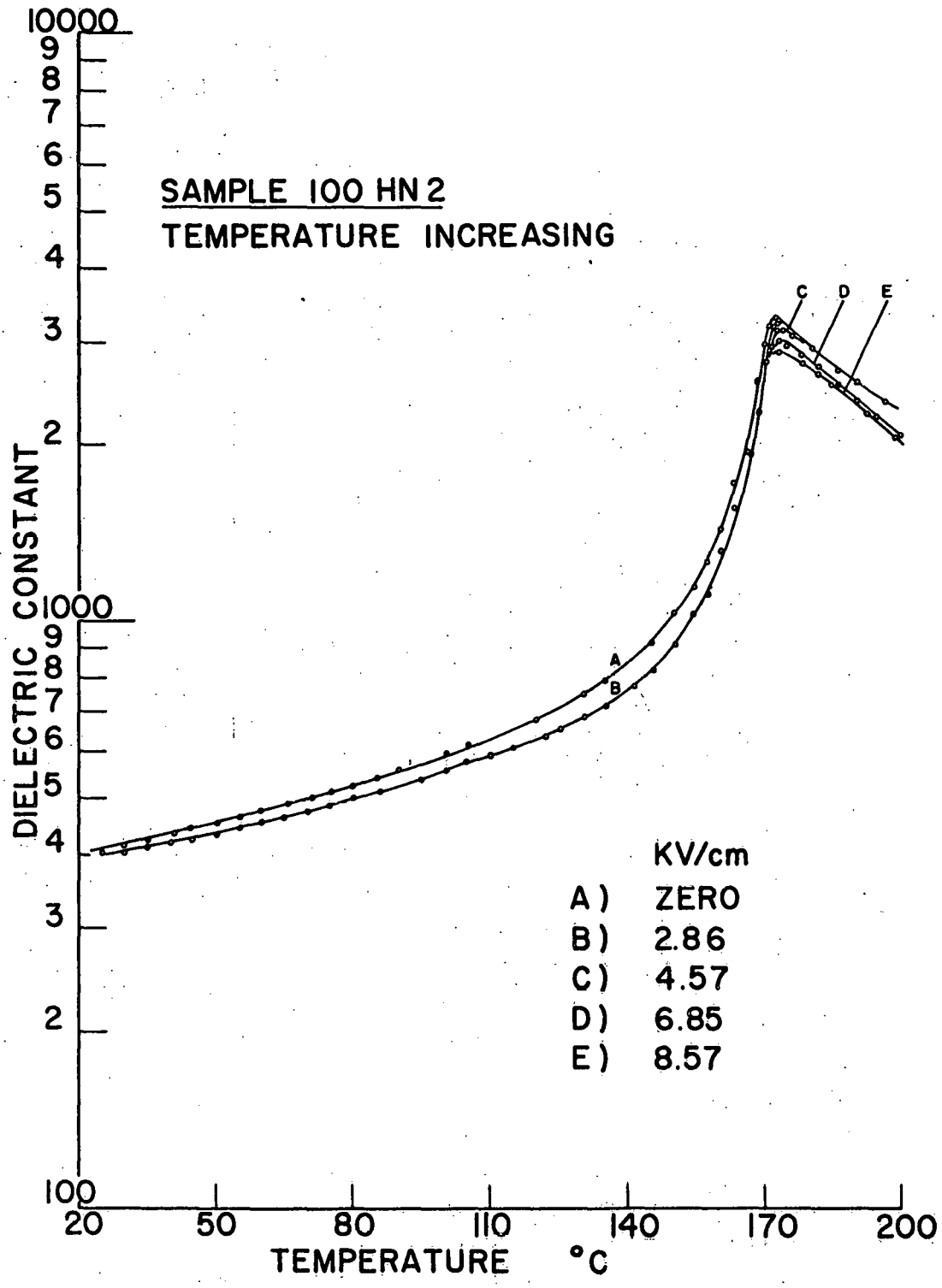

Figure 17. Dielectric Constant vs. Field for Sample 100HN2.

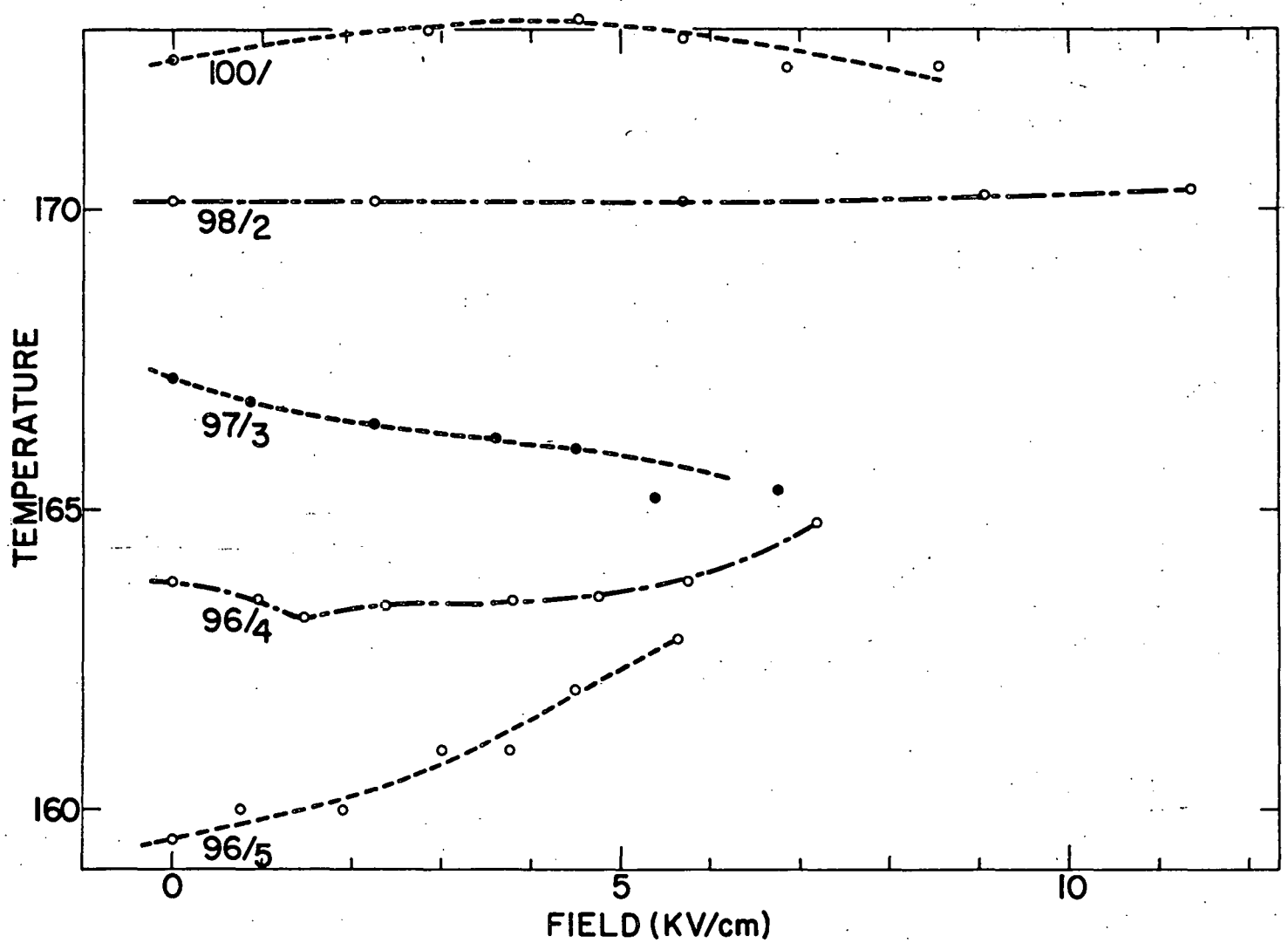

Figure 18. Curie Temperature vs. Bias Field for Lead Hafnate Titanate Compositions.

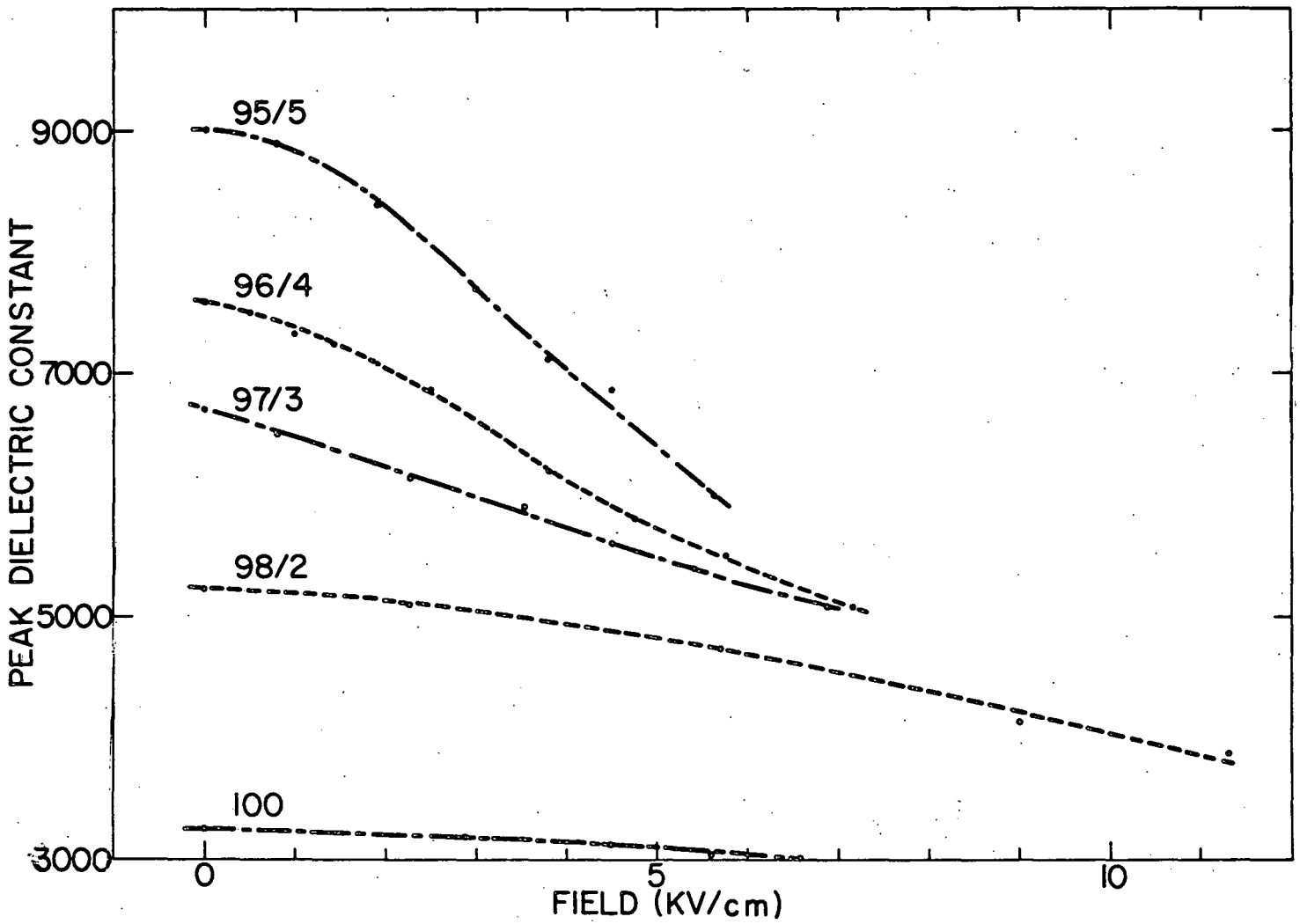

Figure 19. Peak Dielectric Constant vs. Bias Field for Lead Hafnate Titanate Compositions.

95/5, 96/4, and 97/3 materials appear to take on quite similar dielectric characteristics at high fields.

Figure 20 gives a tentative phase diagram for the 96/4 composition. As indicated above, the transitions were not sharp and thus the points indicate only the most probable transition temperatures.

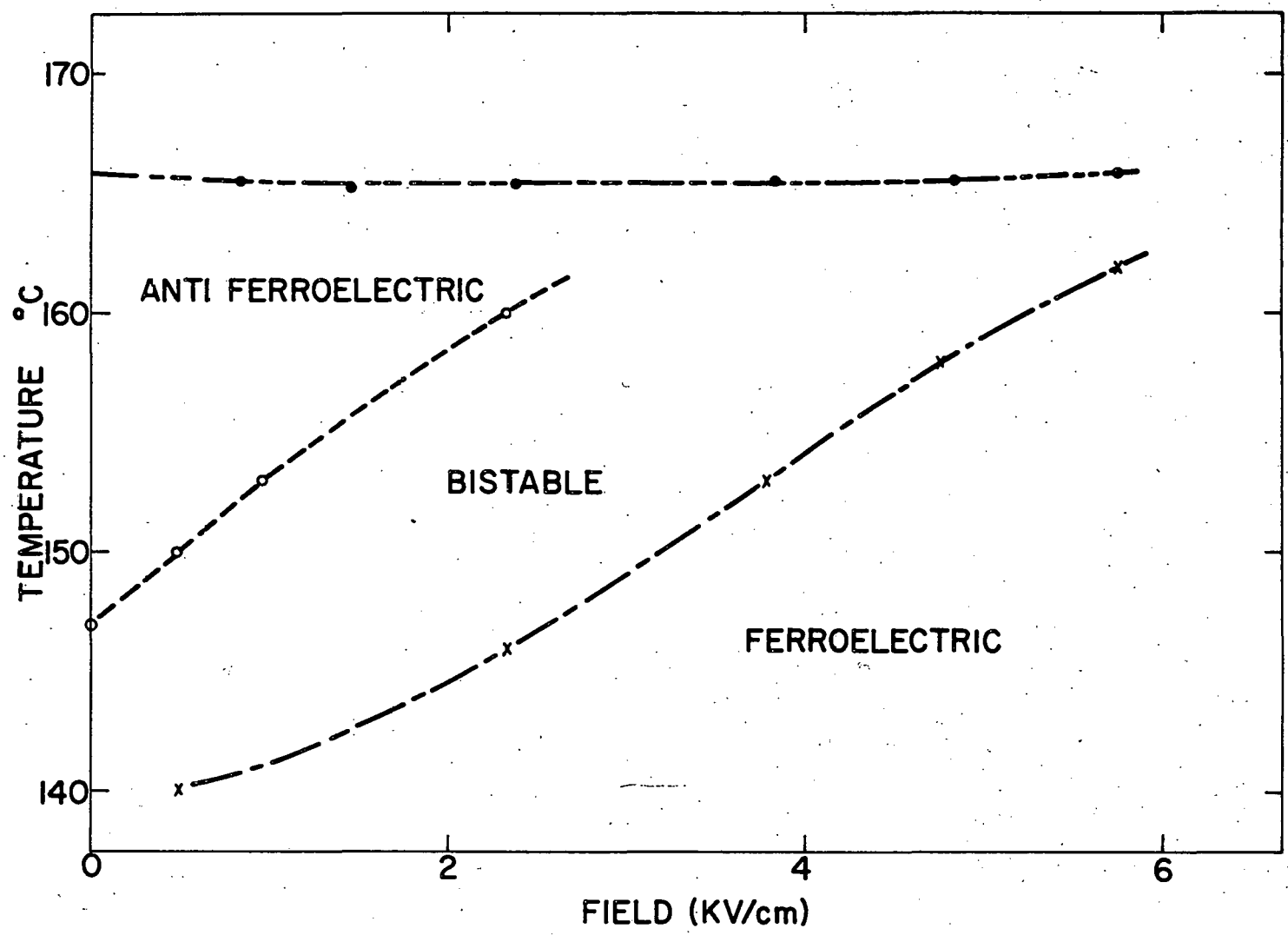

Figure 20. Tentative Temperature-Field Phase Diagram for 96HN2.

CHAPTER V

POLARIZATION MEASUREMENTS

The measurement of polarization has also been of prime interest in the study of ferroelectric materials since these materials are most commonly defined in terms of their possession of a spontaneous reversible internal polarization. This polarization has been used as the basis for the explanation of the other characteristic phenomena associated with ferroelectricity in studies beginning with the interaction theory of Mueller (M3) and culminating with the phenomenological theory of Devonshire (D1).

Two principal methods have been used to measure the polarization of a given ferroelectric sample. The first uses the detection and measurement of charge flow from the sample when it is caused to transform into the nonferroelectric phase, usually either by heating or the application of pressure. Since the polarization is zero in the nonferroelectric phase, the charge which flows through the measuring circuit during the phase transition must represent the original polarization of the material. This technique has the disadvantage of measuring the polarization only by destroying it.

The second method of measuring polarization in these materials utilizes the reversibility of the spontaneous polarization (S6). If the sample is placed in an alternating electric field having sufficient field strength to reverse the polarization on successive half cycles, a

hysteresis loop results. The amount of charge flowing during a single reversal then represents twice the polarization of the material. Also, if the material is subjected to an even number of charge reversals, it can be left in the condition existing before the measurement. Hysteresis loops also have the advantage of giving not only the polarization of the material, but also the electric field necessary to reverse this polarization, the "coercive field". By knowing this field along with the polarization, the energy changes during charge reversal can be found. The area inside a hysteresis loop represents the amount of electrical energy which is converted to thermal energy during one cycle of the applied alternating field.

The random nature of the grain pattern in ceramics leads to basic problems in determining the actual spontaneous polarization of their unit cells. Since perovskite materials have the capability of being polarized along several axes (three in the tetragonal phase, six in the orthorhombic, and four in the rhombohedral), it would seem possible to obtain ceramic polarizations within a few per cent of the single crystal polarization by switching each grain into the lattice direction which most nearly approximates the field direction. In practice, however, mechanical constraints greatly hinder all but the 180° reversals in most materials. In tetragonal barium titanate, for example, only about 15% of the domains not originally optimally aligned can ever be switched 90°. Thus, the polarizations measured on ceramics give only a measure of the actual polarization and precise results must wait until measurements on single crystals are made.

Hysteresis measurements have contributed greatly to the study of FE-AFE transitions through the analysis of the so-called "double loop"

structures given by AFE and cubic materials near a transition point. A typical loop of this type is shown in Figure 21 below.

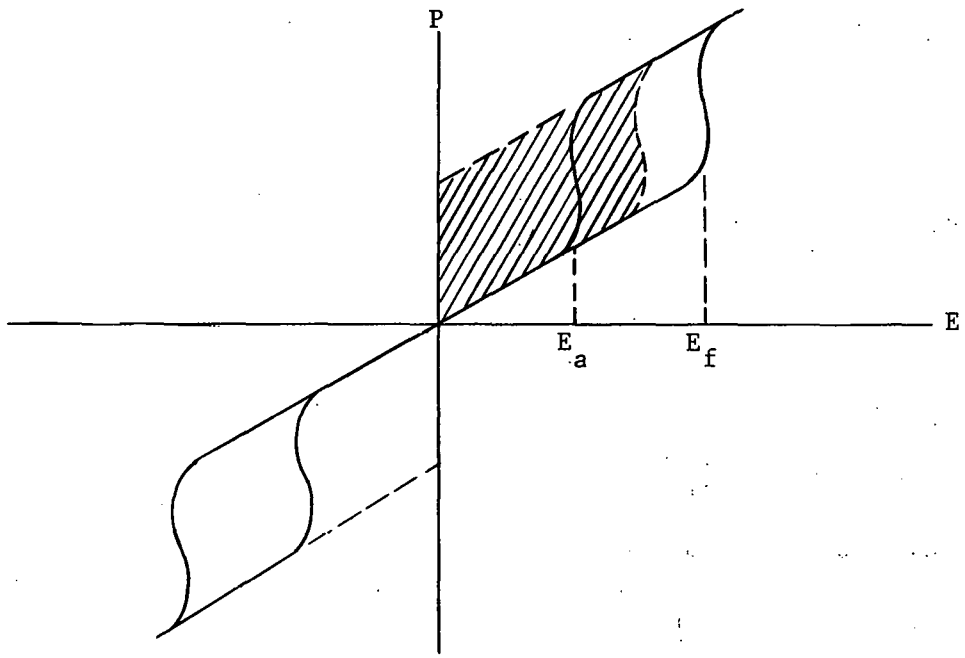

Figure 21. Double Hysteresis Loop Observed During Field-Enforced AFE-FE Transition.

The symbol E_f is used for the field at which the AFE-FE transition takes place, while E_a represents the field at which the FE-AFE transition is observed. If E_f and E_a are approximately equal, a good estimate of the difference in free energies of the two phases is given by the shaded area shown in the figure. In many cases, however, the loops are quite broad and assumptions must be made regarding transition rates and transition probabilities which seriously limit the precision of such estimates.

It has been found that very near the transition temperatures the double loops sometimes reveal a measurable polarization at the zero field point. This phenomenon may be attributed to the coexistence of ferroelectric and antiferroelectric regions within the sample, leading to the superimposing of a normal ferroelectric hysteresis loop on the double antiferroelectric loop.

Experimental Equipment

The systems used for these measurements are shown in Figures 22 and 23. Figure 22 indicates the Sawyer-Tower circuit used to obtain hysteresis loops at 60 cycles. The driving voltage was obtained by connecting to the high voltage transformer of the Beta High Voltage Power Supply immediately before the rectifying stages. In this way a 60-cycle voltage continuously variable from 100 to 2000 volts was available. The resistive divider employed a 100:1 ratio to allow the presentation of the driving voltage as a horizontal sweep of an oscilloscope. The RC integrating network used a 10 microfarad capacitor and a 20 megohm resistor to give an integrating time constant of 200 seconds. The resulting hysteresis loops were then displayed on the oscilloscope and photographed using a Polaroid camera.

For slow-looping measurements the circuit in Figure 23 was used. Driving voltage was supplied by the Beta High Voltage Power Supply and a 400 second integrating circuit was used to detect the polarization changes. A Simpson vacuum tube voltmeter was modified to act as an impedance matching device and allowed the hysteresis loops to be plotted directly on an X-Y recorder. Calibration was done with the aid of a Leeds and Northrup K-3 potentiometer.

Calculation Techniques

The vertical sweep of the oscilloscope or X-Y recorder indicated the voltage across the capacitor in series with the sample. This capacitor acted to integrate the charge flowing across the sample (the change of sample polarization). The spontaneous polarization

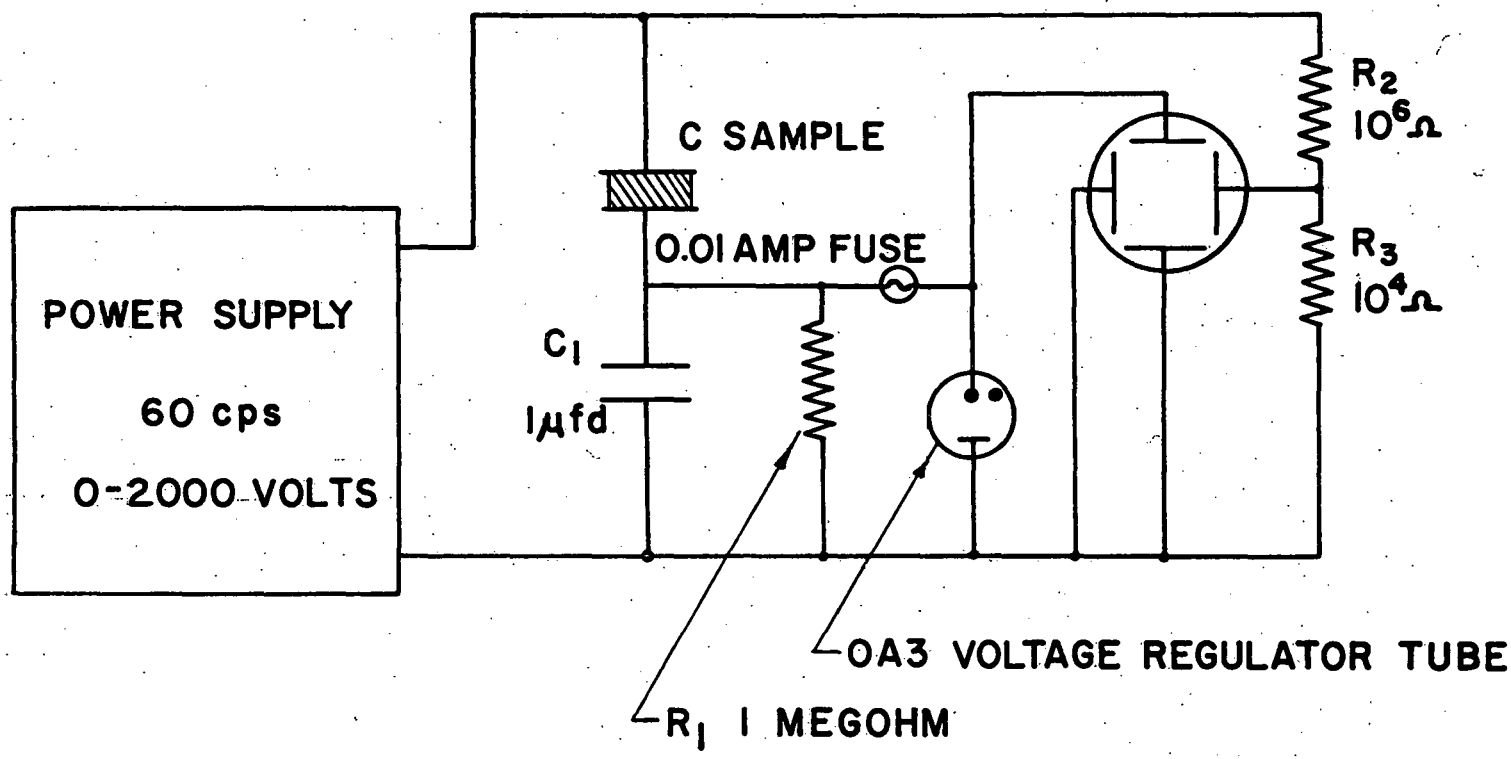

Figure 22. Sawyer-Tower Circuit for 60 cps Hysteresis Loops.

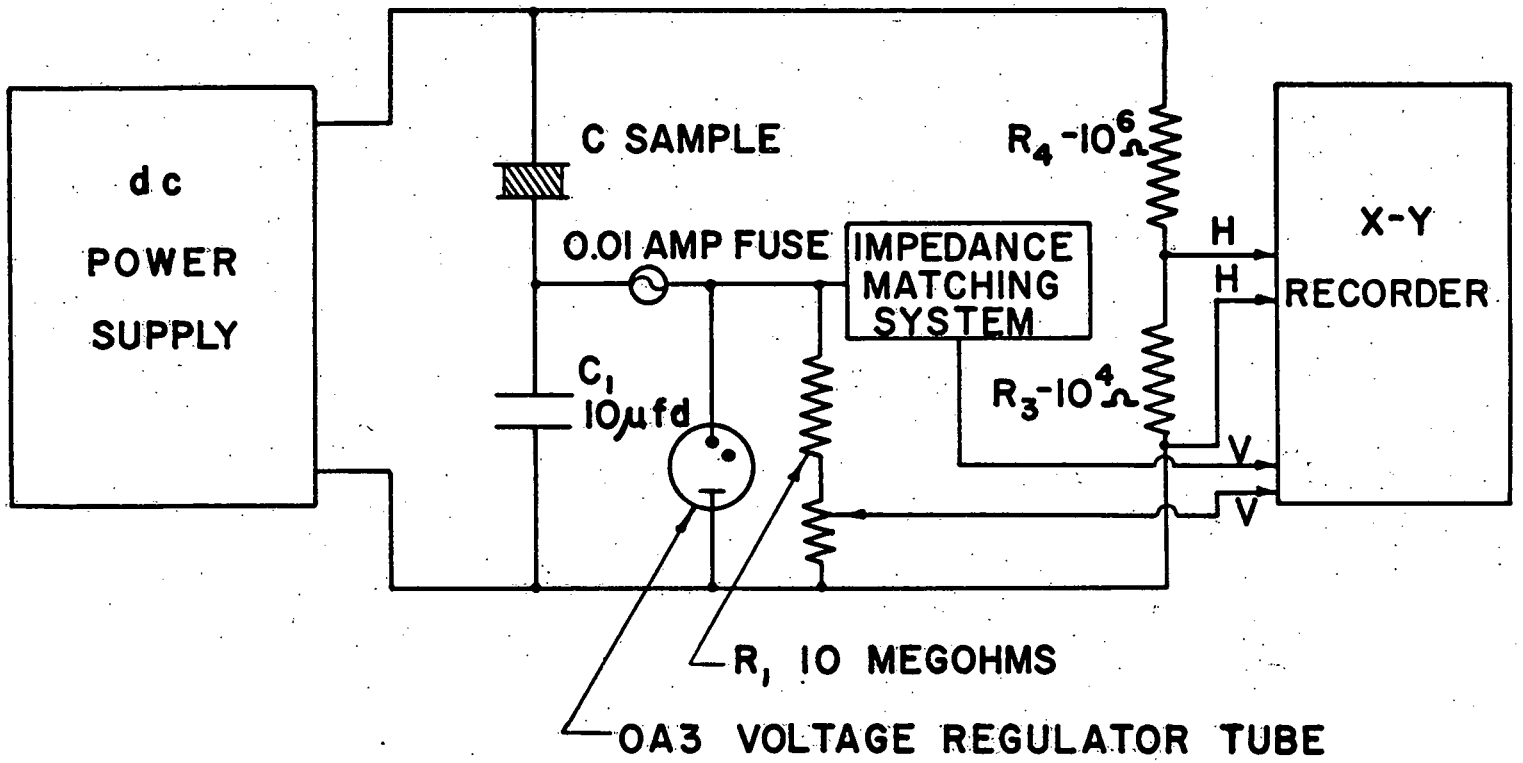

Figure 23. Circuit for Slow-Loop Hysteresis Measurements.

(P_s) was then found by extrapolation of the linear segments at the top and bottom of the loop back to zero field. This polarization is given by

$$P_s = \frac{C_I V_V}{A}$$

where C_I = integrating capacitance

V_V = vertical voltage

A = sample electrode area.

The coercive field of a ceramic sample is usually taken as that field on a symmetric hysteresis loop at which the polarization becomes zero. This is indicated by the horizontal sweep of the oscilloscope, which is driven by the power source through a voltage divider. If the voltage scale of the oscilloscope and the resistive divider ratio are known, the coercive field is obtained directly.

Experimental Results

Results obtained with this equipment were quite similar to those recently obtained at Sandia Corporation. Figure 24 indicates the observed polarization and coercive field as a function of the temperature, as obtained in the present investigations on the 95/5 lead hafnate titanate composition. The apparent decrease of polarization at low temperatures and 60 cycles is probably due to a failure to completely saturate the hysteresis loops. The samples were not subjected to voltages much greater than 10 KV/cm in order to insure against electrical breakdown. Figure 25 is a similar plot for the 96/4 sample. Again the differences between the slow loop polarization and that obtained at 60 cycles are probably due to the limitations of the applied voltage.

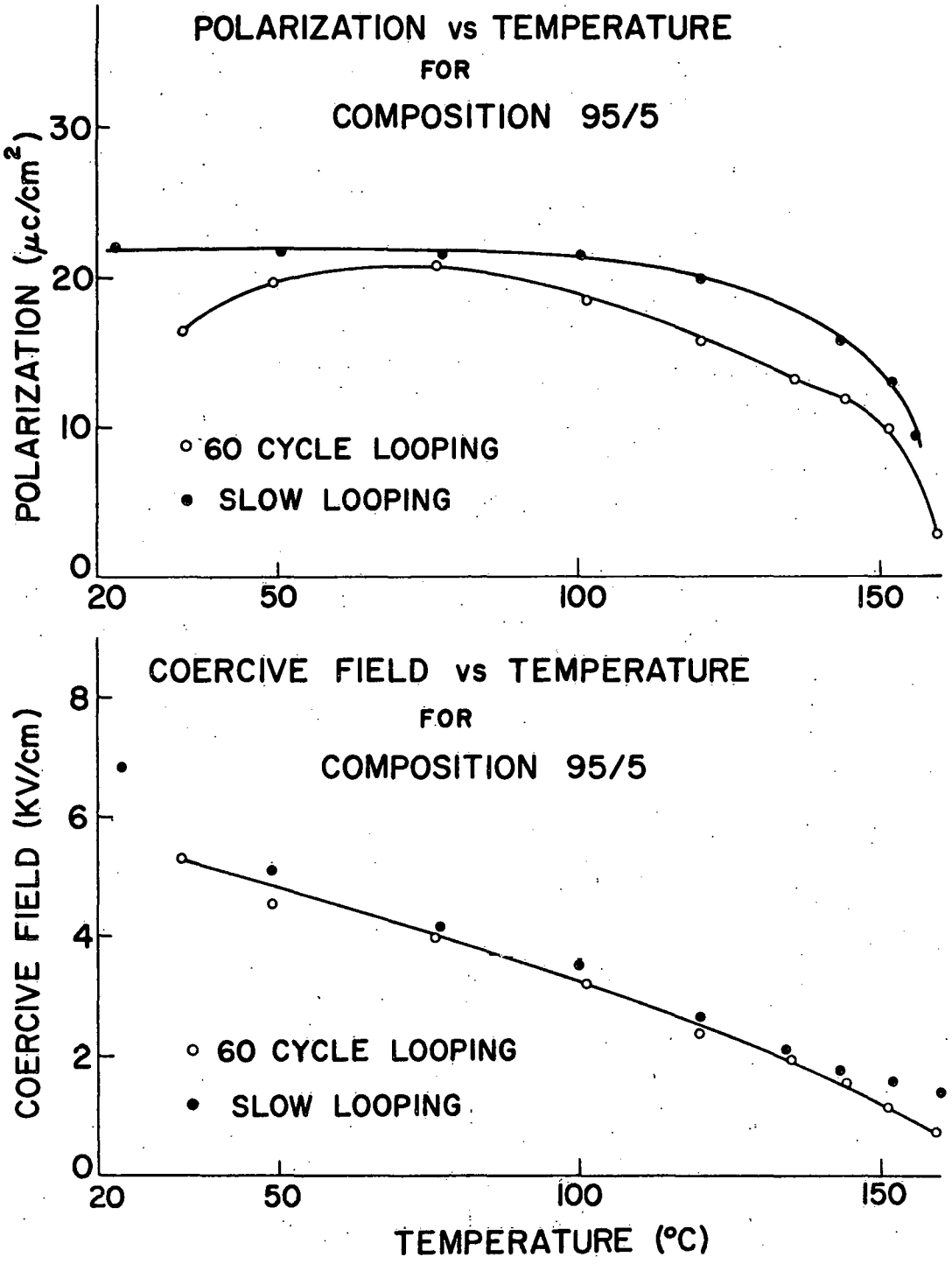

Figure 24. Hysteresis Parameters for the 95/5 Lead Hafnate Titanate Composition.

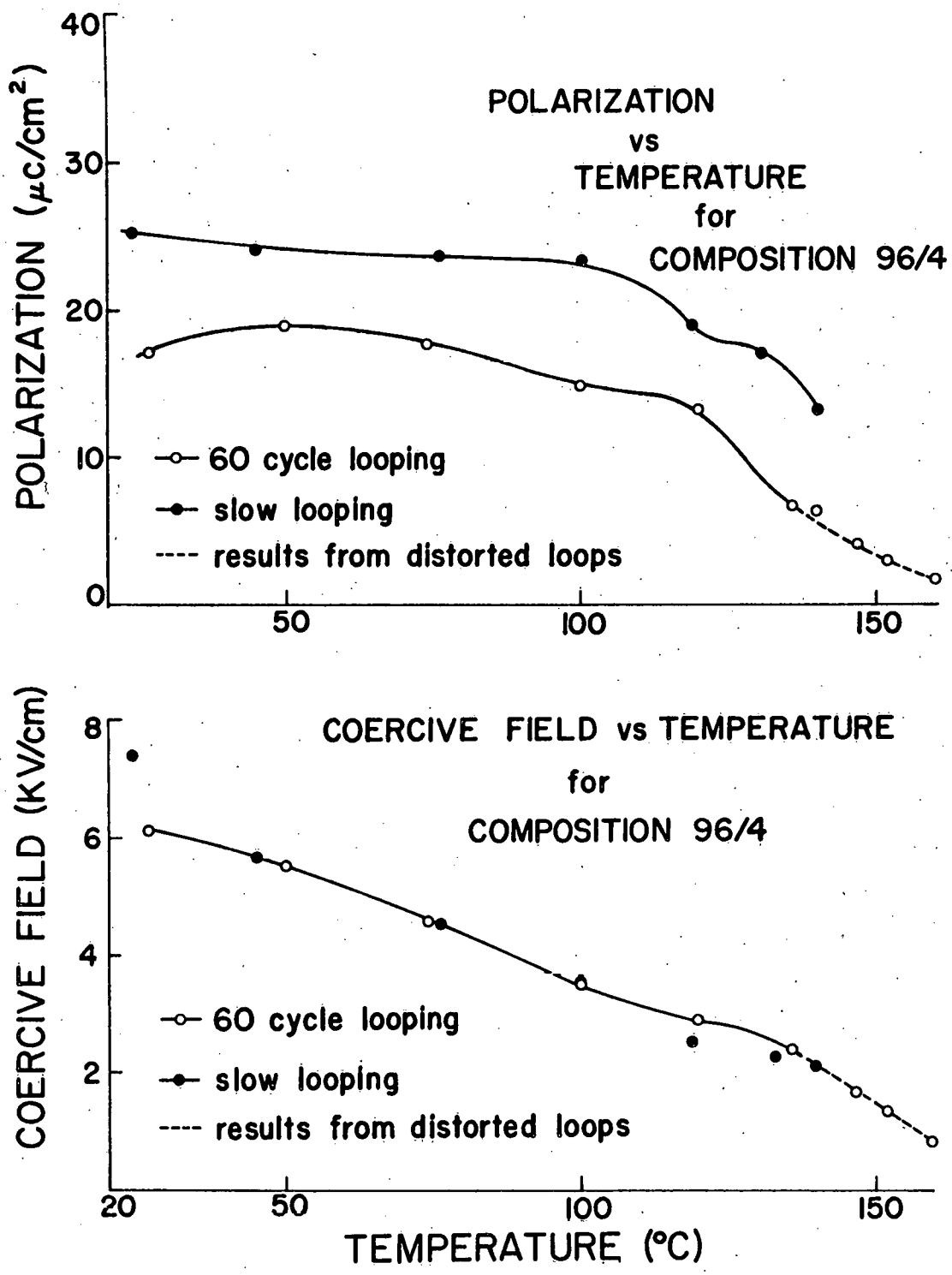

Figure 25. Hysteresis Parameters for the 96/4 Lead Hafnate Titanate Composition.

The loops obtained in the vicinity of the FE-AFE phase transition with the 96/4 material exhibited the characteristic double loop form but failed to close off completely at zero field. In order to establish the presence of some ferroelectric phase within the sample above the transition temperature, the samples were impressed with only the positive half of the voltage cycle. This enabled the positive half of the double loop to be observed in the absence of any ferroelectric switching. The results of this procedure are shown in Figure 26. The fact that the antiferroelectric loops close off at zero bias under these conditions indicates that a certain portion of the material does remain ferroelectric above the transition temperature. The repeatability of the loops is not sufficient to allow a quantitative description of the phenomenon, but qualitatively it appears possible that as much as 25% of the sample remains ferroelectric in the region up to five degrees above the transition temperature.

An attempt was made to apply fields high enough to switch thin samples of the 97/3 and 98/2 material but breakdown of the samples resulted. This has been successfully accomplished at Sandia Corporation and those results are given in a later chapter.

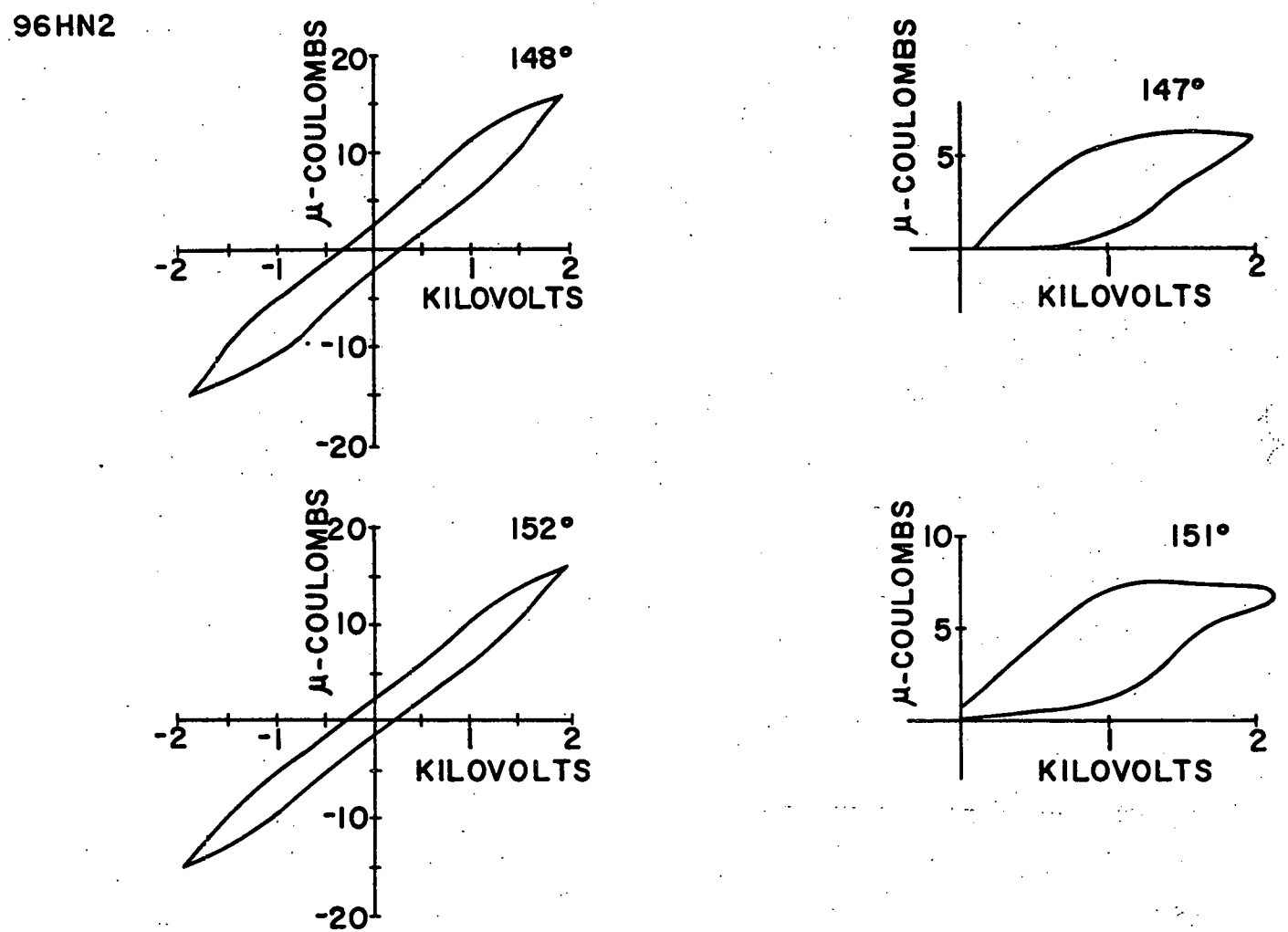

Figure 26. Hysteresis Loops and Portions of Double Hysteresis Loops Showing Field-Enforced Ferroelectric Phase in the 96/4 Lead Hafnate Titanate Composition (Temperature Decreasing).

CHAPTER VI

THERMAL MEASUREMENTS

Calorimetric measurements were made on samples of the materials used in this study in order to determine their specific heats and heats of transformation. The measurements were carried out in a calorimeter designed specifically for measurements on thin discs of ceramic material.

Many of the basic ideas of adiabatic calorimetry were first developed by Sykes (S7). He designed a calorimetric system in which the sample and its container were maintained near the temperature of the calorimeter by means of a heating coil, with a differential thermocouple used between the sample and the calorimeter to detect the growth of temperature differences. By alternately heating the sample above the calorimeter temperature and allowing it to cool slightly below that temperature, Sykes was able to achieve nearly adiabatic conditions of heating. This technique has been modified in the present study by using the ceramic discs themselves to contain the electrical heater and the detection thermocouple, thus doing away with the sample container. The consequent reduction in thermal mass of the sample portion of the calorimeter provides much faster response to changes of input power, allowing the sample to be maintained at the same temperature as the calorimeter for relatively long periods of time.

Two different types of measurements were made on the samples used in this study. In the first type, the sample was mounted in the calorimeter and heated while the calorimeter cup itself remained at room temperature. As described later in this chapter, this technique

permitted the checking of the sample heater and thermocouple and the determination of the room temperature heat capacity and thermal loss parameters of the sample. This information was necessary to detect defects in the sample mounting and to facilitate the procedures used later for more accurate and complete measurements.

In the second type of measurement, the sample was maintained in an adiabatic relationship to the calorimeter while the calorimeter was heated from room temperature to some temperature above the Curie point of the sample material. In this way, the specific heat of the sample could be determined throughout the above temperature range, and the heat of transition absorbed at the Curie point could be obtained. Since these measurements were made under adiabatic conditions, they were more accurate than those of the first type.

Description of Equipment

Figure 27 illustrates the design of the calorimeter. It is constructed of half-inch copper. The outside diameter is five inches and the outside depth five and one-half inches. The inside chamber measures three inches in diameter and three and one-half inches deep. The entire body of the calorimeter is bright nickel plated to resist corrosion and to reduce the radiative emissivity of the chamber. The top of the calorimeter is fitted with three vacuum feedthrough connections for the thermocouples and the heater, as well as a threaded ground post and a metal tube for attachment to the vacuum system. The abutting faces of the calorimeter top and base are fitted with a set of small ridges which aid in the use of an aluminum or lead gasket for vacuum sealing. The two parts of the calorimeter are held together by

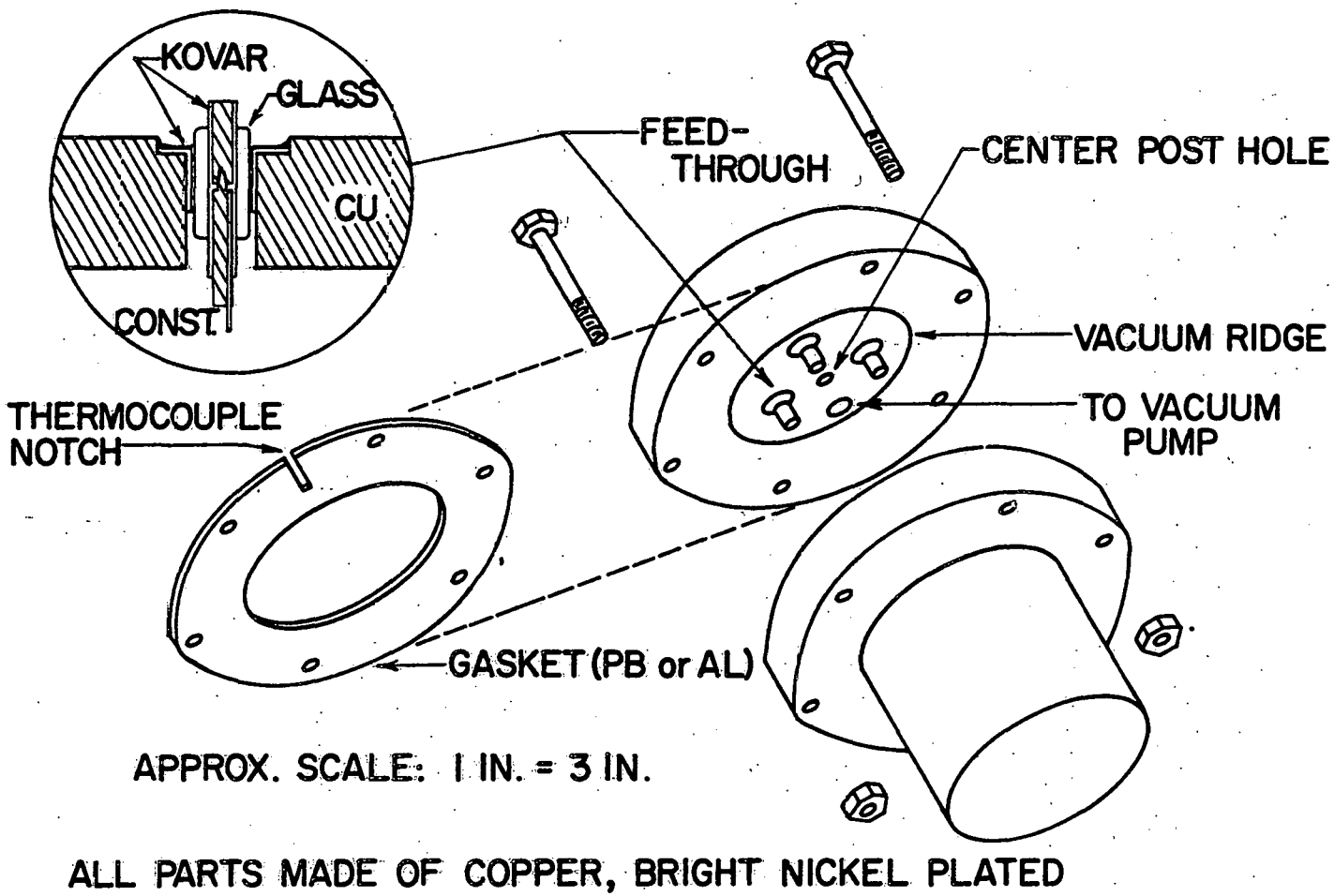

Figure 27. Calorimeter Design.

six equally spaced 1/4" x 1" bolts. A notch is cut in the gasket to allow the burial of a copper constantan thermocouple junction near the inside calorimeter chamber as the calorimeter temperature measurement junction.

Heating of the calorimeter was accomplished by means of a three-gallon oil bath containing Dow Corning DC200 silicone oil. The bath was fitted with a 1400 watt immersible heater at the bottom of the liquid and stirred by means of an Eberbach Model 58 variable speed stirrer. A thermometer was placed in the bath near the calorimeter and used for thermocouple calibration. This bath was capable of heating the calorimeter at rates up to ten degrees Centigrade per minute although rates above three degrees per minute were not used during the measurements of interest.

The maximum temperature variation in the region of the calorimeter was less than one degree during all measurements. Considering the thermal diffusivity of the copper, the variation of temperature within the calorimeter chamber would have been less than this. Since the sample was maintained at the same temperature as the calorimeter cover during adiabatic measurements, radiation exchanges to all parts of the chamber were negligible. The calorimeter was operated under forepump vacuum conditions in order to reduce conduction losses during nonadiabatic measurements.

Description of Samples

Figure 28 illustrates the construction of the sample assembly used in this study. Each sample was built from two discs of the ceramic to be tested. One of these was fitted with a series of grooves and a

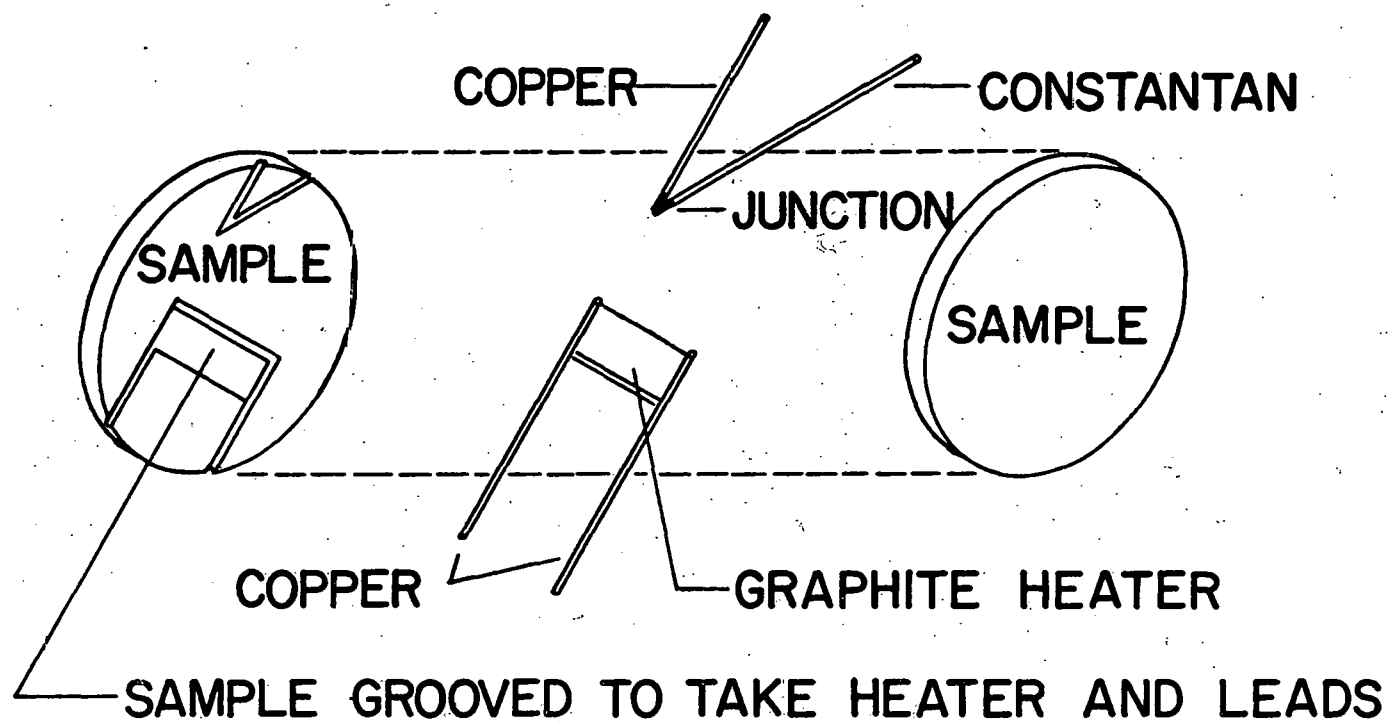

Figure 28. Construction of Sample Assembly.

small flat well to contain the heater plate. This was originally done by masking the sample and sandblasting it with No. 600 alundum powder. Later it was found more convenient to sandblast the well to proper depth and then adjust the depths of the grooves with the aid of a Gulton Model DS-10 ultrasonic drill. This technique allowed the heater and the differential thermocouple junction to be sealed inside the material to be tested. The sample could then be mounted to the calorimeter by means of the electrical connecting wires. Thus both the heat capacity of the sample and the conductive losses to the calorimeter were kept at a minimum relative to the mass of ferroelectric material to be tested.

The sample heater was made of carbon. Originally the heaters were polished into shape from small pieces of graphite rod, but it was found that the use of pieces of carbon arc rod gave higher resistances for the required dimensions, which facilitated measurement of heater power. A typical heater had dimensions of 4 mm x 8 mm x 0.1 mm and a resistance in the range from one to five ohms. This heater plate was then mounted in the well provided in the sample and connections made to the #30 copper lead wires with silver paint. The use of a heater element in the shape of a flat plate allowed a large area of contact between the sample and the heater and resulted in more uniform heating.

The heater was connected to a six-volt battery and control was achieved by means of a ten ohm wire-wound potentiometer. Typical heating conditions consisted of a voltage of about 0.30 volts across the heater and a current of 0.15 amperes through it. Under these conditions the minimum power deviations obtainable were of the order of 0.3 milliwatts. The voltage across the heater was measured by means of a microammeter fitted with various series resistances to provide the optimum

range of measurement, and the current was measured by means of a Simpson Model 269 milliammeter.

The temperature of the sample was measured with a copper constantan thermocouple junction planted in the sample. This junction was made by spot welding a piece of #30 constantan wire to a piece of #30 copper wire and was fitted in the grooves as shown in Figure 28. The copper wire was grounded to the copper of the calorimeter through the threaded central ground plug. The constantan led to the reference junction of the differential thermocouple which was fitted into one of the vacuum feedthroughs as shown in Figure 27. It was found that the thermal resistivity of the glass portion of the feedthrough allowed this junction to heat slightly during the nonadiabatic runs. In order to give better thermal contact between this junction and the calorimeter, a cap was built to fit the exterior central pin of the feedthrough. A thin mica sheet between the cap and the calorimeter cover gave good thermal contact while providing electrical separation.

After insertion of the thermocouple junction and the heater, the two discs comprising the sample were bonded together with Duroplastic epoxy.

Measurement Techniques

Preliminary Measurements

Preliminary measurements were made on each sample by observing the exponential rise and fall of the temperature of the sample when power was applied to the sample heater and the calorimeter was kept at room temperature. This technique allowed the sample heater to be calibrated and permitted the determination of the conduction losses

between the sample and the calorimeter. From these measurements it was also possible to determine the room temperature specific heat of the sample material.

If a sample of material is originally at a temperature higher than its surroundings, and if it is postulated that conduction losses are much larger than radiation losses from the sample, the following condition must hold:

$$c \frac{dT}{dt} + a\ (T - T_o) = 0$$

where c = sample heat capacitance

T = sample temperature

T_o = surrounding temperature

a = thermal loss constant (quantity of heat lost per unit time per unit temperature difference).

Solving this equation for T,

$$T = T_o + \Delta T\ e^{-at/c}$$

where ΔT is the temperature difference at time zero. This implies that under the stated conditions, the sample will cool exponentially with the exponential time constant determined by the ratio c/a.

Likewise, if the sample and its surroundings are initially at the same temperature and power is applied to the sample, the following relation holds:

$$c\ dT/dt + a\ (T - T_o) - Q/t = 0$$

where Q/t is the thermal power being applied to the sample. Solving this equation for T,

$$T = T_o + (T_f - T_o)(1 - e^{-at/c})$$

where T_f represents the equilibrium temperature at which the thermal

losses equal the power input. From this it can be seen that under these latter conditions the temperature will rise exponentially to a final equilibrium temperature, and that the exponential time constant will be the same as that for the cooling curve.

Thus by observing a cooling curve for a given sample mounted in the calorimeter, the ratio of the loss factor to the heat capacity of the sample can be determined. By observing the equilibrium temperature obtained by a given power input, the loss factor can be found from the relation:

$$a = \frac{Q/t}{(T_f - T_o)}$$

The heat capacity of the sample is then the product of this loss factor and the exponential time constant.

In making these measurements, the output of the differential thermocouple was connected to the vertical input of a Moseley Autograf Model 2A X-Y Recorder. The horizontal input was connected to an internal 750 second time base. Thus the actual exponential heating and cooling curves were plotted by the recorder.

Cooling curves were observed over a range of twenty degrees for the accurate determination of the time constant. Then heating curves were observed for various power inputs. Since the time constant of heating was already known, it was only necessary to record a heating curve for a short time in order to calculate the final equilibrium value of the temperature. When these equilibrium temperatures were plotted as a function of power, the result was a straight line whose slope gave the loss factor. Figures 29 and 30 are such a plot and a plot of the cooling curve for a quartz sample which was used to check

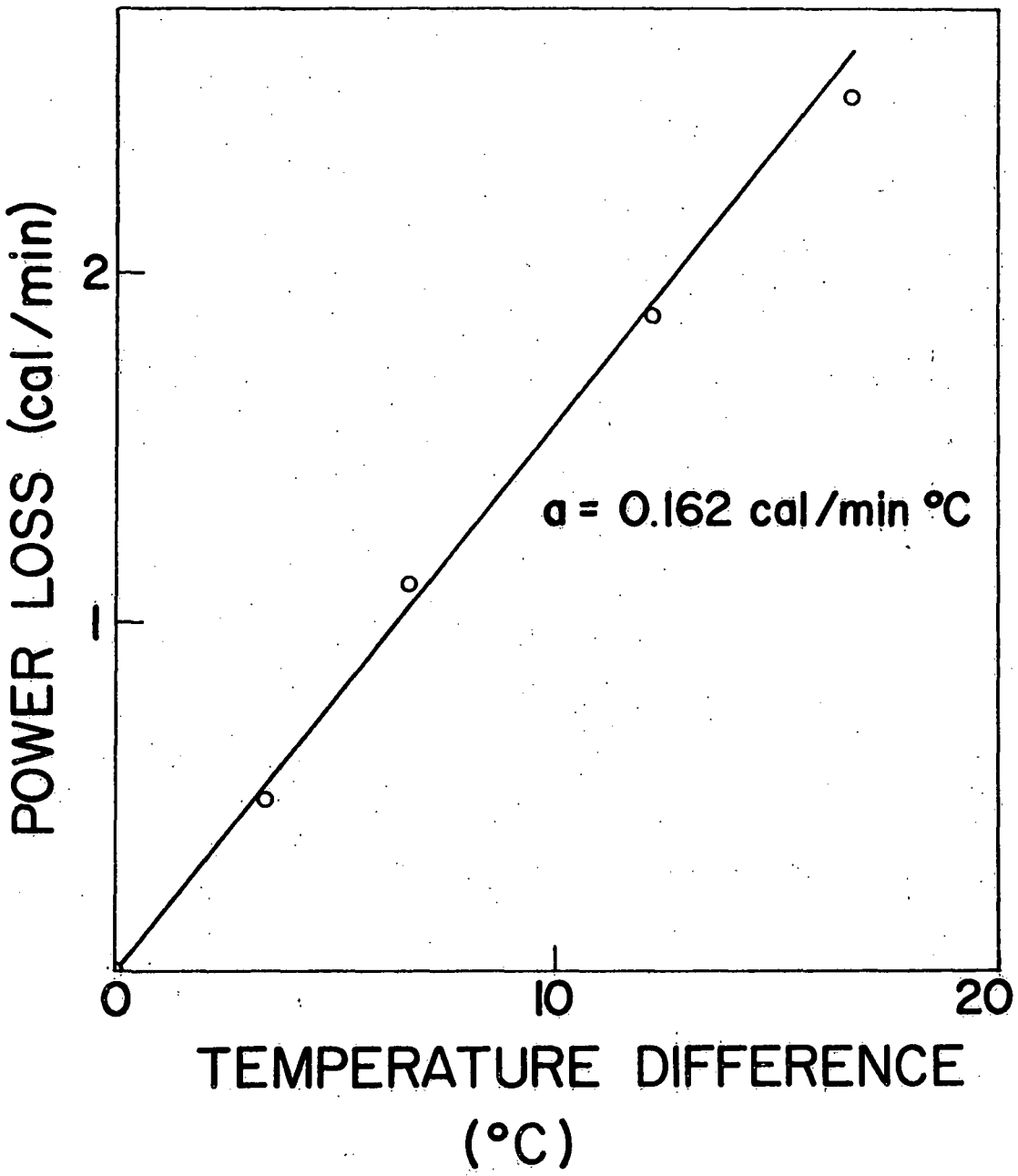

Figure 29. Determination of Loss Factor in Preliminary Measurements.

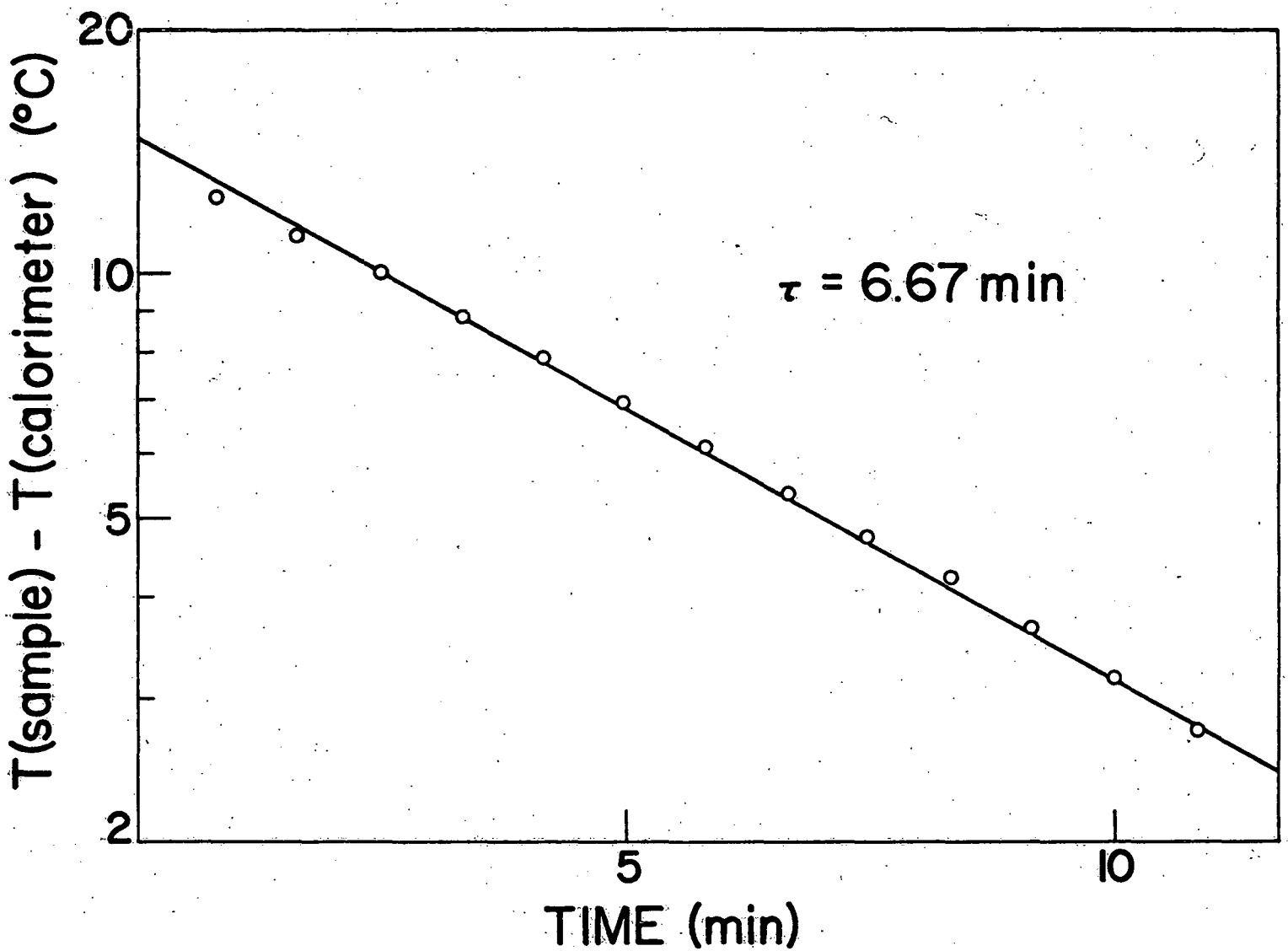

Figure 30. Exponential Cooling Curve for Quartz Check Sample.

out the system. The cooling curve has been plotted on a logarithmic scale to verify the assumption that the loss is primarily through conduction. The value of the specific heat of quartz given by these plots is 0.187 as compared with a handbook value of 0.181. As was stated earlier, it was found that the reference junction of the differential thermocouple tended to heat slightly above the actual calorimeter temperature during nonadiabatic measurements. This caused the reading of the difference temperatures between the sample and the calorimeter to be slightly low, giving erroneously high loss constants. This in turn led to values of the specific heat of the sample which ranged from five to ten per cent high. After installation of the cap to improve thermal contact between the reference junction and the calorimeter, this error was reduced to approximately two per cent.

Adiabatic Measurements

The most precise measurements of this thermal study were those made under adiabatic conditions. As outlined in the introduction to this chapter, these conditions were achieved by using a differential thermocouple as a null detector and varying the input power to the sample to maintain it at the same temperature and the same rate of temperature change as the calorimeter.

In making these measurements, it was found most convenient to apply a constant amount of power to the oil bath throughout a complete run. This caused the rate of heating of the oil to increase during the early part of a run until a steady set of heating conditions was obtained, and then to decrease slowly throughout the rest of the run as losses to the surroundings became greater. The reason that a

constant input power was chosen lay in the high thermal mass of the calorimeter and the oil bath. In contrast to the sample, which could achieve a stable set of thermal conditions within 40 seconds after an input power change, the transient effects of an input power change to the oil bath did not disappear for several minutes. However, the same high thermal mass which prolonged these transients acted to prevent the growth of heating instabilities under the constant input power conditions.

The sensitive detection of adiabatic conditions was accomplished by connecting the differential thermocouple directly into a Leeds and Northrup Type K-3 potentiometer. At its most sensitive settings this potentiometer gave approximately the sensitivity of its Leeds and Northrup Model 2430 galvanometer (one-tenth microvolt per division) and the versatility of the potentiometer circuit was invaluable during periods of instability, troubleshooting, etc. Using this instrument it was possible to keep the temperature of the sample within $0.05^{\circ}C$ of that of the calorimeter during all measurements and to match the two heating rates to within $0.01^{\circ}C/min$. From the loss factors found in this study, a temperature difference of $0.05^{\circ}C$ represents a deviation from the measured input energy to the sample of only 0.2 milliwatts, which is about the same as the sensitivity of setting the input power. This number represents a deviation of less than one per cent of the smallest input power used during the measurements. The probable error in matching the heating rates is also less than one per cent of the smallest heating rates normally used during the measurements.

During these first measurements with this system it was felt advisable to use manual control of the sample power. In this manner

it was possible to get a better feeling for the magnitudes and rates of changes which were occurring in the samples, and of the transient times and accuracies of balance which were characteristic of the system. Where a large number of measurements were to be made, however, it would be advantageous to automate the sample power supply to allow adiabatic measurements to be made and recorded automatically. The block diagram of a preliminary system for this purpose is given in Figure 31. An amplifier having the characteristics necessary for the detection and control of a temperature null between the sample and the calorimeter has been designed by Dauphinee and Woods (D2). A schematic for this amplifier is given in Figure 32. This amplifier has been built, but has not yet been integrated into the measuring system.

During measurements under adiabatic conditions the horizontal section of the X-Y recorder was again operated on the 750 second time base. The vertical section was connected to the calorimeter thermocouple, which was referenced against a junction at 0° C. Thus the curves from the X-Y recorder were direct plots of the calorimeter temperature against time. The rate of change of temperature could then be obtained by measuring the slope of these curves. This rate of change of temperature was thus determined as a function of the temperature.

The power input to the sample which was necessary to maintain it at the same temperature as the calorimeter was listed on the X-Y recorder curves at intervals of a few degrees. From this data a plot could be constructed showing this power as a function of temperature. The ratio of the value of the power applied to the sample at a given temperature to the corresponding rate of change of temperature gives the heat capacity of the sample.

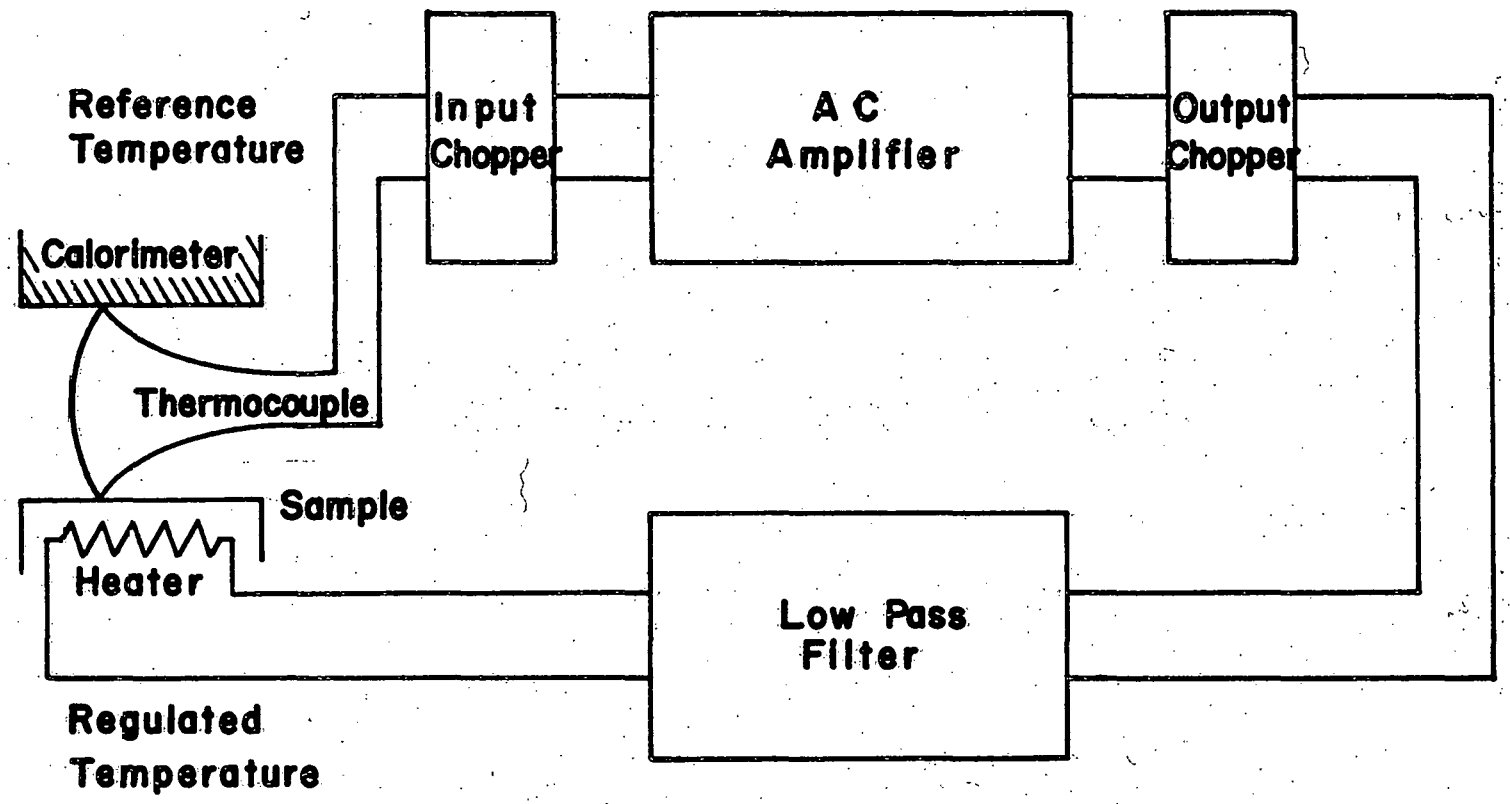

Figure 31. Block Diagram of Automated Thermal Measurement Apparatus.

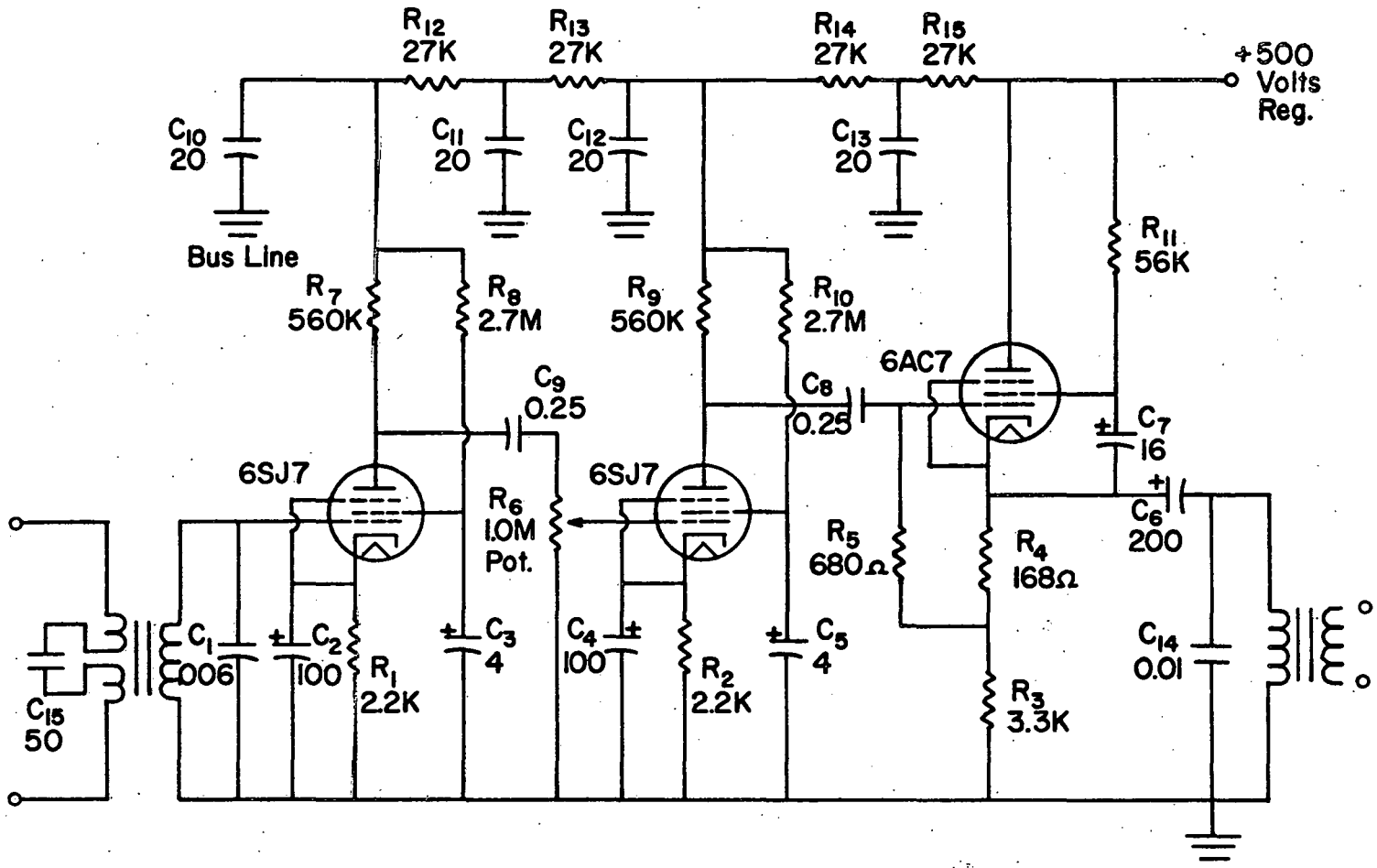

Figure 32. Amplifier Schematic for Automated System (All Capacitances in mfd).

Figure 33 shows a typical plot of input power and rate of change of temperature as a function of temperature. The effect of the heat of transition at the Curie temperature is evident from this graph. In order to calculate this heat of transition, the excess power applied to the sample, as represented by the peak in the power curve near the Curie temperature, was plotted as a function of time. The area under this curve then gives the total excess energy applied to the sample during the transition. Dividing this energy by the mass of the sample gives the transition energy in units of calories per gram, which can be converted to calories per mole by multiplying by the effective molecular weight of the solid solution.

Experimental Results

Table IV lists the characteristics of the samples which were obtained by the preliminary measurements. The sample mass listed is that of the two ceramic discs after sandblasting and cleaning. The tare heat capacity for each sample was calculated by multiplying the masses of the thermocouple wires, the heater connecting wires, the heater plate, and the epoxy binder by their respective specific heats. Although the specific heat of the epoxy was not known exactly, a value of 0.35 calories per gram per degree Centigrade was picked as being representative for this class of material. The exponential time constants and loss factors given were determined from the curves as shown in Figures 34 and 35. The heat capacity of each sample was determined as outlined above, and the specific heat of each material calculated from the relationship:

$$\text{Specific heat} = \frac{\text{Sample heat capacity} - \text{Tare heat capacity}}{\text{Sample mass}} \times \text{Mol. wt.}$$

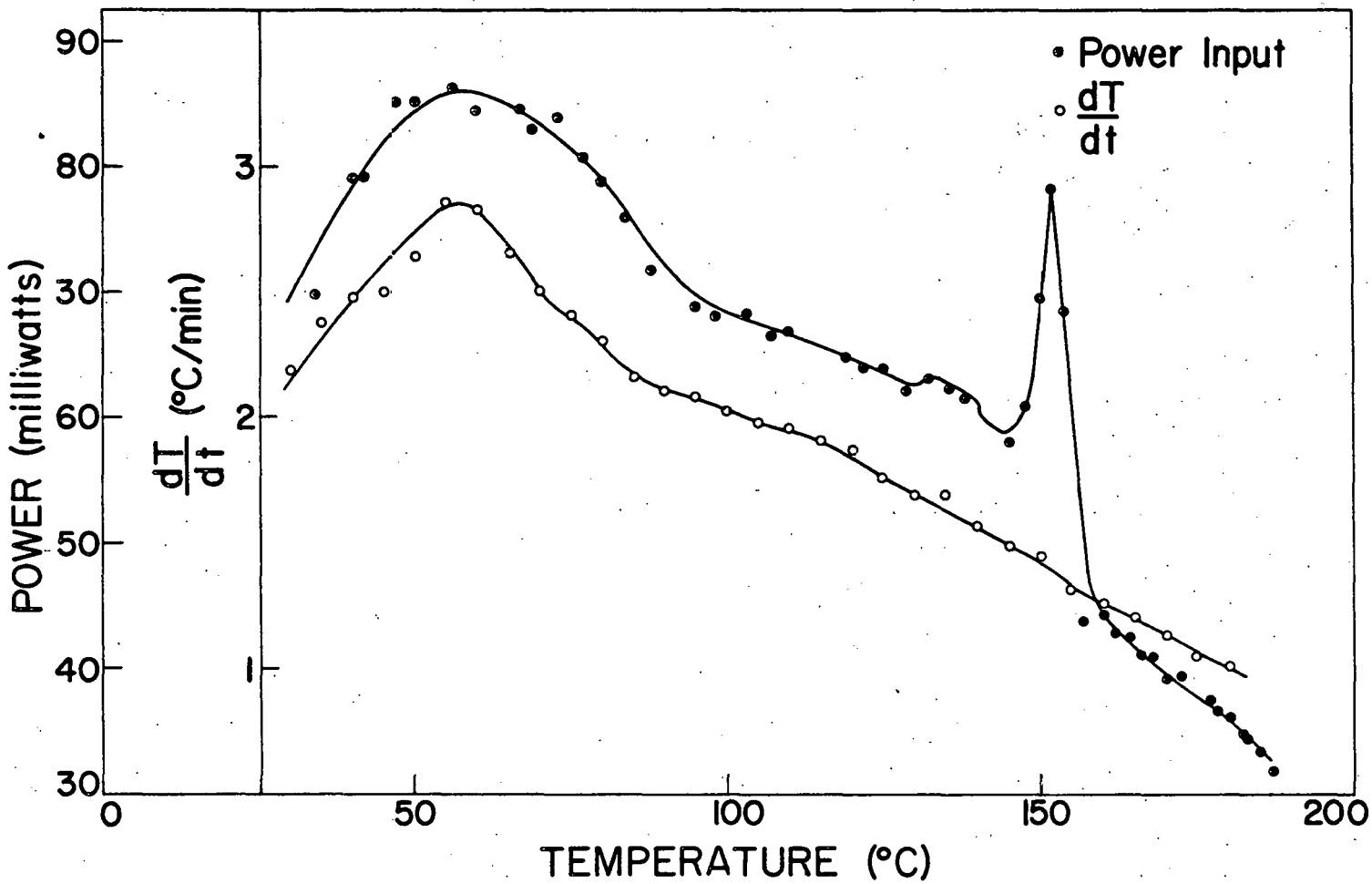

Figure 33. Input Power and Rate of Change of Temperature as Function of Temperature for PZST.

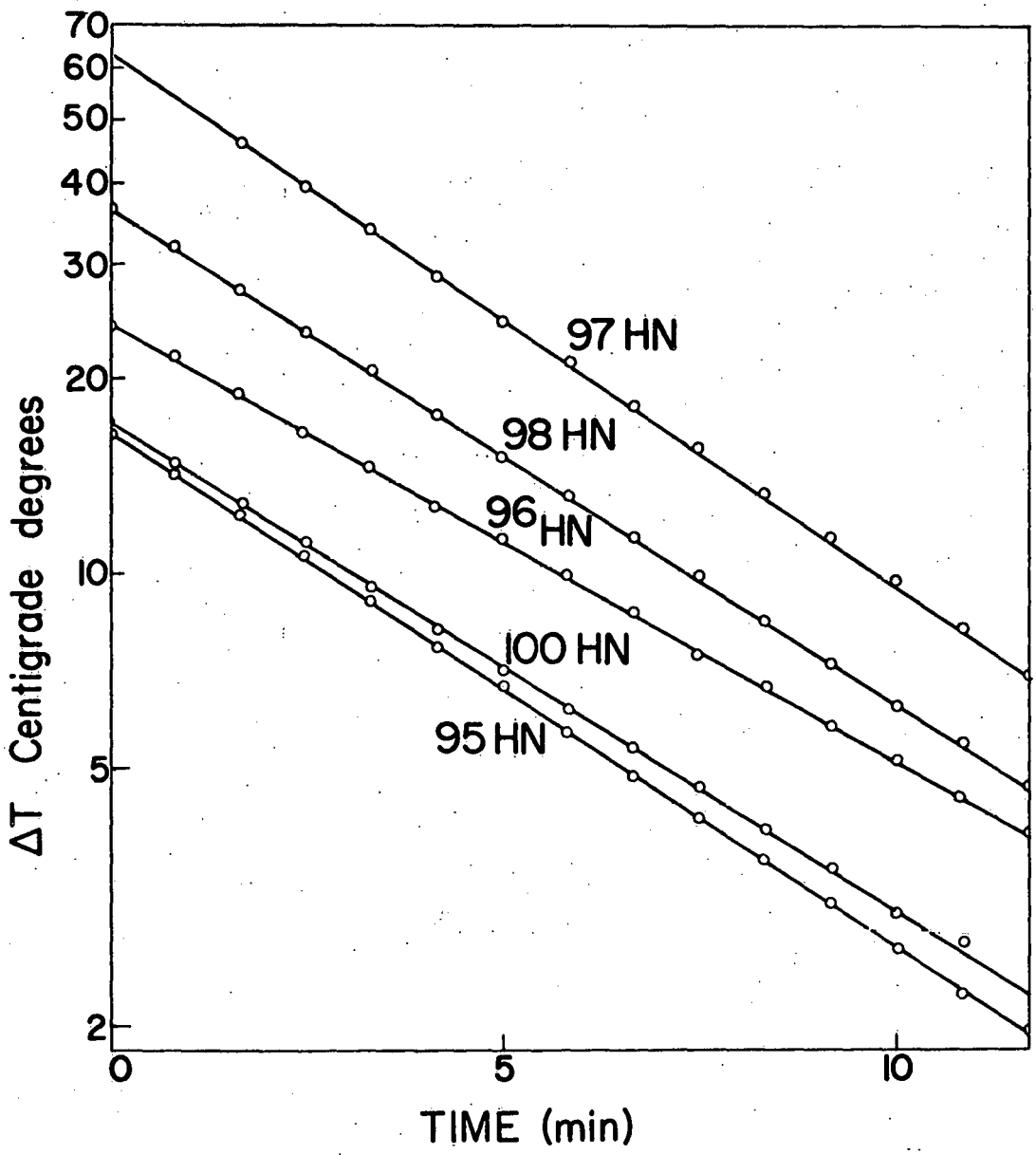

Figure 34. Exponential Cooling for Lead Hafnate Titanate Samples.

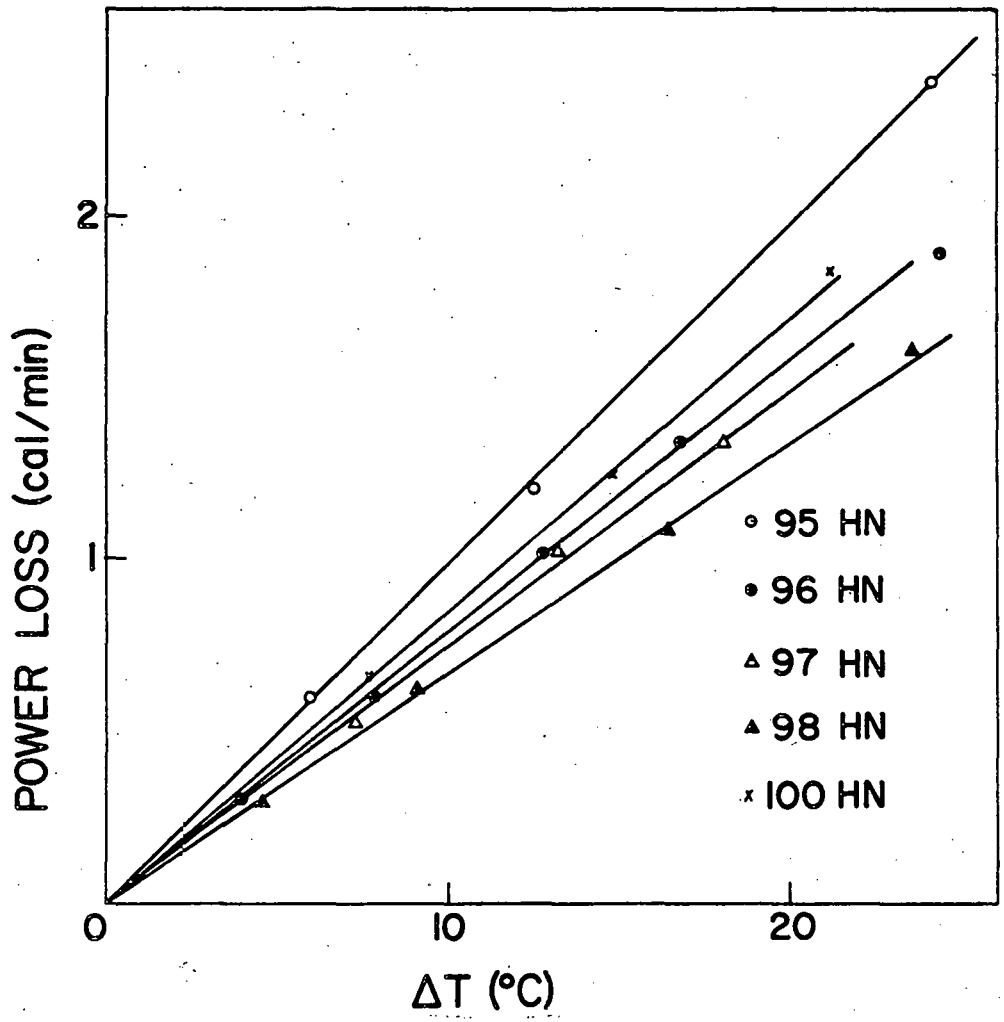

Figure 35. Measurement of Thermal Loss Factor for Lead Hafnate Titanate Samples.

TABLE IV

DATA FROM PRELIMINARY THERMAL MEASUREMENTS

Sample	Sample mass (gm)	Tare heat capacity (cal/gm°C)	Exponential Time Constant (min)	Loss Factor (cal/min°C)	Heat Capacity (cal/°C)	Specific Heat (cal/gm°C)	Specific Heat (cal/mol°C)
95 HN	6.91 gm	0.027	5.50	0.100	0.550	0.076	32.1
96 HN	7.72 gm	0.020	6.48	0.075	0.490	0.061	25.8
97 HN	6.23 gm	0.028	5.30	0.079	0.420	0.063	26.71
98 HN	7.04 gm	0.028	5.61	0.067	0.375	0.049	20.8
100 HN	7.28 gm	0.028	5.78	0.085	0.495	0.064	27.33

Figures 36, 37, 38, 39, 40, and 41, show the variation of specific heat with temperature for the materials used in this study as determined from the adiabatic measurements. Each figure shows the characteristic spike expected of a first order transition at the Curie temperature. The variations below this temperature are much more diffuse and thus less susceptible to interpretation. The 96/4 lead hafnate titanate composition does not show a spike in specific heat curve at the FE-AFE transition, but rather exhibits a general rise in the specific heat, as if the transition is blending with the Curie transition. The PZST sample shows a very small diffuse peak in the power input curve near the FE-AFE transition temperature. The other materials show certain broad peaks and rises, but nothing which can be quantitatively studied.

Figure 42 shows a typical power vs. time plot used to calculate the transition energy in this type of measurement. Table V lists the pertinent data for these calculations and the heats of transition obtained from them. An estimate was also made of the energy involved

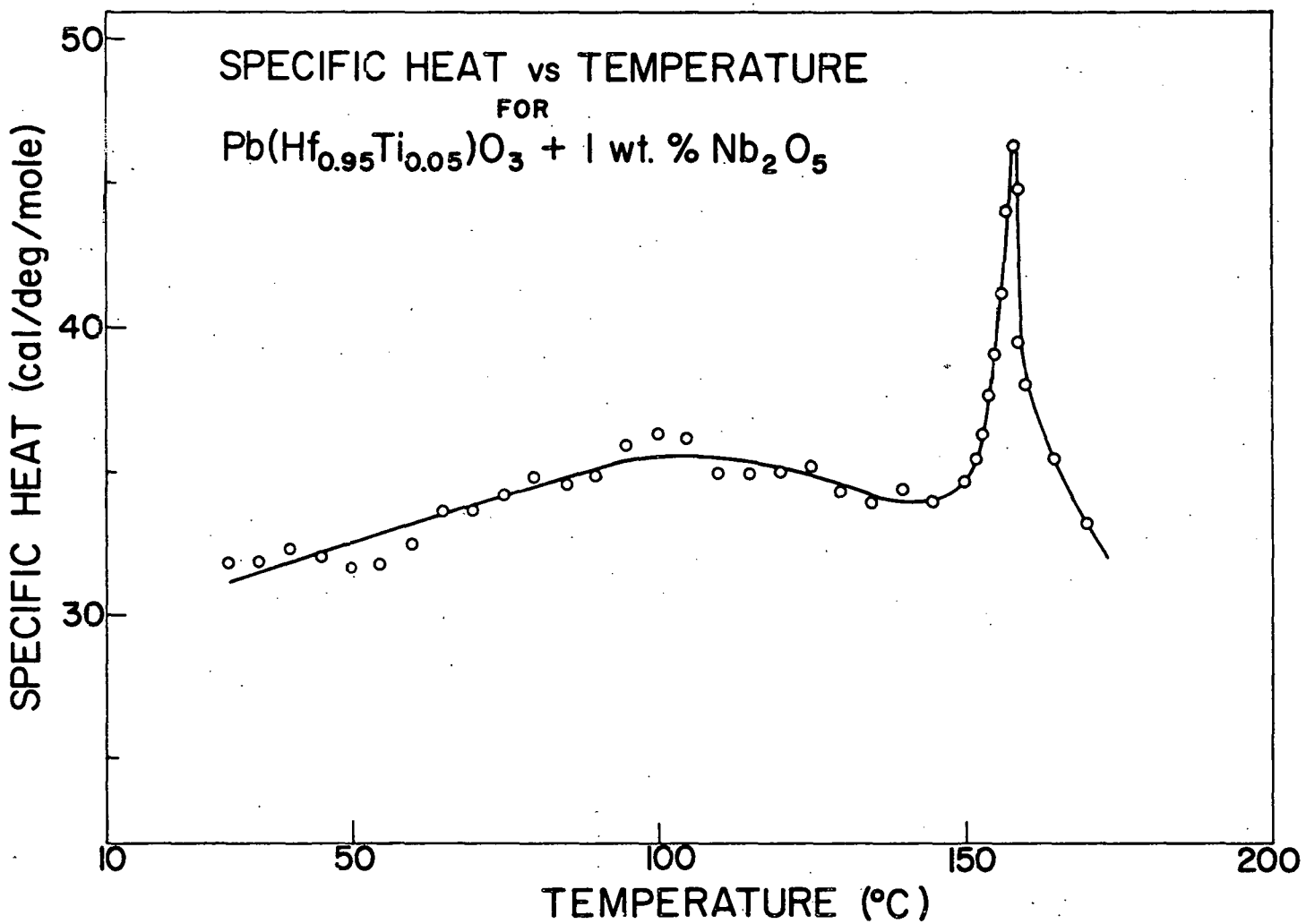

Figure 36. Specific Heat vs. Temperature for $Pb(Hf_{0.95}Ti_{0.05})O_3$ + 1 wt. % Nb_2O_5.

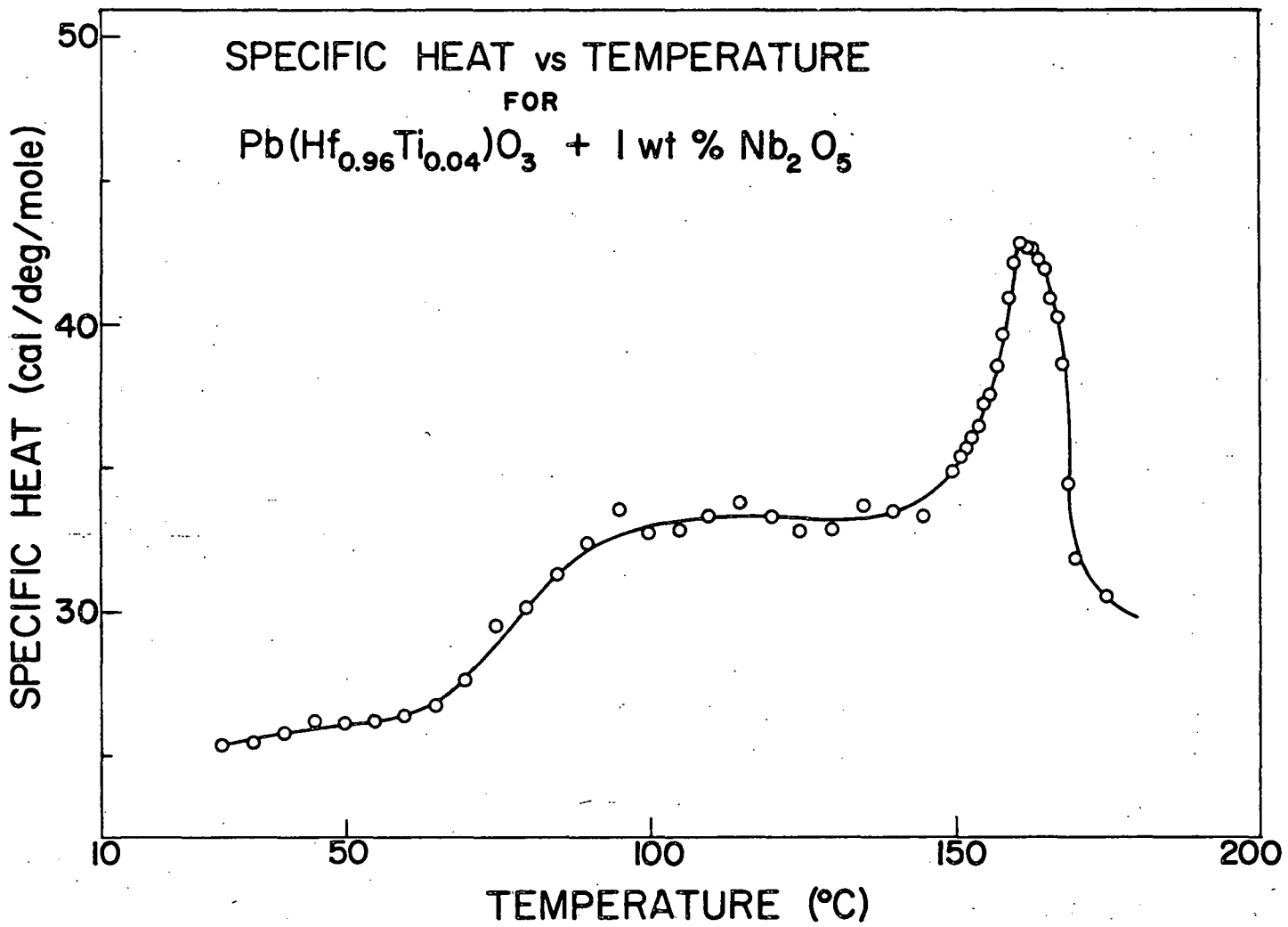

Figure 37. Specific Heat vs. Temperature for $Pb(Hf_{0.96}Ti_{0.04})O_3$ + 1 wt. % Nb_2O_5.

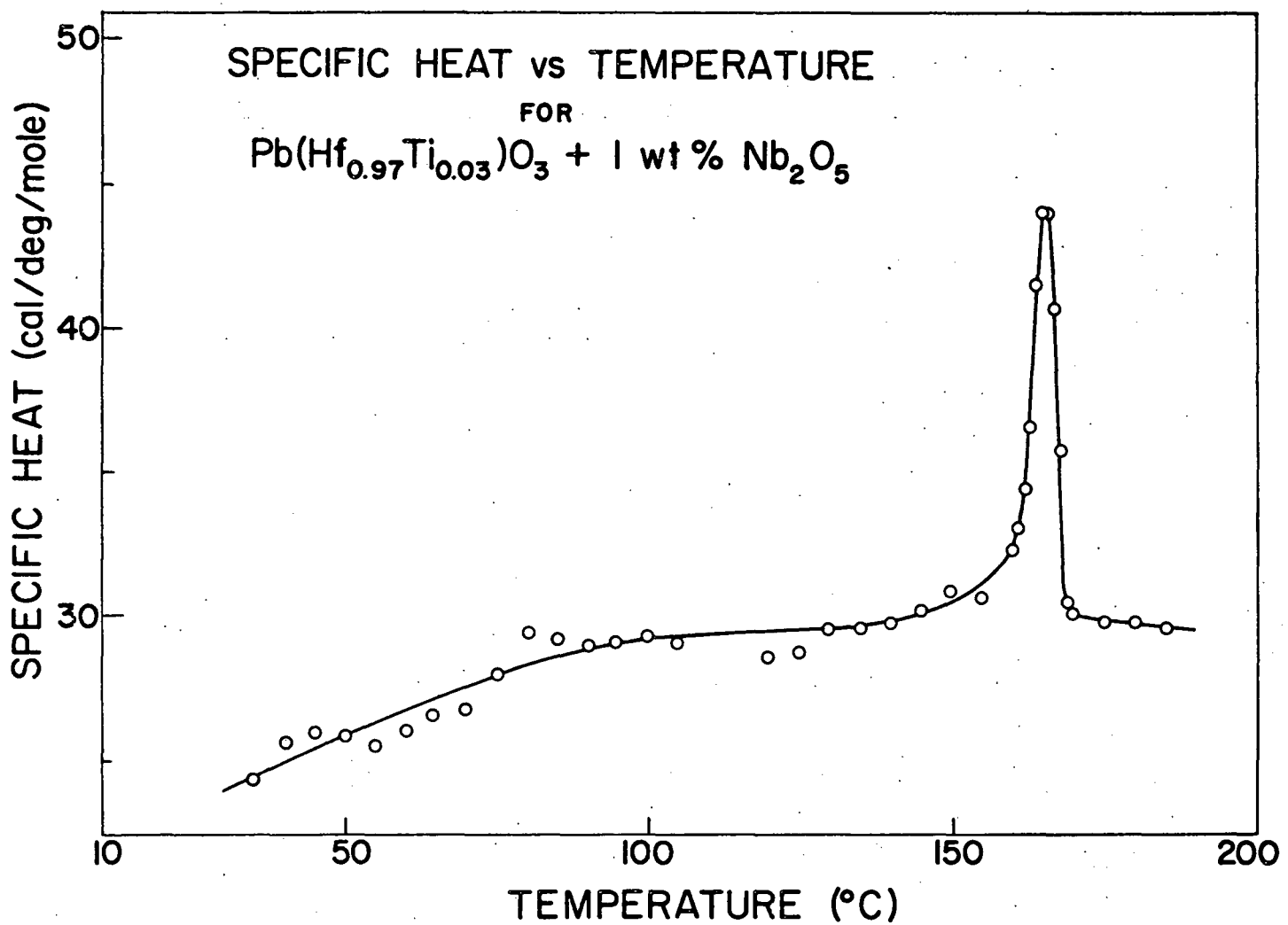

Figure 38. Specific Heat vs. Temperature for $Pb(Hf_{0.97}Ti_{0.03})O_3$ + 1 wt. % Nb_2O_5.

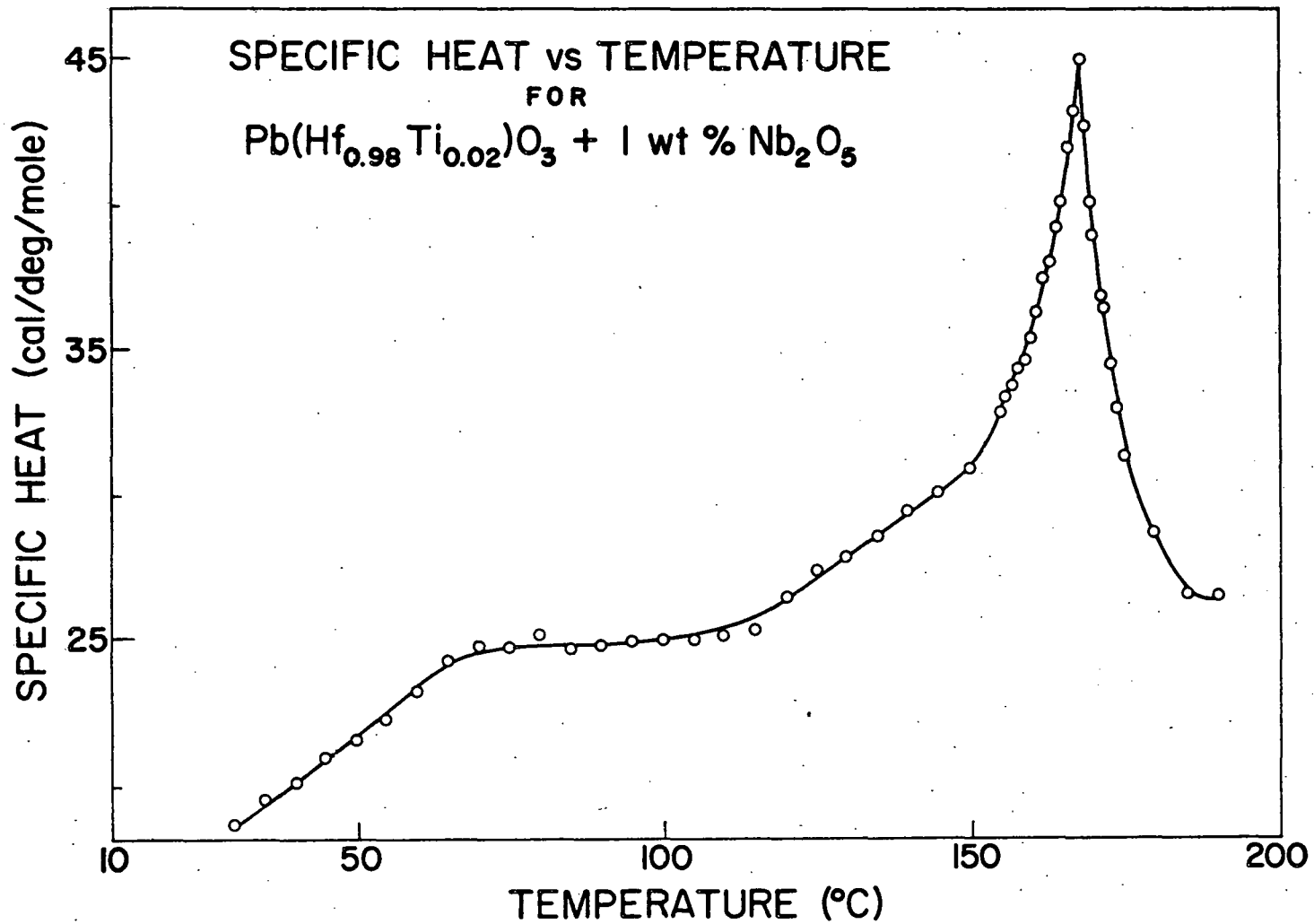

Figure 39. Specific Heat vs. Temperature for $Pb(Hf_{0.98}Ti_{0.02})O_3$ + 1 wt. % Nb_2O_5.

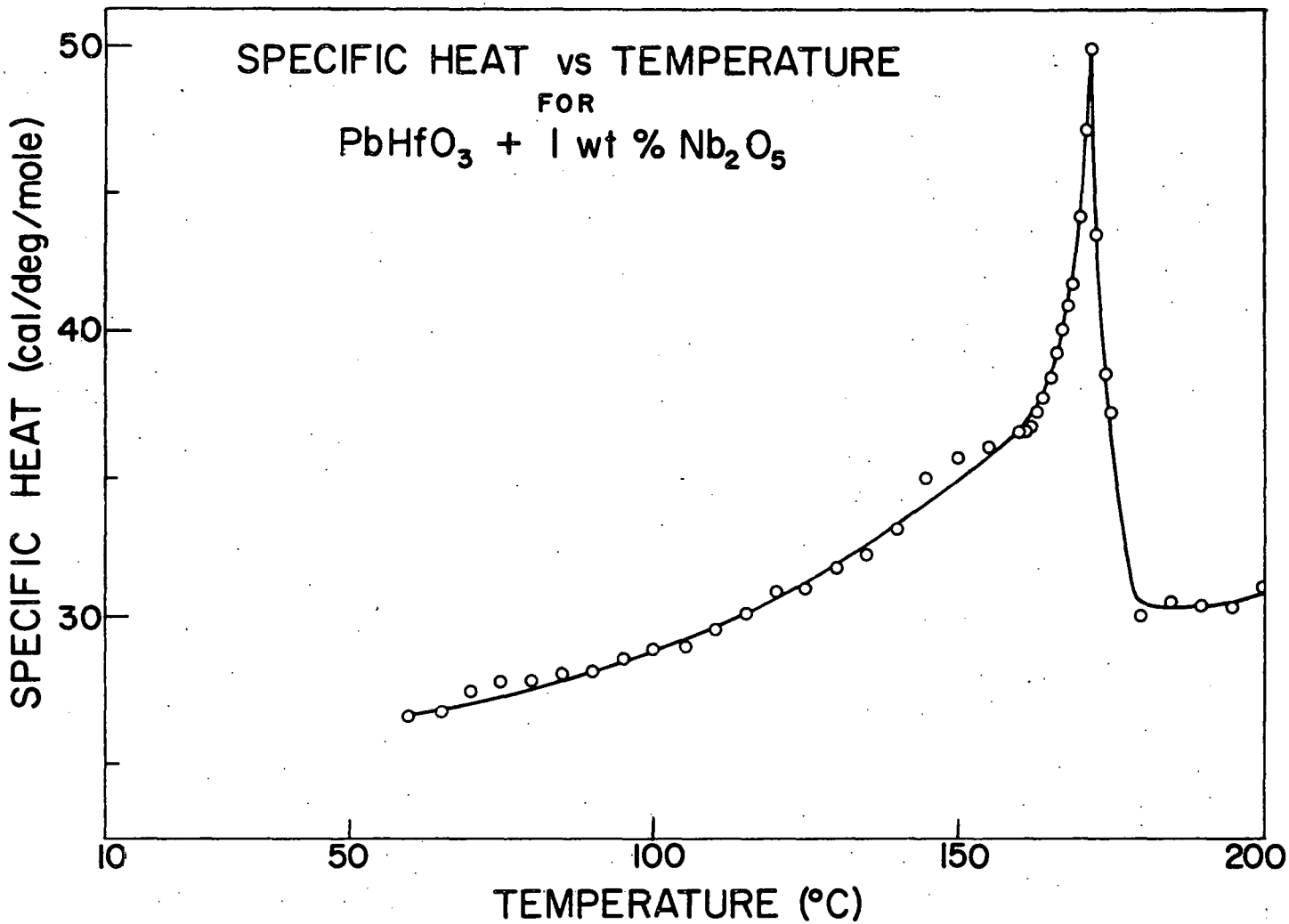

Figure 40. Specific Heat vs. Temperature for $PbHfO_3$ + 1 wt. % Nb_2O_5.

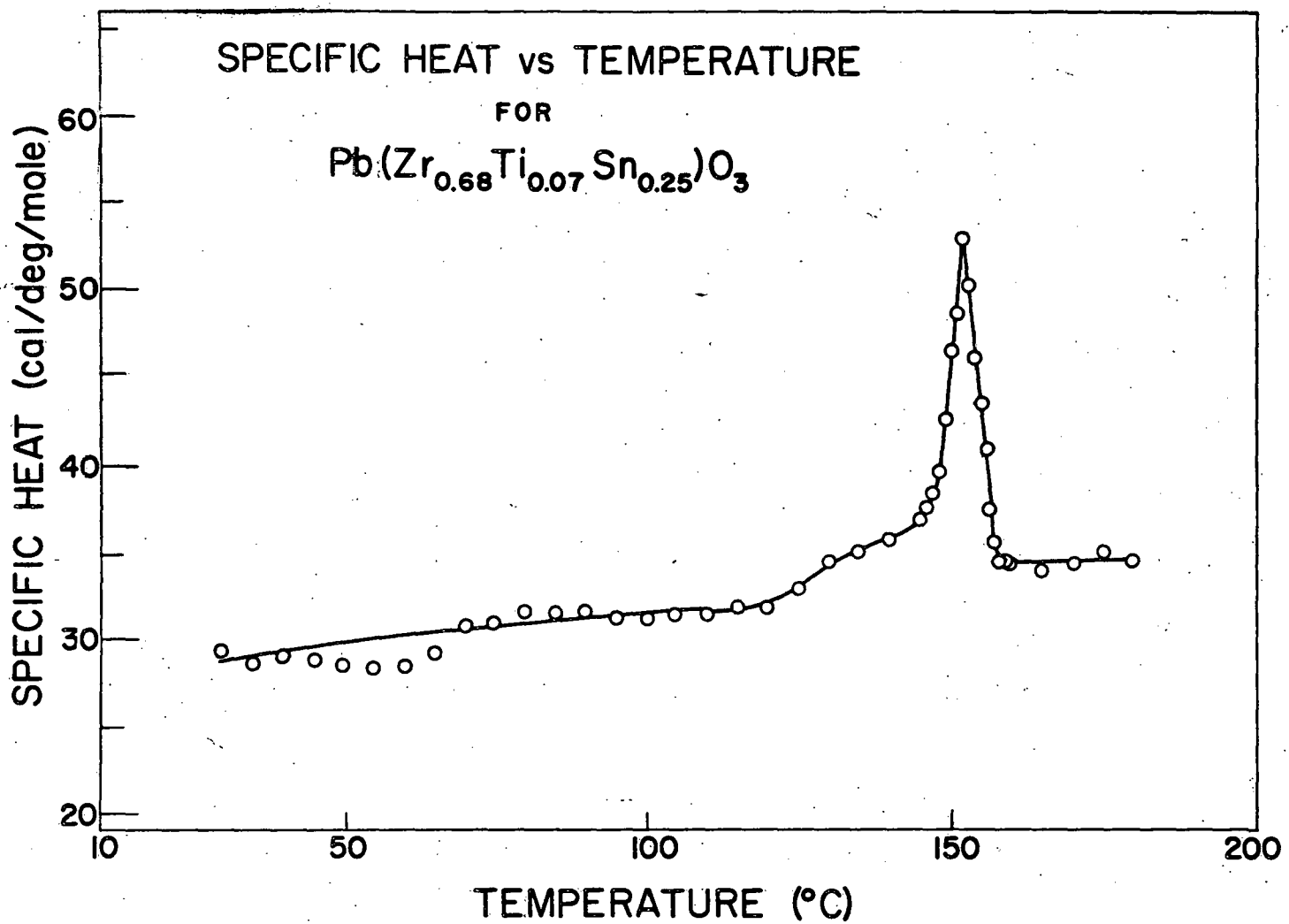

Figure 41. Specific Heat vs. Temperature for PZST.

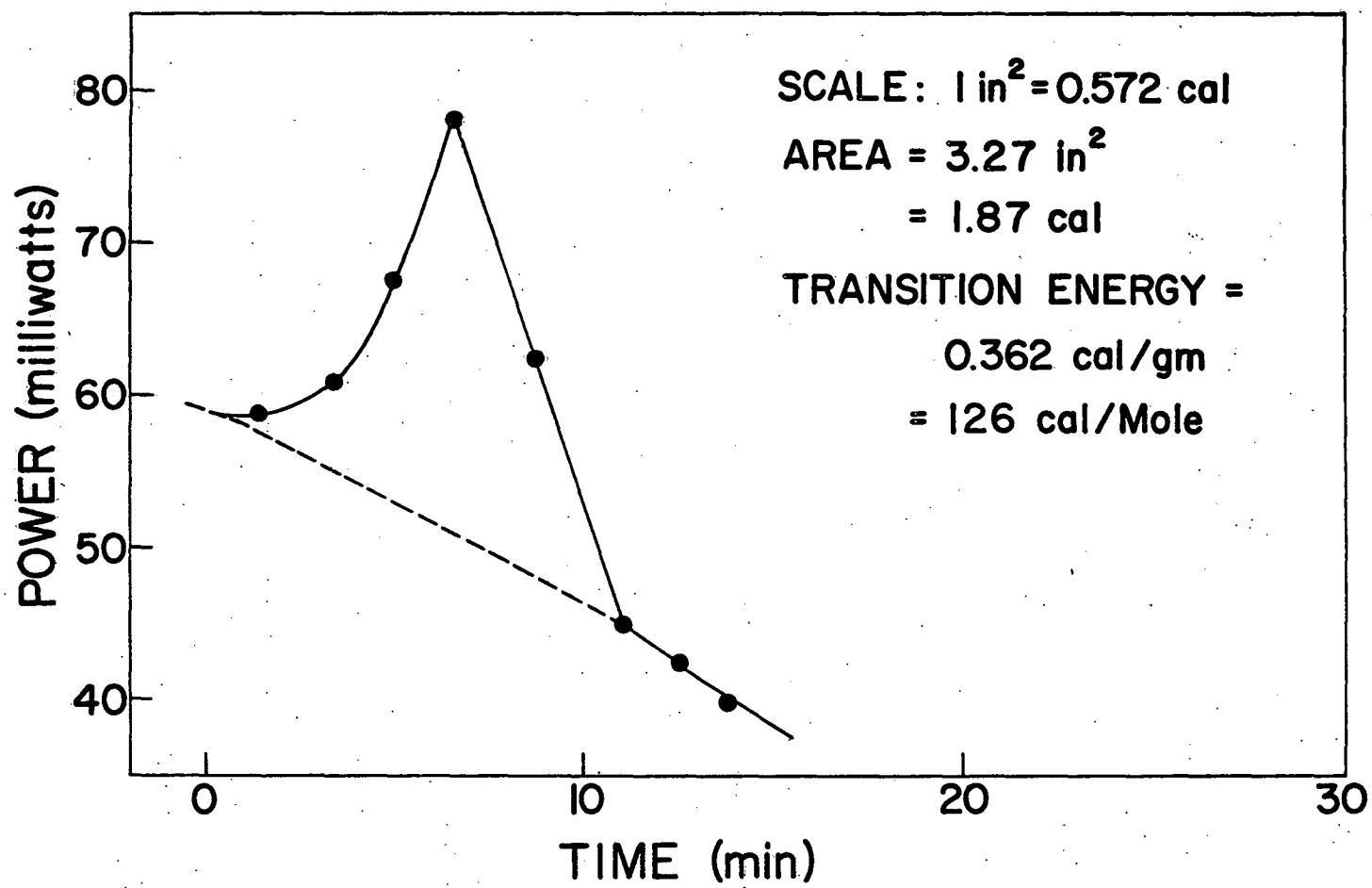

Figure 42. Excess Power vs. Time Plot Used to Calculate Curie Transition Energy for PZST.

in the FE-AFE peak in the PZST sample. Because of the blending of this transition with the Curie transition data this estimate is of limited accuracy but does indicate a very small heat of transition at the FE-AFE transition.

The heats of transition calculated for these materials are smaller than those reported for lead zirconate and its solid solutions. This fact will be discussed later together with a comparison of the techniques used in obtaining them. The heat of transition of the 96/4 material probably appears higher than that of the other members of this family of compositions because of the blending of the FE-AFE transition with the Curie transition.

TABLE V

HEAT OF TRANSITION DATA

Sample	Sample Mass (gm)	Transition Temp.	Excess Heat (cal)	Heat of Transition (cal/gm)	Heat of Transition (cal/mol)	ΔS (cal/mol °C)
95 HN	6.91	160	1.53	0.222	94	0.22
96 HN	7.72	163	2.40	0.311	133	0.31
97 HN	6.23	167	1.49	0.240	102	0.23
98 HN	7.04	170	1.60	0.228	97	0.22
100 HN	7.28	172	1.58	0.218	93	0.21
PZST (Curie)	5.17	152	1.87	0.362	126	0.30
PZST (FE-AFE)	5.17	~130	0.079	0.015	5.3	0.013

CHAPTER VII

RESULTS OF RELATED WORK

This chapter presents certain results obtained during recent studies by other groups which either extend the present study or which can be useful in the interpretation of the present results. Some of the results of the study by Sawaguchi (S4) on lead zirconate titanate are also presented and will be used for comparison with the conclusions obtained for lead zirconate titanate stannate and lead hafnate titanate in the next chapter.

Clevite Work on $Pb_{0.99}Nb_{0.02}(Zr_{0.68}Ti_{0.07}Sn_{0.25})_{0.98}O_3$

A great deal of work on the lead zirconate titanate stannate compositions has been done during the last few years by the Electronic Research Division of Clevite Corporation of Cleveland, Ohio. The work of interest to this study has been selected from three reports by Berlincourt (B2, B3, B4) of the Clevite group.

The work at Clevite has included a study of the characteristics of the FE-AFE transitions in the lead zirconate titanate stannate composition used in the present study and has obtained interesting results concerning the pressure vs. volume relationships in this composition. X-ray studies have shown the AFE phase to be the phase of minimum volume with a change of about 0.36% occurring during transitions between the FE and AFE phases. The change in volume produced in a sample of this material by the

application of hydrostatic pressure was also determined. Again the volume difference between the phases was found to be about 0.35% with the transition occurring at a pressure of about 38,000 psi.

Figure 43 compares the polarization changes produced in this composition by variation of temperature and pressure. It can be seen that while the general shapes of the curves are the same, almost twice as much depoling takes place before the abrupt transition when the temperature is varied as occurs before a pressure-induced transition.

Figure 44 indicates the variation of transition pressure of poled ferroelectric samples as a function of a biasing electric field. Because of the oriented condition of the specimen, the transition pressure for the FE-AFE transition decreases with negative bias until the bias field reaches the coercive field and switching takes place. For the AFE-FE transition there is no original orientation of the polarization and the phase boundary is symmetrical.

A great deal of work has been done by this group in the analysis of the double hysteresis loops characteristic of field induced AFE-FE transitions. Loops taken for PSZT about 8° C above the FE-AFE transition are quite broad, giving E_f equal to about 8 Kv/cm and E_a about 4 Kv/cm.

Figure 45 is a temperature vs. field phase diagram obtained by field variation at constant temperature. This is in contrast to the technique used in this study and described in Chapter IV, which involved the variation of temperature at constant field. It is interesting to note that the shape of the curve representing the AFE-FE transition with increasing field is similar to that which was shown earlier for the FE-AFE transition with increasing temperature.

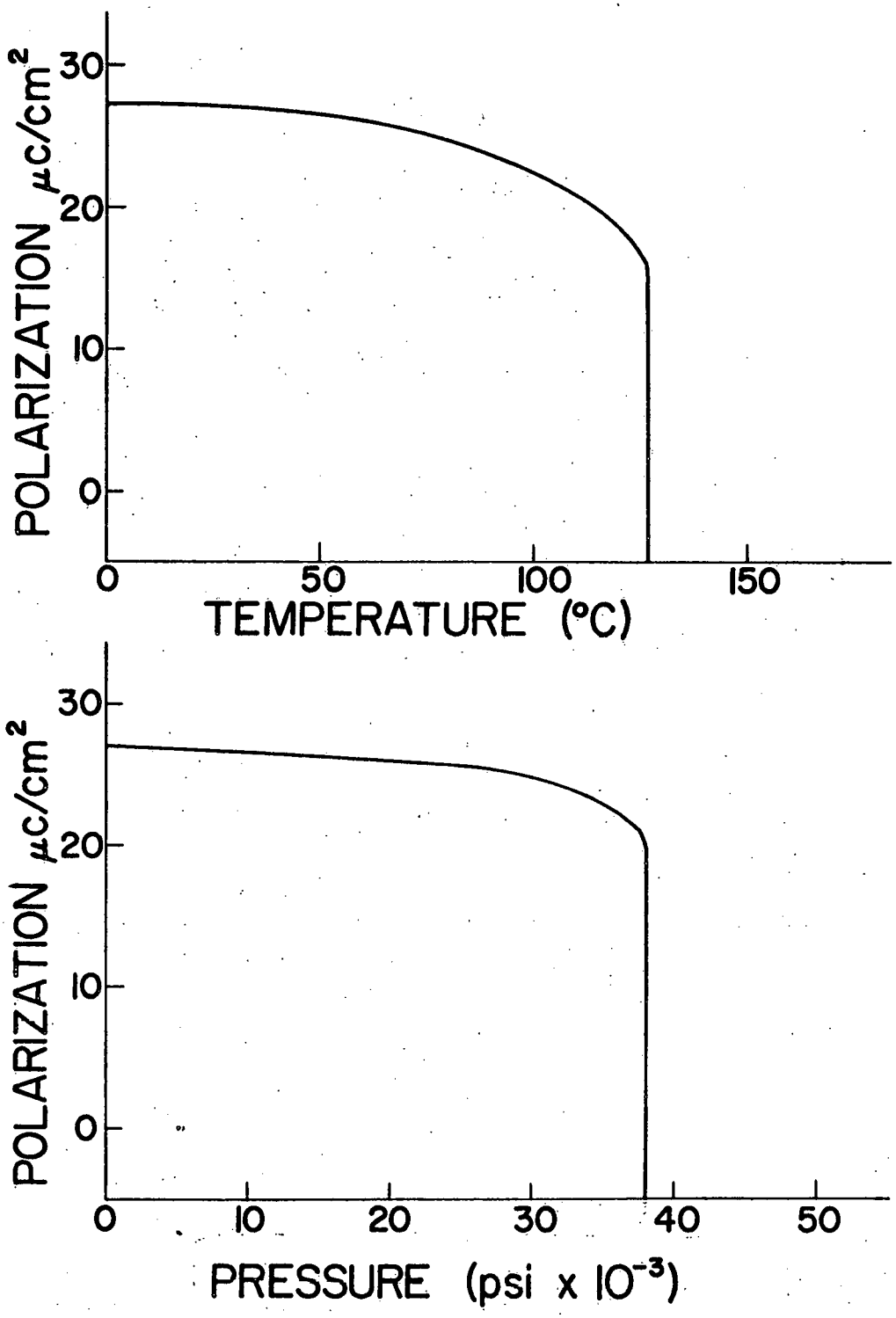

Figure 43. Polarization vs. Temperature and Pressure for PZST. (After Berlincourt (B3)).

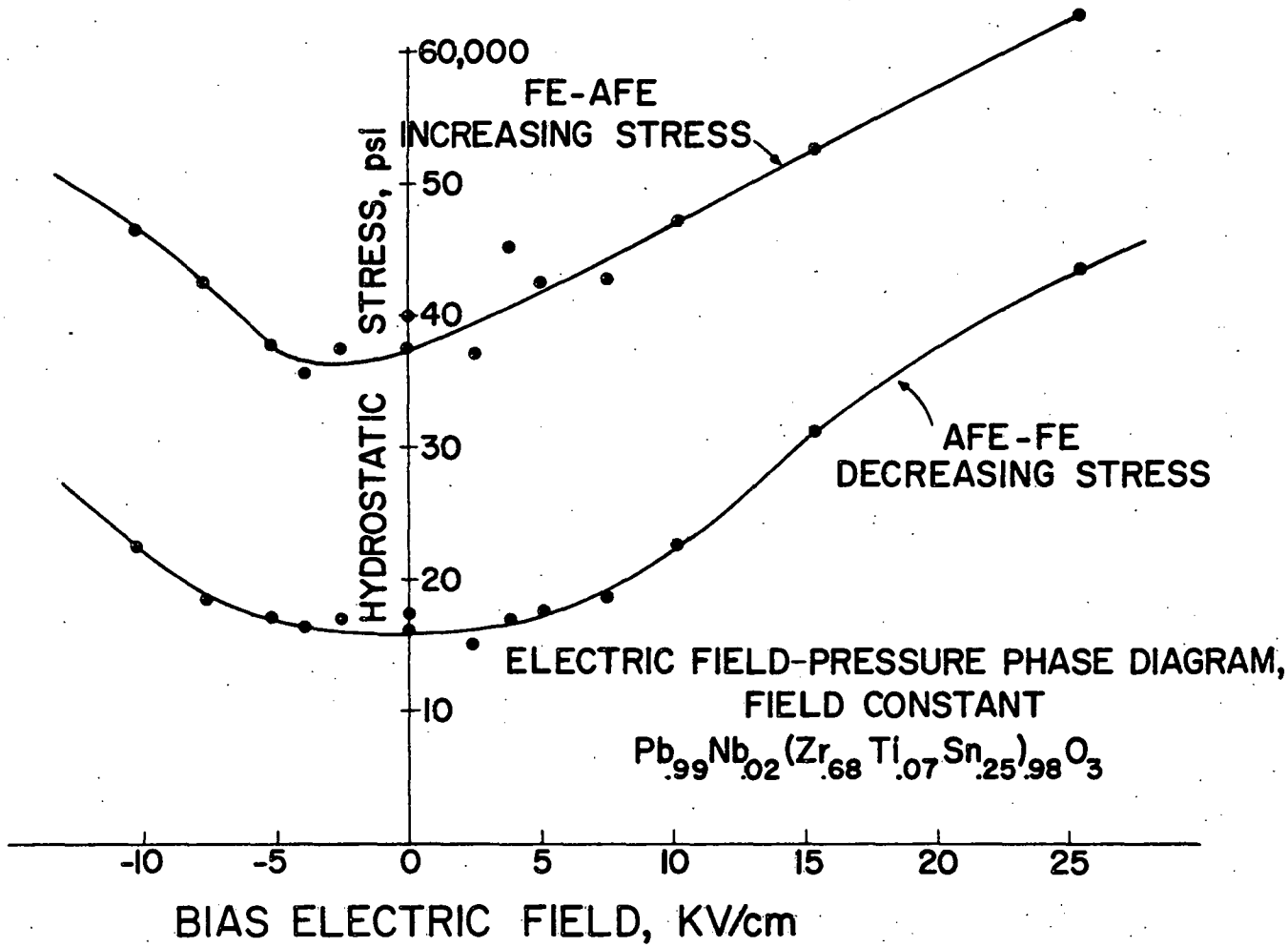

Figure 44. Electric Field-Pressure Phase Diagram for PZST (After Berlincourt (B4)).

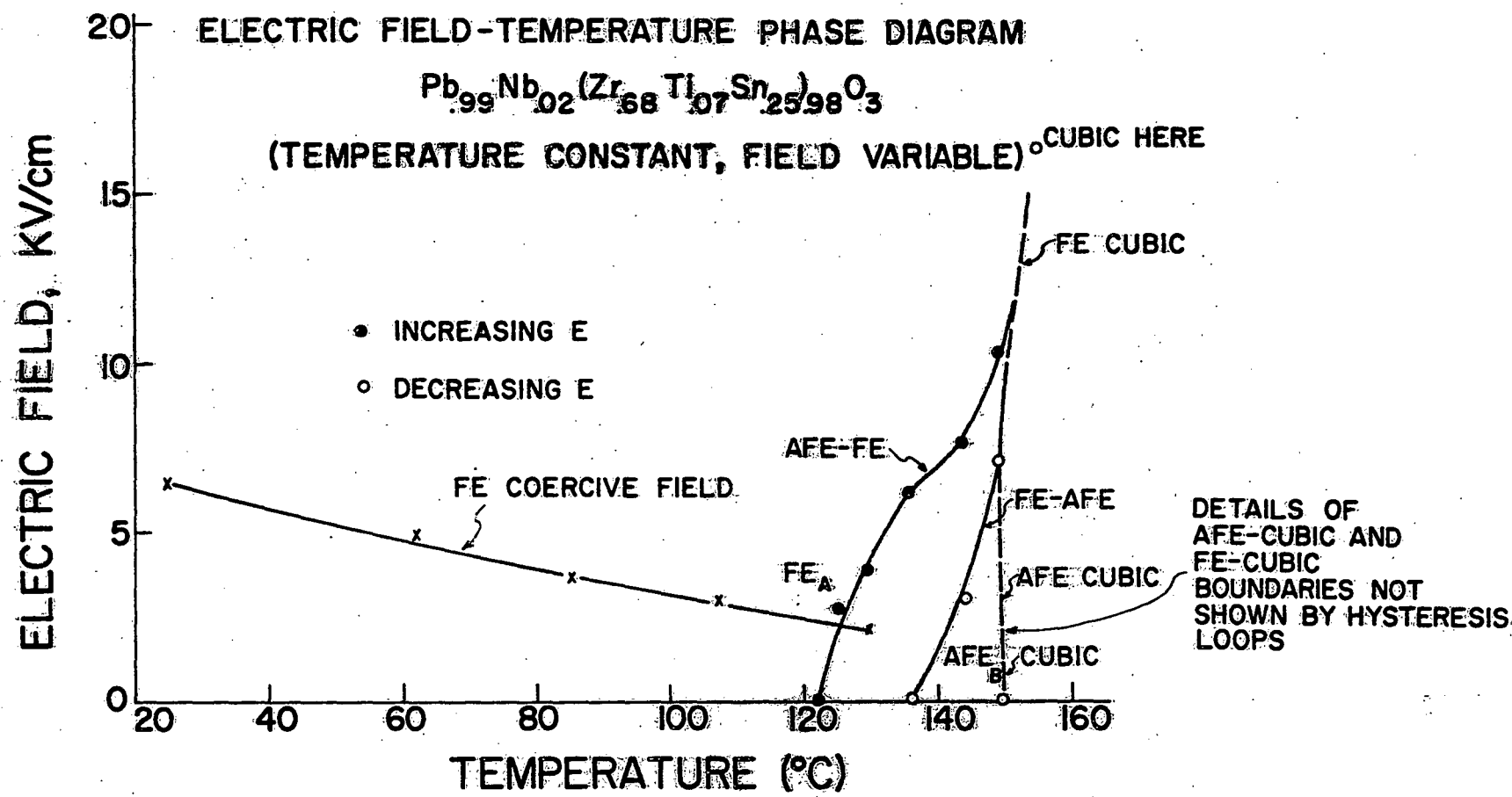

Figure 45. Electric Field-Temperature Phase Diagram for PZST. (After Berlincourt (B4)).

THIS PAGE

WAS INTENTIONALLY

LEFT BLANK

Sandia Studies on Lead Hafnate Titanate Compositions

Studies at Sandia by Hall, Dungan, and others (H1, D3) have continued to reveal new characteristics of the lead hafnate titanate compositions.

Measurements of the variation of E_f and E_a as functions of temperature for the 97/3 and 98/2 compositions revealed that at most temperatures the double hysteresis loops were quite broad and that reliable estimates of the free energy difference between the phases can only be obtained near the transition temperature. However, it should be noted that at temperatures more than 50 degrees below the zero bias transition temperature, the phase change could be produced by fields less than 20 Kv/cm.

Samples having the same compositions as those used in the present study were prepared using a higher purity HfO_2 than had previously been employed (H2). The electrical properties of the samples were quite similar to those previously tested, but the compositional boundary between the FE and the AFE phases covered a much smaller range. Using the purer material, the 96/4 composition was ferroelectric between room temperature and the Curie temperature while the 98/2 composition was antiferroelectric over the same region. An AFE-AFE transition was also observed which had not been reported previously.

Lead hafnate titanate samples without the niobium addition were also prepared. This modification increased the Curie temperature to the 200° C region and moved the AFE-FE phase boundary to the 95/5 composition.

Dungan and Stark (D3) have investigated the lead hafnate titanate stannate compositional family and find it to be strikingly similar to the lead zirconate titanate stannate family.

Hall, in his Ph.D. dissertation (H3), investigated compositions in the lead zirconate hafnate titanate series. In his study of the temperature vs. composition relations for materials having equal molar parts of zirconium and hafnium, he found that the FE-AFE phase boundary had been displaced so as to enlarge the antiferroelectric stability region, but that the boundary slope was still in the same direction as in the lead zirconate titanate compositions. In an extension of this work, he has found that this slope does not appear to reverse until the compositions contain about 80 mole per cent hafnium. Thus the influence of the zirconium ion on the relative stability of the various phases seems to be stronger than that of the hafnium ion.

Sawaguchi (S4), in his study of the high zirconium regions of the lead zirconate titanate series, was able to construct a relative free energy diagram for this system. From calorimetric data, he found that the entropy difference between the two AFE phases (0.22 cal/mole^{o}) was much larger than the difference between the high temperature AFE phase and the FE phase (0.073 cal/mole^{o}). These in turn were both smaller than the entropy difference observed at the Curie transition (0.51 cal/mole^{o}).

From the double hysteresis loops exhibited near the transition temperature, Sawaguchi was able to calculate the difference in free energy between the FE and AFE phases in $PbZrO_3$. The calculations show a free energy difference of about 3 cal/mole at 215° C which decreases to 1 cal/mole near 230° C. From this he concluded that the FE and AFE phases would have equal free energies at about 240° C. Unfortunately, the paraelectric phase becomes dominant below this temperature so that an AFE-FE transition is not actually observed.

From the work with $Pb(Zr_{0.97}Ti_{0.03})O_3$ and $Pb(Zr_{0.98}Ti_{0.02})O_3$, Sawaguchi also determined that additions of lead titanate to lead zirconate decreases the free energy of the FE phase relative to the cubic phase at a rate of 0.5 cal/mole-at% and increases the free energy of the two AFE phases at rates of 5.8 cal/mole-at% and 2.3 cal/mole-at%.

CHAPTER VIII

CONCLUSIONS

Free Energy Relationships in

$Pb_{0.99}Nb_{0.02}(Zr_{0.68}Ti_{0.07}Sn_{0.25})_{0.98}O_3$

The most complete set of data available for any of the compositions used in this study is that on the PZST samples. For this material one now has thermal, electrical, and pressure relationships which involve all three phases. This composition also gave the sharpest transitions and thus the most reliable phase diagrams of all the materials studied. For all of these reasons, the free energy relationships for this composition will be discussed first and the ideas thus obtained then applied to the discussion of the other compositions.

As was shown in Chapter III, the calculation of free energy involves a knowledge of the extensive variables -- volume, polarization and entropy. From the Berlincourt data the molar volume of this composition is found to be about 42 cm^3 and the volume in the AFE phase is approximately 0.35% less than that in the FE phase. The variation of polarization with temperature and pressure was indicated in Figure 43, while the polarization dependence on electric field can be obtained from the plots of dielectric susceptibility vs. field and a knowledge of the spontaneous polarization by using the relation,

$$P(E)=P_s+\int_0^E \epsilon_0 \chi(E)\, dE$$

The calculation of the absolute entropy, however, is a much greater problem. This requires a knowledge of the specific heat at all temperatures above absolute zero. The variation in the vicinity of absolute zero is quite important and is thus far not available. For this reason the absolute entropy of this system cannot presently be calculated and relative entropies must be used to determine the free energy diagrams. The entropy differences between the phases at the transitions are given in Table V.

A correlation of the results of the various measurements is useful as a check on the experimental values obtained. The electrical and thermal data can be compared by using the relationship:

$$\left(\frac{\partial T}{\partial E}\right)_p = -\frac{V\Delta P}{\Delta S}$$

Using the values

$$V = 42\ cm^3/mole$$
$$\Delta P = -16 \times 10^{-6}\ coul/cm^2$$
$$\Delta S = 0.013\ cal/mole^o$$

a value of $(\partial T/\partial E)_p = 12.3\ cm^o/Kv$ is obtained. This compares with a value of about $9\ cm^o/Kv$ which is obtained from the central slope of the FE-AFE phase boundary in Figure 10. The discrepancy seems to indicate that the value of entropy measured was slightly low. This is quite possible since, as was pointed out earlier, the peak used in the calculation of that value was quite small and diffuse. It would seem a value of about $0.02\ cal/mole^o$ might be more accurate for this transition.

The above relation also applies to the ferroelectric Curie transition at high fields. Here the polarization used consists of the spontaneous polarization plus that induced by the field. Using a value of ΔP equal to about 22×10^{-6} coulombs/cm^2 and a value of $\Delta S = 0.30\ cal/mole^o$ (the

entropy difference between the phases at zero field), a value of 0.74 cm^{o}/Kv is calculated. This compares with a value of 0.80 cm^{o}/Kv measured just above the triple point in the PZST phase diagram. In view of the assumptions made, this would seem to be very good agreement.

A comparison of the transition temperature vs. field phase diagrams obtained by varying the temperature in one case and the field in another leads to some interesting conclusions concerning the hysteresis in these transitions. Figure 46 compares the FE-AFE transition with increasing temperature to the AFE-FE transition with increasing field. Since these transitions are in opposite directions, the true phase equilibrium conditions must lie somewhere between them. But a comparison of this figure with Figures 10 and 45 indicates that the true equilibrium line lies much closer to the transition observed with increasing intensive parameter than to that observed with decreasing intensive parameter. Thus the shapes of the curves in Figure 46 are more representative of the shape of the phase equilibrium line than are those for the reverse transitions. The rapid decrease of the slope of the FE-AFE transition as this transition approaches the Curie point would seem to indicate that these two transitions tend to blend causing the change of entropy at the FE-AFE transition to increase rapidly.

The results obtained with hydrostatic pressure can be compared with the electrical results by the relation:

$$\left(\frac{\partial P}{\partial E}\right)_T = \frac{V\Delta P}{\Delta V}$$

Using the values

$$\Delta P = 22 \times 10^{-6} \text{ coul/cm}^2$$
$$\Delta V/V = 0.35\%$$

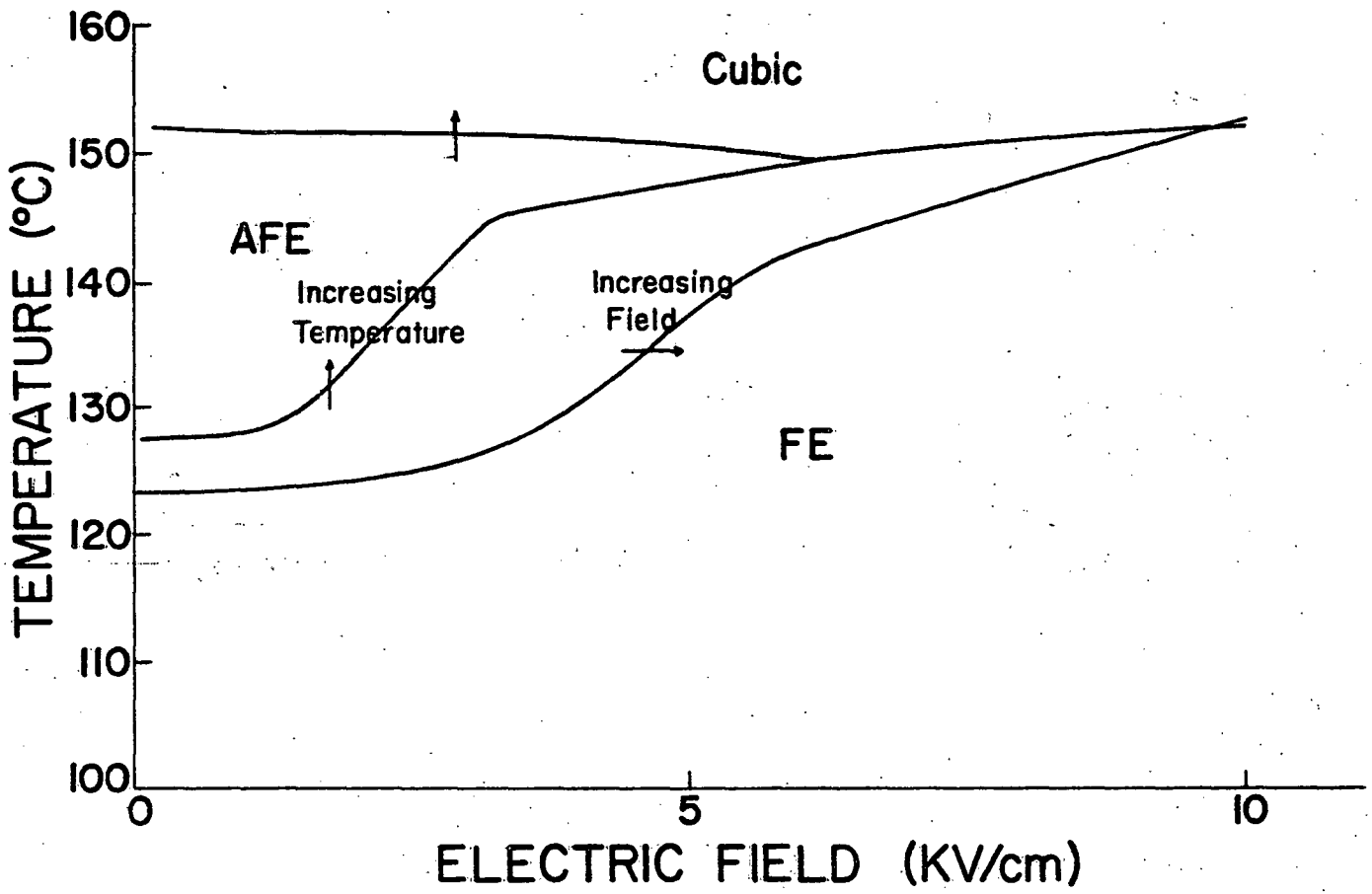

Figure 46. Comparison of Transitions Observed with Increasing Temperature and Increasing Field for PZST.

a value of 62.8 coul/m^2 is found for $(\partial p/\partial E)_T$. This compares with a value of 65.4 coul/m^2 observed in Figure 44.

From the pressure-induced transition data it is possible to estimate the free energy difference between the FE and the AFE phases at room temperature. Sawaguchi (S4) has shown that the free energy difference between two phases observed during a forced ferroelectric transition is essentially the product of the intensive variable necessary to force the transition and the corresponding change of extensive parameter. Authors following him seem to have followed this method of calculation (e.g., the difference in free energy between the phases in the double hysteresis loop is represented by an area equivalent to the average field at the transition multiplied by the change in polarization). An assumption that the difference in entropy and internal energy between the two phases are approximately constant over the temperature range considered, on the other hand, leads to a correction of the above value by a factor of $\Delta S(T-T_o)$ where ΔS is the observed entropy difference, T is the temperature of the forced transition, and T_o is the temperature of the transition with the intensive parameter equal to zero. Over the temperature ranges used in this study however, this correction amounts to less than 20% of the principal value, so that the Sawaguchi assumption will be used in subsequent calculations. The values given for free energy differences between the phases should therefore be understood to give at least a reasonable approximation to the true free energy difference.

Using the above approximation, Berlincount's pressure-induced transition gives:

$$\Delta G \cong p\Delta V$$
$$= 38 \times 10^3 \text{ psi} \times 15 \times 10^{-8} \text{cm}^3$$
$$\Delta G(\text{molar}) = 9.4 \text{ cal/mole}$$

While this is only an estimate, it is comparable to the values of difference of free energy between the ferroelectric and antiferroelectric phases observed by Sawaguchi in lead zirconate titanate solid solutions. Because of the possible presence of hysteresis, this value should be taken to represent an upper limit to the free energy difference between the phases.

An estimate of the free energy difference at 135° may be obtained from the field-induced hysteresis loops of Berlincourt. Since these loops are broad this estimate is of limited accuracy but a maximum and minimum value can be established from E_f and E_a for the transition. Again using the previous assumptions, the following values are obtained:

Maximum value:

$$\Delta G(\text{molar}) = \Delta P E_f V(\text{molar}) = 0.96 \text{ cal/mole}$$

Minimum value:

$$\Delta G(\text{molar}) = \Delta P E_a V(\text{molar}) = 0.48 \text{ cal/mole}.$$

In order to establish free energy differences involving the paraelectric phase, the entropy difference at the transition must be used, since this is the only information at hand regarding this phase. The entropy difference of 0.30 cal/mole° indicates that the free energy of the cubic phase falls quite rapidly below that of the AFE phase above the Curie temperature. Extrapolations of this difference to temperatures far from the Curie point depends on a knowledge of the curvature of the free energy lines as a function of temperature.

The curvature of these lines is given by the relation:

$$\left(\frac{\partial^2 G}{\partial T^2}\right)_{E,p} = -\left(\frac{\partial S}{\partial T}\right)_{E,p} = -\frac{C_p}{T}$$

Thus from the measurement of specific heat, the curvature of the free energy lines can be found, and relative free energy curves calculated. Figure 47 shows a plot of C_p/T calculated from the curve of Figure 41. The points in the vicinity of the Curie transition have been left out since the change of entropy in this region has been calculated as the entropy change at the transition. This plot indicates that the curvature of the free energy lines is almost constant over the entire range, decreasing only about 15% between 30°C and 170°C. There is no noticable abrupt change of curvature for the material in the cubic phase.

Figure 48 is a construction of a relative free energy diagram using the above curvatures and the free energy differences found earlier. In drawing this diagram only the entropy difference relative to the entropy of the FE phase at 100°C has been used. Therefore to obtain the true free energy differences from this state a further slope equivalent to the absolute entropy of the FE phase at 100°C must be superimposed on each of the curves. From this it can be seen that the variation of free energy with temperature completely dominates all other variations in all three phases and that the differences in free energies between the phases are quite minor compared to this variation.

In order to show a free energy relationship explaining the experimental findings Figure 49 can be used. In this figure the free energies of the AFE and PE phases have been plotted relative to that of the FE phase at all temperatures. The phase relationship pictured is for zero pressure and field. The FE-AFE equilibrium point has been set at 125°C to be consistent with the hysteresis observed in Figure 10. The AFE-PE equilibrium has been placed at the Curie temperature observed with rising temperature because of the small hysteresis connected with this transition.

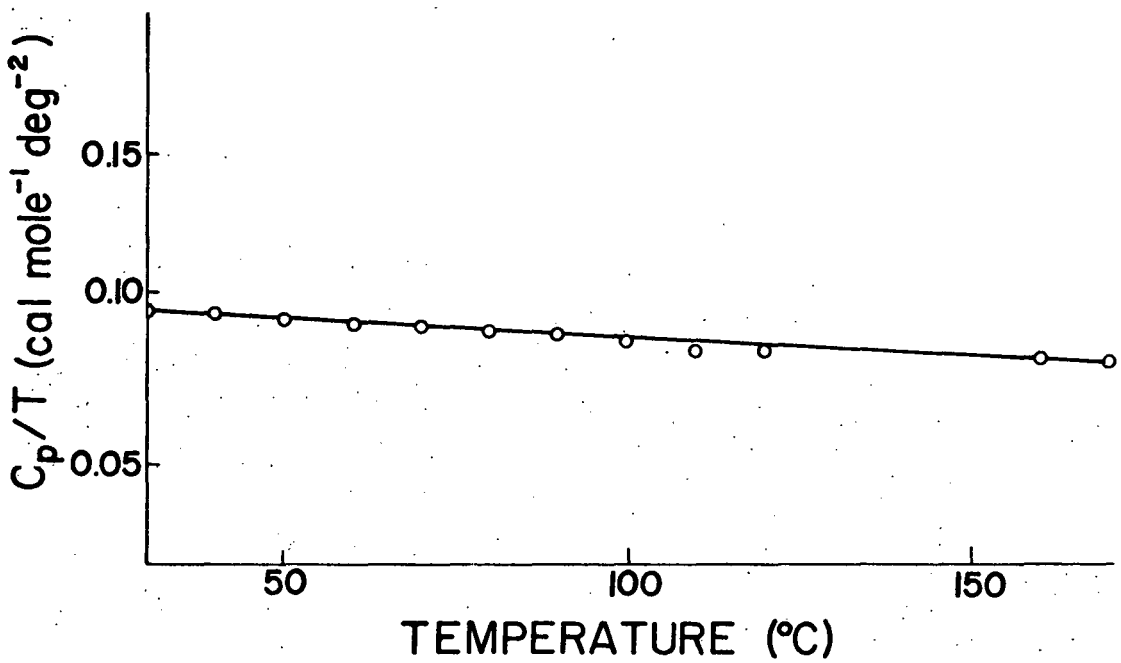

Figure 47. C_p/T for PZST Sample.

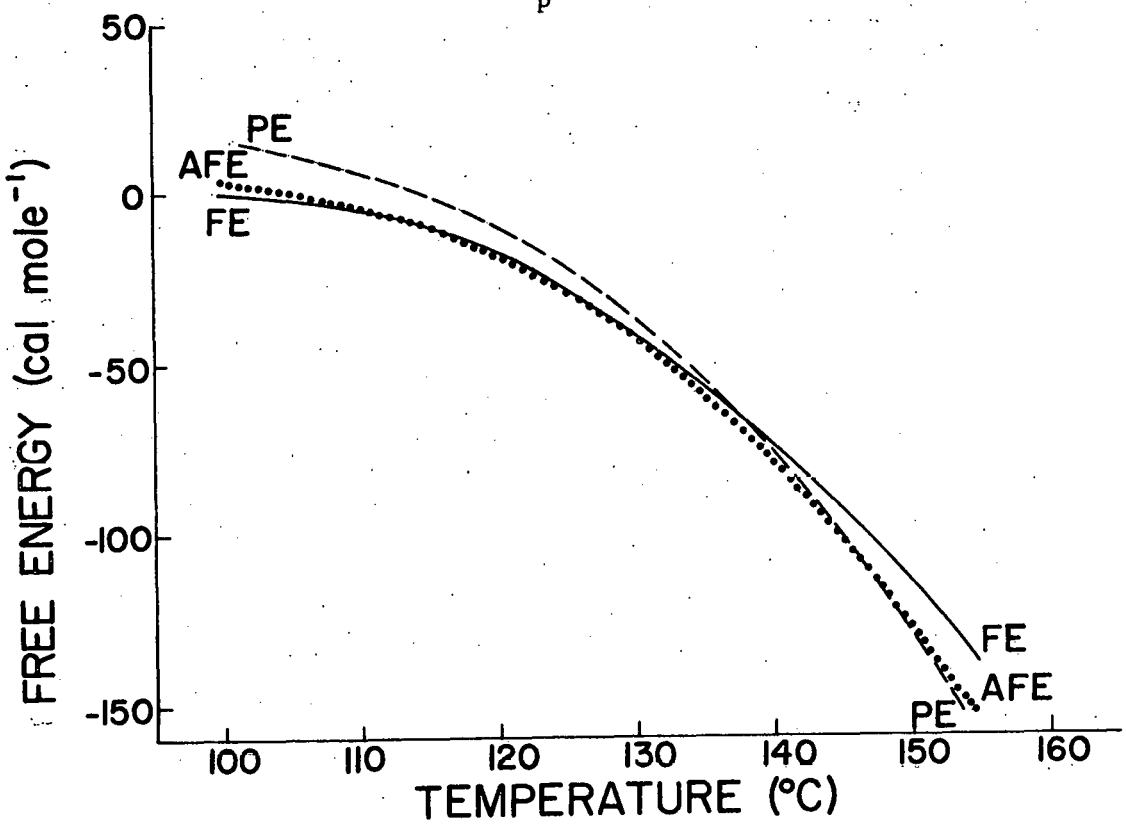

Figure 48. Free Energy vs. Temperature for PZST. (Relative to FE Phase at 100°C)

Lines have been drawn at the observed FE-AFE and AFE-FE transitions in order to indicate the free energy differences present at the temperatures at which these transitions occur. The free energy difference is approximately 0.10 cal/mole at the FE-AFE transition and nearly 1.75 cal/mole at the reverse transition.

Figure 50 represents the relative free energies at a field of 5 Kv/cm. This field lowers the free energy of the FE phase approximately 1 cal/mole relative to the other phases and lowers the PE phase line slightly with respect to the AFE phase line. Here the AFE-FE transition is observed at a temperature corresponding to about 1.25 cal/mole. The FE-AFE transition occurs at a temperature where the PE phase becomes energetically competitive, leading to the possibility of a blending of the transitions. At fields greater than about 7 Kv/cm the AFE phase disappears completely since the junction of the FE free energy curve and the PE free energy curve occurs below the AFE free energy curve.

From this treatment it can be seen that although the absolute values of the free energies cannot be calculated exactly and approximations must be made in order to calculate the free energy differences between the phases, the behavior of the relative free energies of the various phases leads to an explanation of the dependence of transition temperature and hysteresis on the external electric field.

Results for the Lead Hafnate Titanate Samples

As has been pointed out previously, the lead hafnate titanate samples gave less quantitative information regarding free energies since the transitions tended to be more diffuse. Thus a quantitative discussion of the relative free energies of these materials would not be productive with the present results. Qualitatively, the fact that AFE-FE transitions have been induced at temperatures as much as fifty degrees below the normal

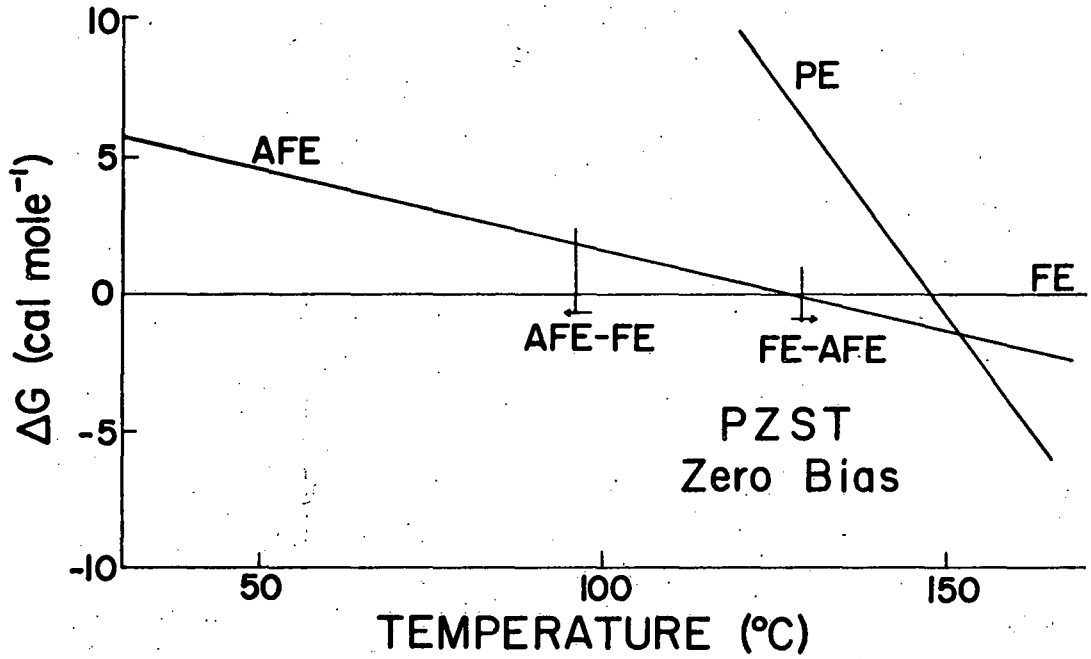

Figure 49. Relative Free Energies of the Various Phases for a PZST Sample at Zero Field.

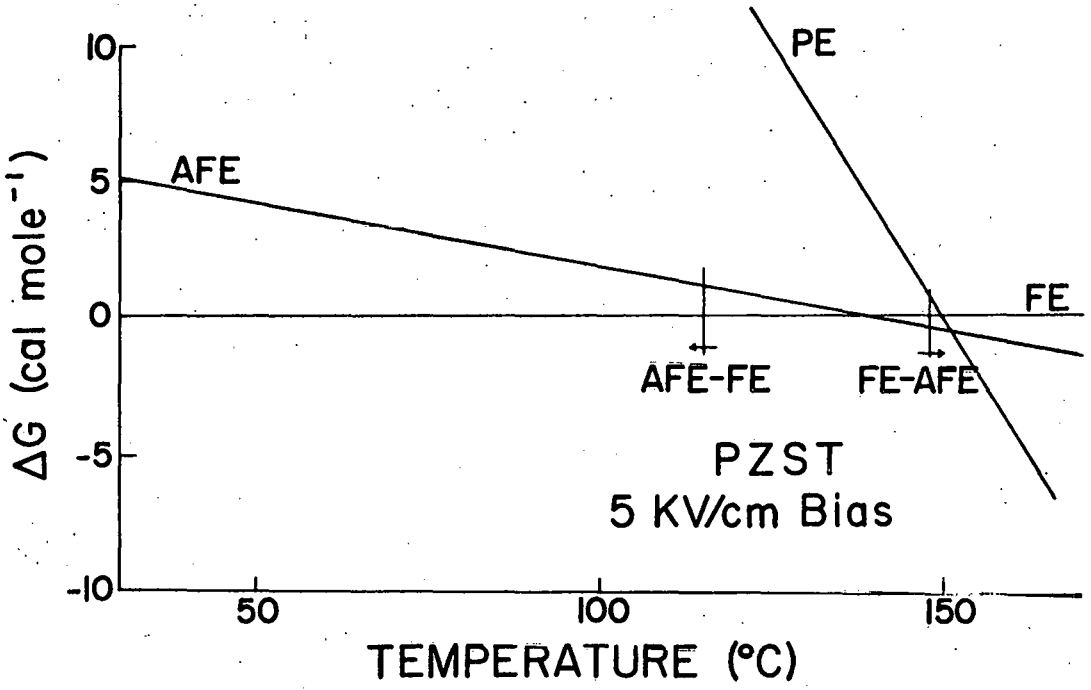

Figure 50. Relative Free Energies of the Various Phases for a PZST Sample with External Field of 5 KV/cm.

transition temperature shows that the phases are more nearly equal in free energy than corresponding phases in the PZST material. Thus, in these materials too, the free energies and entropies of the FE and AFE phases differ only very slightly.

Qualitative Theory of FE-AFE Transitions in Lead Perovskites

From the preceding discussions it appears that the reversal of the direction of phase transformation with rising temperature in these ferroelectric materials does not represent a drastic difference in the thermodynamic character of the material but rather a relatively minor difference which changes the delicate balance of thermodynamic parameters from one mode of behavior to another. Regardless of whether the transition with rising temperature is FE-AFE or AFE-FE, both the free energies and the entropies of the two phases are nearly equal under conditons of room temperature, atmospheric pressure, and zero electric field. If the free energy of the FE phase is lower than that of the AFE phase at room temperature and the entropy of the FE phase is higher than that of the AFE phase, the FE phase will prevail at all temperatures between room temperature and the Curie temperature. If the entropy of the AFE phase happens to be greater than that of the FE phase, there is a possibility that the AFE phase will become energetically favorable below the Curie temperature and an FE-AFE phaze transition may occur. Likewise, a room temperature dominance of the AFE phase coupled with a slightly higher entropy in the FE phase leads to the possibliity of an AFE-FE transition. Since the free energies involved are small, the entropy differences necessary are extremely minute.

It is interesting hereto compare the energies associated with the FE-AFE transitions with those observed in other common transformations. Chemical transformations are accompanied by energy changes of the order of 10^4 to 10^6 calories per mole. For example, the heat of combustion of carbon

is about 8000 calories per gram, or 100,000 calories per mole. Changes of state normally involve changes of energy two orders of magnitude smaller than this. For example, the energy change during the melting of ice is about 1440 calories per mole. Thus it can be seen that the energy differences involved in FE-AFE transformations (about 10 calories per mole) are quite small when compared with most transformation energies.

By using the above considerations, the relationship between the FE and AFE phases with regard to free energy and entropy may be outlined for the lead perovskite compositions used in this study.

In both pure lead zirconate and pure lead hafnate, the AFE phase is the phase of minimum free energy. The free energy difference between the FE and AFE phases at room temperature is great enough that differences in entropy cause no AFE-FE phase transformations below the Curie temperature. However, the difference between the zirconium ion and the hafnium ion is great enough to cause a difference in the entropy relationships between the two phases. In lead zirconate the entropy of the FE phase is greater than that of the AFE phase, while in lead hafnate the opposite is true. These differences are brought out by the addition of the titanium ion. The addition of a small amount of titanium to lead zirconate produces a situation in which the AFE phase is still dominant at room temperature but the larger FE phase entropy can lead to an AFE-FE phase transformation at higher temperatures but before the paraelectric phase becomes dominant. In lead hafnate, on the other hand, certain amounts of titanium ion produce a condition in which the FE phase is dominant at room temperature but the higher entropy of the AFE phase causes an FE-AFE transformation to take place below the Curie temperature. Thus, this small entropy difference between the phases in the two materials produces radically differing behavior.

The addition of a small amount of stannate ion to lead zirconate titanate increases the entropy of both phases but affects the AFE phase more than the FE phase, causing the AFE phase to become the phase of highest entropy. Again when enough titanate ion is available to cause the FE phase to be only slightly dominant at room temperature, the greater entropy of the AFE phase is sufficient to cause an FE-AFE transformation to occur at higher temperature. Thus the behavior of this material is found to be similar to that of lead hafnate titanate rather than lead zirconate titanate.

This behavior of the FE and AFE phases would therefore seem to emphasize that the only drastic difference between the two phases is in the electrical properties. The fact that the unit cell polarizations sum in the case of ferroelectric materials and cancel in antiferroelectrics leads to large variations in behavior with only minor structural and energy differences. This in turn explains the great influence that structural and thermal parameters exert on the observed properties of these materials.

Resume of Experimental Techniques

Dielectric Measurements

The most important results of the dielectric portion of this study lie in the use of the equivalent conductance as a technique for the study of FE-AFE phase transitions and in the measurement of the dielectric saturation associated with the peaks of dielectric constant in the vicinity of the Curie transition.

As has been pointed out previously, the use of equivalent conductance in the place of the more conventional tan δ allows a truer observation of the actual loss mechanism in the dielectric material. By eliminating the effects of the rapidly changing dielectric constant in the vicinity of a

transition, it becomes easier to distinguish the various types of transformations which occur and allows a better estimate of transition temperatures.

The effect of dielectric saturation at high electric fields has a pronounced bearing on the application of these materials in thermal-to-electric energy conversion. The highest dielectric constants observed in this study were found under triple point conditions, that is, near that temperature and field at which the FE, AFE, and cubic phases show nearly equal free energies. Unfortunately, this is also the region where the dielectric constant is most degraded by the application of a further electric field. Thus the conversion efficiencies and amplifications to be gained by thermally changing the dielectric constant are lessened and stability becomes a problem. Because of the absorption of charge in the unit cells of the FE phase as the temperature of the material decreases from the Curie temperature, it seems that the best amplification characteristics will be found by using the change of dielectric constant of an AFE material in these parametric devices. Results of the present study indicate that amplifications of three to five should be possible with the present materials.

Thermal measurements

This study has indicated that while thermal measurements are much less sensitive than electrical measurements in the vicinity of an FE-AFE transition, they nevertheless reveal valuable information concerning the energy relationships between the phases. The interpretation of thermal data with regard to accurate determination of excess specific heat and heats of transition will require further study with improved ceramics and single crystals. As was pointed out earlier, in this study only the excess heat occurring in the spike at the transition was used in calcu-

lating heats of transition and transition entropies. Materials exhibiting sharper transitions should cause these peaks to be more pronounced and thus give more accurate results.

A final result of this study is the indication that in many cases, what has been considered as a single phase sample may actually contain two or more phases coexisting over a temperature range which extends many degrees away from the "transition temperature". One cause of this behavior lies in the ceramic nature of the material with the accompanying stresses and variations of particle size and texture. Another cause probably lies in the lack of true chemical homogeniety throughout the samples. Since the electrical character of these materials shows such a strong dependence on structural characteristics, very slight compositional variations will spread transitions appreciably, causing a blending of transition characteristics when more than one transition is occurring in any small temperature region. As material processing techniques are improved, the experimental techniques described in this report will allow much information to be gained about the thermodynamic characteristics of FE-AFE phase transitions in lead perovskites.

BIBLIOGRAPHY

A1 Anderson, J. A., Rept. Nat. Res. Council, April (1918).

B1 Buerger, M. J., "Crystallographic Aspects of Phase Transformations", Phase Transformations in Solids, John Wiley & Sons, New York (1951).

B2 Berlincourt, D. A., Research on Piezoelectric Materials and Phenomena, Annual Progress Report (1961).

B3 Berlincourt, D. A., Research on Piezoelectric Materials and Phenomena, Fifth Progress Report (1961).

B4 Berlincourt, D. A. and H. H. A. Krueger, Phase Transitions in $Pb(Zr, Sn, Ti)O_3$ Compositions (1962).

C1 Cady, W. G., Rept. Nat. Res. Council, May (1918).

C2 Cross, L. E. and B. J. Nicholson, Phil. Mag. 46, 453 (1955).

D1 Devonshire, A. E., "Theory of Ferroelectrics", Advances in Physics 3, 85 (1954).

D2 Dauphinee, T. M. and S. B. Woods, Rev. Sci. Instr. 26, 693 (1955).

D3 Dungan, R. H. and A. H. Stark, Investigation of Solid Solutions in the Antiferroelectric Region of the $PbHfO_3$-$PbTiO_3$-$PbNb_2O_6$ System, Sandia Corporation Technical Memorandum 224-62(11) (1962).

G1 Goodman, G., J. Am. Ceram. Soc. 43, 105 (1960).

H1 Hall, C. A., Preparation and Investigation of Solid Solutions in the High Hafnate Region of the $PbHfO_3$-$PbNb_2O_6$-$PbTiO_3$ System, Sandia Corporation Technical Memorandum 21-62(11) (1962).

H2 Hall, C. A., personal communication.

H3 Hall, C. A., Ph.D. dissertation, University of Illinois, 1962.

J1 Jaynes, E. T., Ferroelectricity, Princeton University Press, Princeton, (1953).

J2 Jona, F. and G. Shirane, Ferroelectric Crystals, The McMillan Co., New York (1962).

J3 Jaffe, B. R., S. Roth, and S. Marzullo, J. Res. Nat. Bur. Stand. 55, 239-254 (1955).

K1 Kanzig, W., "Ferroelectrics and Antiferroelectrics", Solid State Physics 4, 1-197, Academic Press, Inc., New York (1957).

M1 Megaw, H., Ferroelectricity in Crystals, Methaen and Co., Ltd., London (1957).

M2 Megaw, H. D., Acta Cryst. 7, 187 (1954).

R1 Roth, R. S., J. Research Nat. Bur. Stand. 58, 75 (1957).

S1 Sachse, H., Ferroelectrika, Springer-Verlag, Berlin (1956).

S2 Shirane, G., R. Pepinsky, and B. C. Frazer, Acta Cryst. 9, 131 (1956).

S3 Sanderson, R. T., Chemical Periodicity, Reinhold Publishing Co., New York (1960).

S4 Sawaguchi, E., J. Phys. Soc. Japan 8, 615 (1953).

S5 Shirane, G. and R. Pepinsky, Phys. Rev. 91, 812 (1953).

S6 Sawyer, C. and C. Tower, Phys. Rev. 35, 267 (1930).

S7 Sykes, C., Proc. Roy. Soc. 148, 422 (1935).

W1 Wells, A. F., Structural Inorganic Chemistry, Oxford University Press, London (1962).

THIS PAGE

WAS INTENTIONALLY

LEFT BLANK

SECTION B

DISPERSION OF DIELECTRIC CHARACTERISTICS

ABSTRACT

The frequency dependence of the dielectric parameters of some polycrystalline materials exhibiting ferroelectricity and/or antiferroelectricity was examined under varying conditions of temperature and static electric field. Work was performed in the frequency range from 10^2 to 10^5 cps on lead zirconate stannate titanate and lead hafnate titanate solid solutions. The dielectric constant and "equivalent conductance" were determined over a range of temperatures extending from 20^oC to 200^oC and up to field strengths of 8 Kv/cm although the most extensive measurements were made at room temperature and zero field. Both ferroelectric and antiferroelectric phases of the materials were investigated and the trends of the results compared.

The samples in general showed a loglinear decrease in dielectric constant with increasing frequency. The antiferroelectric samples displayed a decrease approximately one-third to one-half that of the ferroelectric materials. For all samples, the equivalent conductance values plotted on a log-log scale against frequency yielded a straight line with a slope of very nearly one, suggesting the presence of hysteresis-type losses. These variations with frequency could be altered in various degree by changing temperature or field. Using as a basis the apparent hysteresis-type loss mechanism, a model is proposed which explains the equivalent conductance results and also remains consistent with the dispersion in the dielectric constant. The model involves the concept of minute polarization reversals by domain wall motion. The results at varying temperatures and field strengths are also incorporated into the model. The experimental findings for both the ferroelectric and

antiferroelectric compositions show a great deal of consistency with the model, and with this as a foundation, it is suggested that perhaps the solid solution samples are neither purely ferroelectric nor purely antiferroelectric but rather a combination of the two phases with one more dominant.

TABLE OF CONTENTS

Chapter		Page
I.	INTRODUCTION	1
	Definitions of Terms	1
	Selected Background	4
	Nature of the Present Investigation	10
II.	DESCRIPTION OF SAMPLES	12
	Introductory Statements	12
	Lead Zirconate Stannate Titanate	13
	Lead Hafnate Titanate	13
III.	INSTRUMENTATION AND PROCEDURE	17
	General Considerations	17
	Measurement Technique	20
	Bias Measurements	24
	Sample Holder Assembly	26
IV.	RESULTS	29
	Zero Bias Measurements	29
	Bias Measurements	35
	Poled Sample Measurements	39
V.	DISCUSSION AND CONCLUSIONS	43
VI.	AREAS FOR FURTHER STUDY	56
BIBLIOGRAPHY		60

LIST OF TABLES

Table		Page
I.	List of Samples	15
II.	Comparison of Power Supply Values to Actual Values.	25

LIST OF FIGURES

Figure		Page
1.	Ferroelectric Hysteresis Loop	2
2.	The Perovskite Structure	12
3.	Phase Diagram for PZST-6	14
4.	Ferroelectric Equivalent Circuit	18
5.	Vector Representation	18
6.	Block Diagram of Assembly for Zero Bias Measurements	20
7.	Simplified Bridge Circuit	22
8.	Block Diagram of DC Bias Measurement Assembly	24
9.	Sample Holder Assembly	27
10.	Typical Result of Dielectric Constant versus Measuring Frequency	30
11.	Results for Samples at Room Temperatures and Zero DC Field	32
12.	Typical Equivalent Conductance Curves at Zero DC Field	33
13.	Results of Varying AC Measuring Field Strength with Zero DC Bias	36
14.	Typical Bias Measurement Results	37
15.	Dielectric Parameters as Functions of DC Field Strength	38
16.	Resonance in PZST-6 at Room Temperature	40
17.	Resonance in 95 HN at Room Temperature	41
18.	Relaxation Equivalent Circuit	43
19.	Resonance Equivalent Circuit	44
20.	Domain Wall Motion Switching Model	46
21.	Vector Diagram Showing Components of Total Polarization	48

22. Polarization Components Plotted on a P-E Diagram 48

23. Equivalent Conductance Curves Showing the Presence of Joule Losses 58

CHAPTER I

INTRODUCTION

Definitions of Terms

A ferroelectric material may be defined as one which shows both a spontaneous electric polarization and hysteresis effects in the relation between dielectric displacement and electric field. Such anomalous behavior is normally observed within specific temperature regions, above which the material displays a normal dielectric behavior and no longer possesses a spontaneous polarization. This upper temperature point has come to be called the Curie temperature (or Curie point) and above it the material is said to be "paraelectric". The terms "ferroelectric", "Curie point" and "paraelectric" originate from the similarity of behavior between ferroelectrics and ferromagnetics and, although the physical causes of their behaviors are quite different, they have been carried over from the study of ferromagnetics.

Above the Curie point the paraelectric (or non-polar) phase obeys a Curie-Weiss law,

$$\epsilon = \epsilon_o + \frac{C}{T - T_o}$$

where C is the Curie constant and T_o the Curie-Weiss temperature. In the vicinity of the Curie-Weiss temperature the dielectric constant becomes very large. For a second order phase transition from the ferroelectric (polar) phase to the non-polar phase, the Curie temperature (T_c) and Curie-Weiss temperature (T_o) nearly coincide, but for materials which undergo first order phase changes, T_o and T_c do not coincide.

Within a ferroelectric material, alignment of the electric dipoles may extend over only a portion of the material, while another region may possess dipoles aligned in some other direction. A region in which the spontaneous polarization is all in the same direction is said to be a domain. Different domains are separated by walls, and in the tetragonal ferroelectric perovskites such as barium titanate, these are generally referred to as 90° or 180° domain walls. Basically, a 180° wall is one in which the polarizations on either side of the wall are antiparallel, and a 90° wall exists when the polarizations on either side are normal to each other. In the latter case the positive end of one domain must be perpendicular to the negative end of the second domain, since there can be no charge existing on the domain wall itself.

A typical ferroelectric hysteresis loop is illustrated in Figure 1. At the origin, O, the domains are oriented so that the net polarization

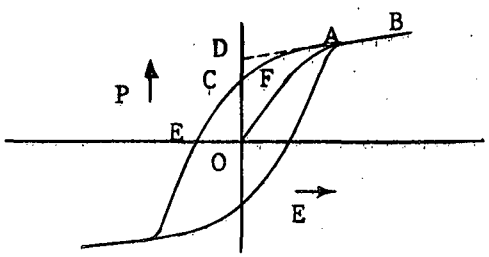

Figure 1. Ferroelectric Hysteresis Loop

is zero. As the field is increased, the domains tend to align with the field until at portion AB all the domains are aligned to form one single domain and a state of saturation exists. As the field is reduced to zero, some domains remain aligned in their previous direction and so the polarization does not go to zero. Thus there exists a remanent polarization indicated in the figure as OC. The linear portion AB of the curve extrapolated back to the polarization axis represents the spontaneous polarization P_s (OD) of the material. The value of the field required to

reduce the polarization to zero is called the coercive field E_c (OE).

In addition to the ferroelectric materials, there exists a group of materials in which neighboring dipoles are antiparallel. Such materials are said to be "antipolar" in comparison to those which are called "polar" where neighboring dipoles are parallel. A substance which exhibits such an antiparallel dipole array is said to be antiferroelectric. A more formal definition of an antiferroelectric material is "an antipolar material whose free energy is comparable to that of a polar material" (J1). The problem of antiferroelectricity has received general treatment by Känzig (K1) and Forsbergh (F1).

Prior to the last decade, the most extensive investigations were done on three ferroelectric materials: Rochelle salt, potassium dihydrogen phosphate, and barium titanate. Recently many new ferroelectrics and antiferroelectrics have been discovered. As Jona and Shirane (J1) mention in their book, however, "our knowledge of the basic phenomenon has not been appreciably enhanced."

Some of the more notable works in the literature providing reviews of ferroelectric properties and problems involved in the field of ferroelectricity are given in references F1, J1, K1, K2, and M1. The reader is referred to these works for a more complete discussion of ferroelectrics and antiferroelectrics.

In the study of ferroelectrics the dielectric constant has played an important role. The dielectric constant k is normally defined as the derivative of the electric displacement D, with respect to the field E, or

$$k = \frac{\epsilon}{\epsilon_o} = \frac{1}{\epsilon_o}\frac{dD}{dE} ,$$

From the relationship (in MKS units),

$$D = \epsilon_o E + P$$

one can obtain the susceptibility χ, defined as

$$\chi = \frac{1}{\epsilon_o} \frac{dP}{dE}$$

or

$$\chi = k - 1.$$

In the vicinity of a Curie point, or where ever k is much greater than one, the susceptibility and dielectric constant become nearly equal, or

$$k = \frac{1}{\epsilon_o} \frac{dD}{dE} \doteq \frac{1}{\epsilon_o} \frac{dP}{dE} .$$

Selected Background

Since the dielectric constant exhibits an anomaly at the transition temperature between structural phases, it is usually measured as a function of temperature and/or field. Less emphasis has been placed upon measurements of dielectric characteristics as a function of frequency. Those studies which have been done were almost exclusively performed on barium titanate -- probably since it was one of the first ferroelectrics to display striking characteristics, was relatively easy to produce, and showed excellent commercial possibilities.

Such an early investigation of dielectric constant as a function of frequency was done by Roberts (R1) on polycrystalline barium titanate. Roberts found no pronounced anomaly in dielectric characteristics within the frequency range 0.1 to 25 megacycles per second. He found a piezoelectric resonance, however, when the samples were polarized in a strong electric field.

Had Roberts extended his measurements into the microwave range, he would have discovered a relaxation spectrum as did von Hippel and Westphal (V1) and later Powles and Jackson (P1). The important feature

of this relaxation is an abrupt decrease in dielectric constant by more than an order of magnitude, beginning near 10^8 cycles per second and tapering off past 10^{10} cycles per second.

Kittel (K3) was one of the first to propose a workable, qualitative explanation of this phenomenon. He introduced the idea that the observed dispersion was due to processes of domain wall displacement. A domain wall displacement, in a direction perpendicular to the wall, will increase or decrease the effective polarization parallel to the wall. Recently Sannikov (S1) has presented a more rigorous approach considering the frequency dependence of the dielectric constant associated with domain wall displacements. Sannikov's expression for the complex electric susceptibility χ^* is

$$\chi^*(\omega) = \frac{\chi_0 \omega_0^2}{\omega_0^2 - \omega^2 + j(\omega_r + \omega_r')\omega} .$$

In this equation ω_0 $(=2\pi f_0)$ is the resonance frequency of the material, ω_r and ω_r' are two ionic damping frequencies, $\omega(=2\pi f)$ is the frequency of the applied field and χ_0 is the susceptibility at $\omega = 0$ and is related to the resonance frequency by

$$\chi_0 = \frac{4P_0^2}{lM\omega_0^2} .$$

In this expression P_0 is the static polarization in the uniform ferroelectric, l is the mean domain width, and M the effective mass of the domain wall. Although Sannikov's result is valid only for ferroelectrics which undergo second order phase changes into the nonpolar phase and assumes domain walls undergo only small distortions, it yields satisfactory numerical results for the observed phenomena in barium titanate.

It is desirable to know more about the phenomenon which takes place when the polarization is reversed from one direction to another (switching).

A potential means of obtaining information about this process is by making dielectric constant measurements (since $k \propto dP/dE$) while the sample is being simultaneously switched by a slowly varying biasing field (sweeping field).

One of the earliest of such experiments was done by Drougard and Young (D1), who subjected a single crystal of barium titanate to a low amplitude audio frequency sine wave to measure the dielectric constant and at the same time imposed a slowly varying field to produce switching. Drougard and Young regarded their results, among other things, as giving no indication of domain walls moving to any appreciable extent in response to the audio frequency field.

Similar investigations by Drougard, Funk and Young (D2) studied the dielectric characteristics as a function of measuring frequency, sweeping frequency, sweeping voltage and the rate of switching polarization (current). They found that the measuring frequency and the switching current were both significant variables. At constant switching current, the real part of the complex dielectric constant, k' #, showed a strong frequency dependence, decreasing as the measuring frequency was increased. This frequency dependence was described by a Debye relaxation type of spectrum,

$$k^* = \frac{\epsilon^*}{\epsilon_0} = k_\infty' + \frac{a}{1 + j\omega T}$$

where k^* is the complex dielectric constant and T is the relaxation time. The real part of the dielectric constant is given by

$$k' = k_\infty' + \frac{a}{1 + \omega^2 T^2} .$$

For single crystals of barium titanate and at various switching current

The complex dielectric constant is discussed fully in Chapter III.

densities the value of T was around 5.2 - 5.5 microseconds.

Merz (M2) also did extensive study on the switching process. He found experimentally that at low fields, the rate at which the polarization reverses itself is proportional to $\exp(-\alpha/E)$, where α is a temperature dependent quantity, and E is the applied field. In other words, the field at which a crystal will switch its direction of polarization depends on the time that is allowed for the switching, or more simply, the rate at which the hysteresis loop is traversed determines the shape of the loop. Using Merz's exponential law as a basis, Landauer, Young and Drougard (L1) assumed the rate at which polarization is reversed may be given by

$$\frac{dP}{dt} = F(P)\exp(-\alpha/E(t)),$$

where F(P) permits the switching rate to depend on the extent to which the crystal has already reversed its polarization as well as on the field. Making several assumptions concerning the functions F(P) and E(t) this equation was integrable and gave rise to a family of curves showing the dependence of the coercive field of barium titanate on the rise rates and the applied field. The results of Drougard, Funk and Young (D2) are thus partially explained by the work of Landauer, Young and Drougard using Merz's exponential law, but the question of whether $\exp(-\alpha/E)$ was a rate of domain nucleation (formation of new domains) or a rate of domain expansion remained essentially unanswered.

The increase in dielectric constant during switching as found by Drougard, Funk and Young was also investigated by Fatuzzo (F2) who, in addition to observing their low frequency relaxation, also discovered a new relaxation above 2×10^9 cycles. These relaxations were also present in triglycine sulfate, another ferroelectric. Fatuzzo's model attributes

the increase in dielectric constant and losses to oscillations of the "side" walls of the domains in the case of the high frequency relaxation, but in the case of the lower frequency relaxation, to oscillations of "front" walls of the newly formed domains. The model proposed agrees well with the experimental results.

In general, a ferroelectric domain is said to grow through (1) forward domain wall motion in which case the wall moves in the direction of the ferroelectric axis (2) sideways domain wall motion where the wall moves in a direction perpendicular to the ferroelectric axis, or (3) by a combination of these two.

Little (L2) studied the dynamic behavior of domain walls in barium titanate single crystals by optical techniques. She observed the 180° walls moving perpendicular to the polar axis, an effect Merz did not perceive. It was found from electrical measurements that the equivalent susceptibility was strongly dependent upon both measuring field strength and frequency, in agreement with Drougard, Funk and Young (D2). The dependence upon frequency was attributed to the optically observed domain wall motion which damped out around 10^4 cycles per second. Little also concluded that 180° domain walls did not move sideways in reasonable laboratory times with fields less than 2.4 kilovolts per centimeter (kv/cm).

Chynoweth (C1), studying ferroelectric Barkhausen pulses in barium titanate, theorized that a Barkhausen pulse could arise from the nucleation and growth through the thickness direction of a domain. Since the charge represented by the Barkhausen pulse accounted for only 0.1 to 1 per cent of the total charge required for complete polarization reversal, Chynoweth proposed a further growth of these domains through sideways expansion, hence accounting for the entire charge.

Although the experimental investigations mentioned thus far have been varied in technique and conclusions, they were all similar in that they were performed with metal electroded samples. In order to eliminate internal stresses and deformations caused by metal electrodes, Miller (M3) used single crystal barium titanate samples with aqueous LiCl electrodes. The samples were observed to undergo polarization reversal with electric fields of several hundreds of volts per centimeter, a value much less than that quoted by Little. Miller ascertained that polarization reversal can take place by extensive sideways motion of a few 180° domains. In addition it was found that polarization reversal could be accomplished with few or even no Barkhausen pulses, and that Barkhausen pulses occurred when two growing domains came together.

Using the same techniques, Miller and Savage (M4, M5) have done extensive investigation of the dynamics of domain wall motion as a function of temperature and field. They have also studied carefully the geometry of individual domains and have proposed a model for the mechanism by which the boundary moves. Later work by Miller and Savage (M6, M7) included the investigation of 180° domain wall motion with metal electroded barium titanate crystals. Wall velocities were studied as functions of electric field, crystal thickness and impurity content added to the crystal growth melts. Generally the dependence upon field was the same as that found for the liquid electrode studies, but the pronounced dependence upon sample thickness was attributed to nonferroelectric surface layers adjacent to the metal electrodes. Miller and Savage expanded on a surface layer model proposed by Drougard and Landauer (D3) to explain the switching speed dependence upon sample thickness as observed by Merz (M8).

The effect of such a surface layer would be to reduce the applied field E to a value E_b in the bulk of the material. Since the surface layer is assumed to have a low dielectric constant, an appreciable part of the applied voltage appears across it. From this it can be seen that the thinner the crystal, the more important the surface layer becomes. There is a considerable amount of disagreement as to the thickness and dielectric constant of the layer, but the values proposed by Savage and Miller are perhaps the most consistent with experimental results. They estimate the thickness to be of the order of 100 Angstroms and the dielectric constant to be about 100.

In light of a number of theoretical and experimental observations, Gerson (G1) reasoned that the dielectric constant of ferroelectrics should increase at very low frequencies since there should be a contribution to the dielectric polarization due to switching. Using lead titanate zirconate ceramics, he determined the dielectric properties in the frequency range 0.1 to 10 cycles per second. A slight increase in dielectric constant was observed but this was interpreted as an effect due to interfacial polarization rather than an effect due to ferroelectric switching.

Nature of the Present Investigation

The purpose of this study has been to determine if there exists any frequency dependence of the dielectric characteristics in lead hafnate titanate and lead zirconate stannate titanate compositions within the frequency range 10^2 to 10^5 cycles per second and if possible to correlate the observed behavior with the previous experimental studies mentioned. Another interesting aspect to consider here is that the dielectric

behavior of antiferroelectric materials as well as ferroelectric materials was studied in hopes of gaining further insight into the characteristics of this class of substances.

CHAPTER II

DESCRIPTION OF SAMPLES

Introductory Statements

All the samples employed in this work were polycrystalline (ceramic) solid solutions of various members of the perovskite family. The general formula of the compounds belonging to this family is ABO_3. In the formula A is a monovalent, divalent or trivalent metal and B is a penta-valent, tetravalent or trivalent metal respectively. The ideal perovskite structure is illustrated in Figure 2. A complete and comprehensive

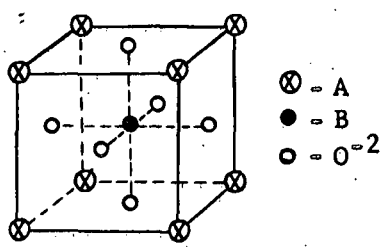

Figure 2. The Perovskite Structure

discussion of the perovskite-type oxides, their solid solutions and the related phenomenon of ferroelectricity is given by Jona and Shirane (J1).

All samples were furnished by Sandia Corporation and with the exception of PZST-6 were prepared by C. Hall of that corporation. The samples were solid solutions of lead hafnate titanate and lead zirconate stannate titanate. In addition all samples had Nb_2O_5 added (one per cent by weight). In general the effects of the niobia are to lower the coercive field of the sample by an appreciable amount and to raise its

resistivity by several orders of magnitude (B1). Gerson (G2) studied the variations in ferroelectric characteristics due to the addition of niobium and lanthanum, and concluded that this led to high mobility of domain walls.

Firing temperatures of the ceramics were from 1400 to 1430 ^{o}C. Silver electrodes were fired on the entire surface area.

Lead Zirconate Stannate Titanate

The majority of experimental work in this study was done on sample PZST-6 whose composition is $Pb(Zr_{0.68}Sr_{0.25}Ti_{0.07})O_3$. This sample was extremely well-behaved, exhibiting both a ferroelectric and an antiferroelectric phase and well defined transition regions. With zero electric field upon increasing temperature the sample exhibited ferroelectric properties up to 127 ^{o}C and became antiferroelectric from 127 ^{o}C to 151 ^{o}C. At 151 ^{o}C (the Curie point) the sample transformed into the paraelectric (cubic) phase. With decreasing temperature the antiferroelectric phase persisted down to 97 ^{o}C at which point the sample became ferroelectric once again. This composition in the ferroelectric phase has a rhombohedral unit cell structure, and in the antiferroelectric phase a pseudotetragonal structure. Figure 3 is a phase diagram of PZST-6 as a function of field and temperature (N1). Dimensions and density for the sample are recorded in Table I.

Lead Hafnate Titanate

Work was also carried out on various solid solutions of lead hafnate titanate. The composition $Pb(Hf_{0.95}Ti_{0.05})O_3$ was ferroelectric at temperatures below the Curie point (159 ^{o}C), while the compositions

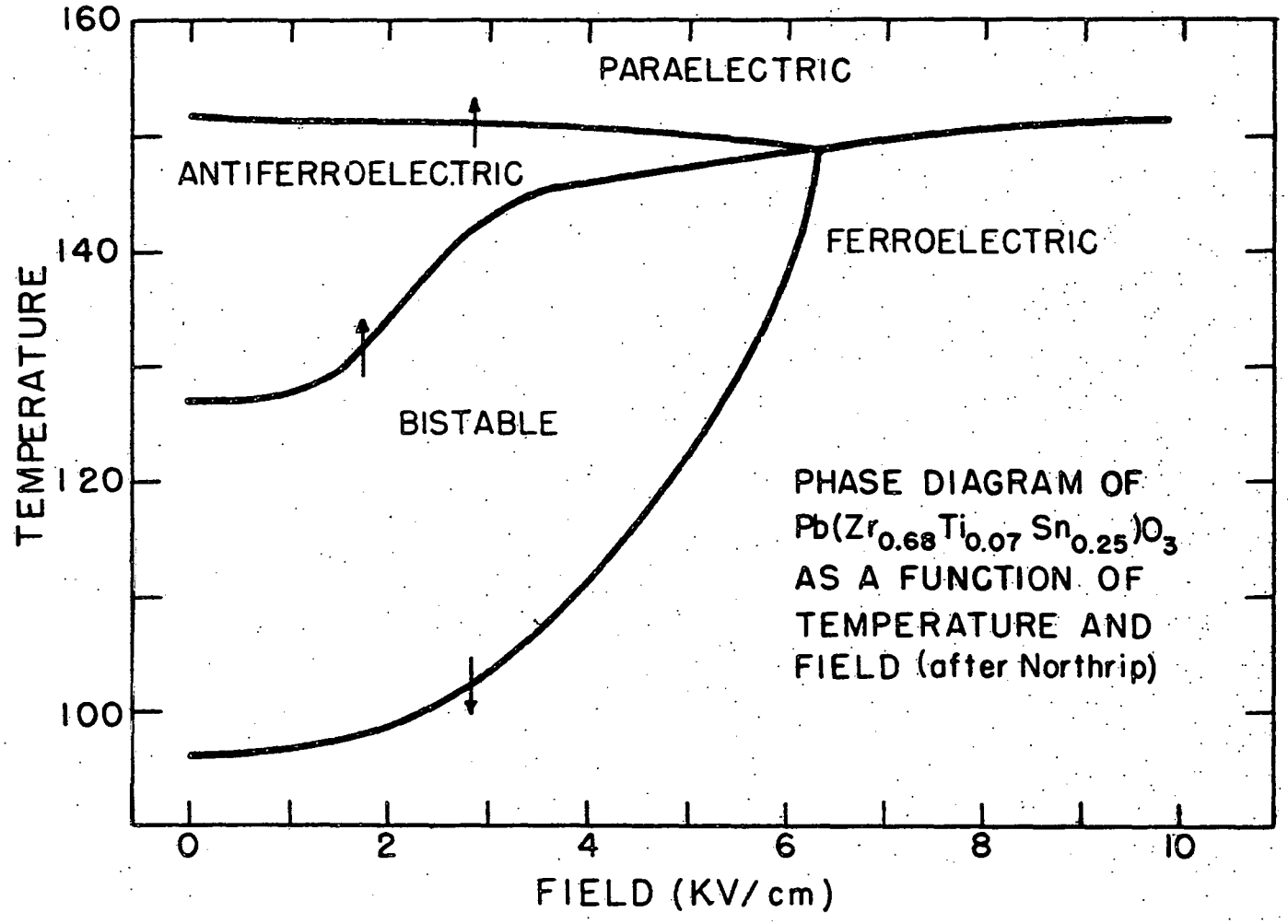

Figure 3. Phase Diagram for PZST-6

TABLE I

LIST OF SAMPLES

Sample	Composition*	Area (cm^2)	Thickness (cm)	Density (gm/cm^3)	Curie Temp. (^oC)
PZST-6	$Pb(Zr_{0.68}Sn_{0.25}Ti_{0.07})O_3$	1.986	0.174	7.94	151
95 HN	$Pb(Hf_{0.95}Ti_{0.05})O_3$	1.528	0.265	8.93	159
96 HN	$Pb(Hf_{0.96}Ti_{0.04})O_3$	1.577	0.209	9.00	164
97 HN	$Pb(Hf_{0.97}Ti_{0.03})O_3$	1.524	0.219	8.99	170
100 HN	$PbHfO_3$	1.579	0.175	8.99	170

*All compositions have one per cent by weight of Nb_2O_5 added.

$Pb(Hf_{0.97}Ti_{0.03})O_3$ and $PbHfO_3$ were antiferroelectric all the way to their Curie points. The composition $Pb(Hf_{0.96}Ti_{0.04})O_3$ showed traces of antiferroelectricity in a small temperature range at low fields and otherwise was ferroelectric. Northrip (N1) has done extensive work on the thermal and electrical properties of the lead hafnate titanate system and the reader is referred to his work for a more complete discussion of these compositions. Sample densities and dimensions are recorded in Table I.

CHAPTER III

INSTRUMENTATION AND PROCEDURE

General Considerations

A capacitor, connected to a sinusoidal voltage source

$$V = V_o \exp(j\omega t)$$

will store, with a vacuum dielectric, a charge

$$Q = C_o V.$$

C_o is called the geometrical (or vacuum) capacitance of the capacitor, and, fringing effects neglected, is equivalent to $\epsilon_o A/d$ where ϵ_o is the permittivity of free space, A the surface area of one capacitor plate, and d the distance between plates. In this case the charging current

$$I_c = \frac{dQ}{dt} = j\omega C_o V$$

$$= I_o \exp\left[j\left(\omega t + \frac{\pi}{2}\right)\right]$$

leads the voltage by a phase angle of 90°.

If the capacitor is filled with some substance, the capacitance increases to

$$C = C_o \frac{\epsilon'}{\epsilon_o} = C_o k',$$

where ϵ' and k' represent the real parts of the complex permittivity and dielectric constant respectively. In addition to the charging current there now appears a loss current, so that the total current is

$$I_t = I_c + I_l.$$

In other words, the capacitor can be characterized by a loss parameter as well as a capacitance parameter. This loss parameter is representable

as either a series or parallel resistance.

A ferroelectric is conventionally represented in parallel notation as the equivalent circuit of Figure 4. In the circuit, R_x represents

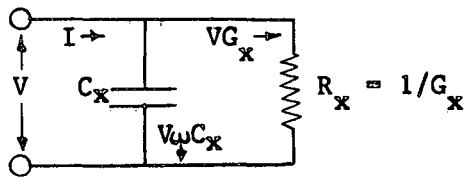

Figure 4. Ferroelectric Equivalent Circuit

the loss component (Joule heating, hysteresis losses, etc.) and C_x the pure capacitive component. The loss current therefore is expressible as

$$I_l = G_x V,$$

and so the total current traversing the capacitor is

$$I_t = (j\omega C_x + G_x)V.$$

A vector diagram for this equivalent parallel circuit is shown in Figure 5. In the figure θ is the phase angle and δ is the dielectric loss angle.

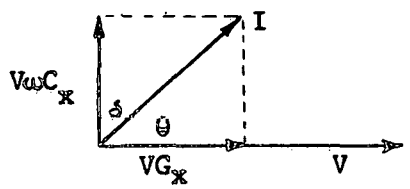

Figure 5. Vector Representation

Hence the dissipation factor D, defined as the cotangent of the phase angle is

$$D = \cot\theta = \tan\delta = \frac{G_x}{\omega C_x}.$$

It is customary to describe the charging current and the loss current by the introduction of a complex permittivity,

$$\epsilon^* = \epsilon' - j\epsilon'',$$

or a complex dielectric constant,

$$k^* = \frac{\epsilon^*}{\epsilon_0} = k' - jk'',$$

where ϵ'' and k'' are the loss factor and relative loss factor respectively.

The total current may now be written

$$I_t = j\omega C_0 k^* V,$$

and the loss tangent becomes

$$\tan\delta = \frac{\epsilon''}{\epsilon'} = \frac{k''}{k'}.$$

In the past, loss mechanisms in ferroelectrics have been recorded in terms of tan δ, since this value is usually directly readable or calculable from the measuring apparatus. However, as Northrip (N1) points out, this method of measuring losses gives a number which depends not only on the value of the loss current but also on the value of the capacitive current. In other words changes of tan δ are caused by both changes in loss mechanism and changes in capacitance. For ordinary dielectrics this creates no special problem but in ferroelectrics many regions of interest are accompanied by both changes in loss mechanism and very large changes in capacitance (e.g. near a Curie point). For this reason the loss tangent is not a particularly sensitive indicator of loss mechanism changes when dealing with ferroelectrics. Northrip has proposed the use of an "equivalent conductance" defined as

$$G_x = 2\pi f C_x \tan\delta.$$

The term "equivalent" denotes that all types of losses are considered.

A convenient aspect of the use of "equivalent conductance" rather than the loss tangent is that it permits corrections to be made with relative ease for losses and capacitances in the measuring system, since

conductances in parallel are additive. More will be said of this later in the chapter.

Measurement Technique

All measurements of capacitance and dielectric loss were made with a General Radio Capacitance Measuring Assembly Type 1610-A. This assembly is a general purpose capacitance bridge integrated with the necessary generator, amplifier and cables. It is possible to determine dissipation factor and equivalent series capacitance from zero to 1150 micromicrofarads ($\mu\mu$f) with this assembly over a frequency range from 30 to 10^5 cps. At a frequency setting of one kilocycle per second (kcps) the capacitance range extends to one microfarad. A block diagram of the assembly used for zero bias measurements is shown in Figure 6.

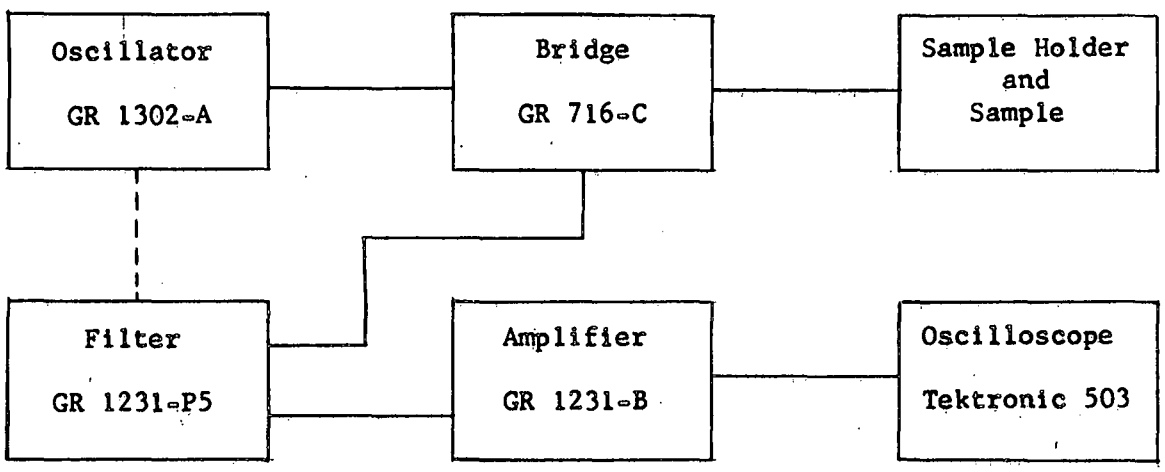

Figure 6. Block Diagram of Assembly for Zero Bias Measurements

The oscilloscope connected to the output of the 1231-B amplifier was used as a null detector to provide for a more sensitive balance of the bridge.

The frequencies at which the sample capacitance and loss could be most easily determined were dictated by the frequency settings on the General Radio Type 1231-P5 filter. These frequencies were 0.1, 0.2, 0.5, 1, 2, 5, 10, 20, 50, and 100 kcps. A frequency setting of 50 cps was also available, but sensitive bridge balance was hindered at this setting by low frequency ac pickup which could be attributed to the magnetic stirrer used in the sample bath as well as other stray 60-cycle noise. Occasionally it was necessary to substitute a Hewlett-Packard Model 200CD oscillator in place of the General Radio oscillator in order to achieve frequencies greater than 100 kcps. A sensitive bridge balance was possible to 200 kcps with the oscilloscope despite the upper frequency setting of 100 kcps on the filter.

Since measurements of capacitance greater than 1150 $\mu\mu$f were required over the frequency range from 10^2 to 10^5 cps, it was necessary to calibrate capacitors for use as external standards over this frequency range. An explanation of the use of these external standards as well as corrections made for them follows.

Consider Figure 7 which is a circuit diagram of the General Radio 716-C Capacitance Bridge. In this modified Schering bridge, C_n is the precision internal standard reading from 100 to 1150 $\mu\mu$f. C_a is the variable air capacitor and decade capacitor, which compose the dissipation factor controls. R_a and R_b are the ratio arms controlled by the range selector on the bridge. Equal ratio arms are provided at 0.1, 1, 10 and 100 kcps and multiplying factors of 10, 100, and 1000 are provided at 1 kc.

The previously mentioned external standards were used in parallel with C_n, and allowed measurements of capacitance greater than 1150 $\mu\mu$f to be made over the desired frequency range. In Figure 7 the calibrated

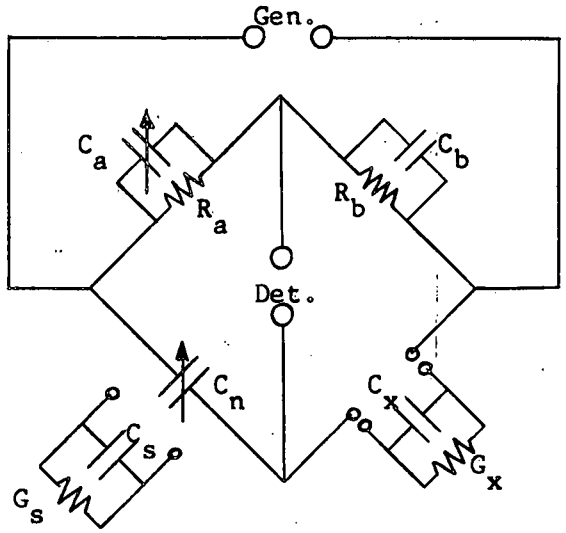

Figure 7. Simplified Bridge Circuit

external standard is represented in parallel notation as C_s and G_s. When an unknown capacitance (C_x, G_x) is balanced against C_n and the external standard the capacitance is given by

$$C_x = C_n + C_s.$$

The bridge, however, reads a value of the loss tangent that is not unique to G_x but rather to a value slightly less than the true value of G_x. The error induced is due to the loss factor of the external standard. The magnitude of this loss is of the order of the loss tangent of the internal standard, both being quite small, and so no corrections were made for either. This induced an error in the calculated value of G_x of less than 2 per cent of its actual value. The value of G_x is thus calculated from

$$G_x = 2\pi f C_x \tan \delta .$$

The use of external standards extended the effective capacitance range

to 0.01 μf, well over the values of capacitance of the samples used. Mica capacitors with values near 1000, 2000 and 5000 $\mu\mu$f were calibrated for use as external standards over the previously mentioned frequency range. Mica capacitors were used because of their relatively low loss.

The cable from the bridge to the sample holder, as well as the sample holder itself, also presented a capacitance and loss which required corrections. The capacitance and equivalent conductance of the cable and sample holder can be symbolized by C_c and G_c respectively. These are effectively in parallel with the sample so that the actual values of the unknown are

$$C_x = C_n + C_s - C_c,$$

and

$$G_x \doteq (C_x + C_c)\tan\delta - G_c.$$

The calculated value of G_x is still smaller by an amount less than 2 per cent of the actual value due to the loss in the external standard. The cable and sample holder, however, required calibration for capacitance and equivalent conductance over the mentioned frequency range.

Using this method of measurement, the capacitance could be determined to within ± 1 $\mu\mu$f and the dielectric loss to within ± 0.0008. These limitations are inherent in the bridge and external standards with this nature of measurement and exclude any errors due to environmental changes affecting the external system. The latter, however, are apparently small and may be considered negligible.

The output of the General Radio amplifier was non-linear over the three decade frequency range and so precautions were taken to insure that all measurements were made at the same measuring field strength. Over most of the frequency range the variation in measuring field strength was less than 10 per cent, and so induced no great error in the dielectric

constant measurements.

The dielectric constant is directly calculable from the capacitance using the relation

$$k' = \frac{C_x d}{\epsilon_o A},$$

where A, d and C_x are the sample surface area, thickness and capacitance respectively.

Bias Measurements

A block diagram of the assembly used for measurements with a biasing dc voltage impressed across the sample is depicted in Figure 8. A Beta 10 kilovolt dc power supply was used to provide biases up to 2000 volts across the sample.

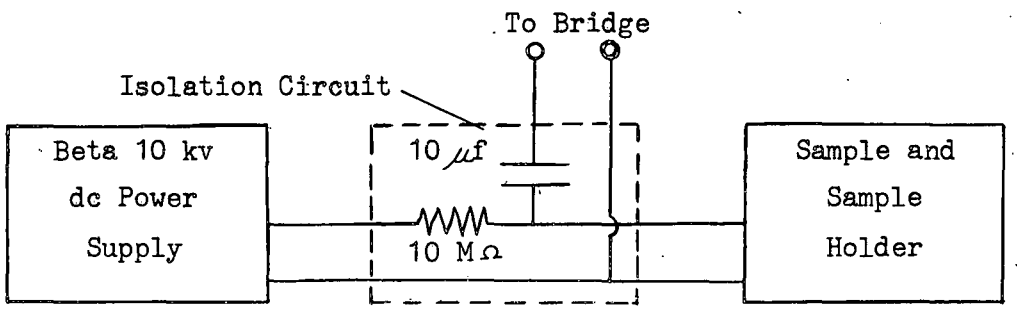

Figure 8. Block Diagram of DC Bias Measurement Assembly

The isolation circuit was employed to keep the dc off the bridge circuit as well as to effectively keep the ac measuring voltage across the sample. The 10 μf oil capacitor offered an ac impedance of the order of 10^3 to 10^5 times smaller than the sample impedance itself, over the entire frequency range. The isolation circuit caused some inconvenience in making the dc bias measurements in that it offered a 100 second time constant to the power supply. In other words, for the bias across the sample to read within one per cent of its final value, it was necessary to wait at least 5 time constants before taking a reading.

Although time consuming, this presented no special difficulty.

The power supply meter readings did not agree with the actual voltage impressed across the sample so it was convenient to make a table (Table II) showing both, together with the corresponding field strengths for that particular sample. The use of these tables allowed reproduction of settings with comparative ease.

TABLE II

COMPARISON OF POWER SUPPLY VALUES TO ACTUAL VALUES

Power Supply Meter Readings (volts)	Voltage Impressed Across Sample (volts)	Corresponding Field Strength (for PZST-6) (kv/cm)
100	98	0.56
200	199	1.14
300	280	1.61
400	375	2.16
500	480	2.76
600	560	3.22
700	660	3.79
800	760	4.37
1000	960	5.52
1200	1140	6.55
1500	1440	8.28

As would be expected, the power supply and isolation circuit introduced a large capacitance and loss into the measurements. This capacitance was of the order of 1700 to 1750 $\mu\mu$f and the loss tangent about 0.01 to 0.1. This presented no special problem, however, as both C and G for the system were determined over the employed frequency range and the corrections in sample capacitance and loss could then be made as mentioned earlier. In order to keep errors at a minimum it was necessary to calibrate the system for capacitance and loss at each of the bias voltage settings used.

In general, however, the bias measurement results must be examined with caution since the large number of corrections necessary, can provide a large source of error. This results from the fact that the power supply calibration required the use of large external standards as did the actual bias measurement. These large external standards in turn had been calibrated against a smaller external standard. While these calibrations and corrections cause only a small error (about 1%) in dielectric constant, whose total range extends over approximately a tenth of an order of magnitude, a sizeable error is prevalent in the equivalent conductance results due to the expanded range (three orders of magnitude). Also, errors in capacitance and loss tangent can provide a considerable error in equivalent conductance since it is proportional to the product of these two values. Normally the magnitude of these errors is less than 10 per cent of the given value of equivalent conductance. Although this represents quite a large error, the general trend of the results can still be ascertained.

Sample Holder Assembly

The sample holder assembly (Figure 9) was constructed by J. Northrip of this laboratory. The sample itself was held between two large brass plates and immersed in Dow Corning 200 Silicone oil. A 250 watt immersion heater controlled by a variac was used in conjunction with a magnetic stirrer. The thermometer was kept close to the sample to prevent any errors due to possible gradients in the oil bath.

The external surfaces of the 3000 ml beaker containing the oil were covered with a reflective coating and insulation to reduce thermal losses due to radiation and conduction. With these precautions and the variac

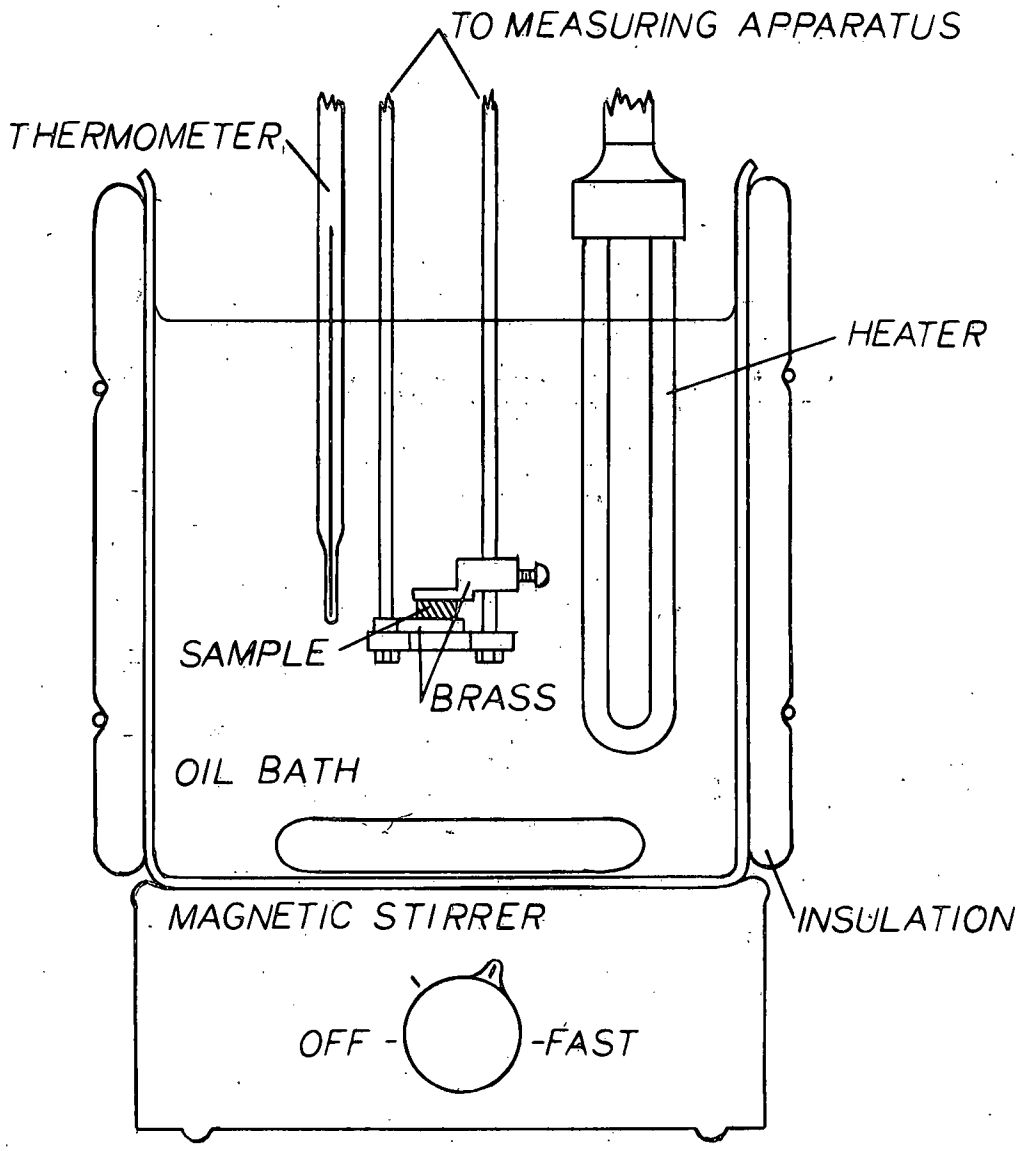

Figure 9. Sample Holder Assembly

controlled heater, temperatures from 25 to 230 ^{o}C could be achieved and held constant within ± 0.5 ^{o}C. Measurements were not made too near the transition points of the sample used, so that any change in capacitance due to thermal drift would be small in comparison to the dependence upon frequency.

CHAPTER IV

RESULTS

Zero Bias Measurements

A typical result of the dielectric constant versus measuring frequency investigations is depicted in Figure 10, for sample PZST-6 at zero biasing field and low (less than 20 volts/cm) measuring field strengths. Recalling that at 25 ^{o}C this sample is ferroelectric, one observes from the figure that the dielectric constant displays a linear log dependence upon the measuring frequency. This can be most easily represented by an equation of the form

$$k' = k_o' + b \ln(f/f_o)$$

where b and k_o' are constants with k_o' the dielectric constant at f equal to f_o equal to one cycle per second.

It is also possible to express the dependence as

$$k' = k_i' + k_s' \left[1 - a \ln(f/f_o)\right]$$

where now k_i' represents a frequency independent contribution to the dielectric constant and the frequency dependent term appears in a mathematical form more convenient to the later discussion. The values of the constants for the curve in the ferroelectric phase in Figure 10 are:

$$k_i' = 385$$

$$k_s' = 188$$

$$a = 0.0469.$$

To provide some means of comparing data it was found useful to

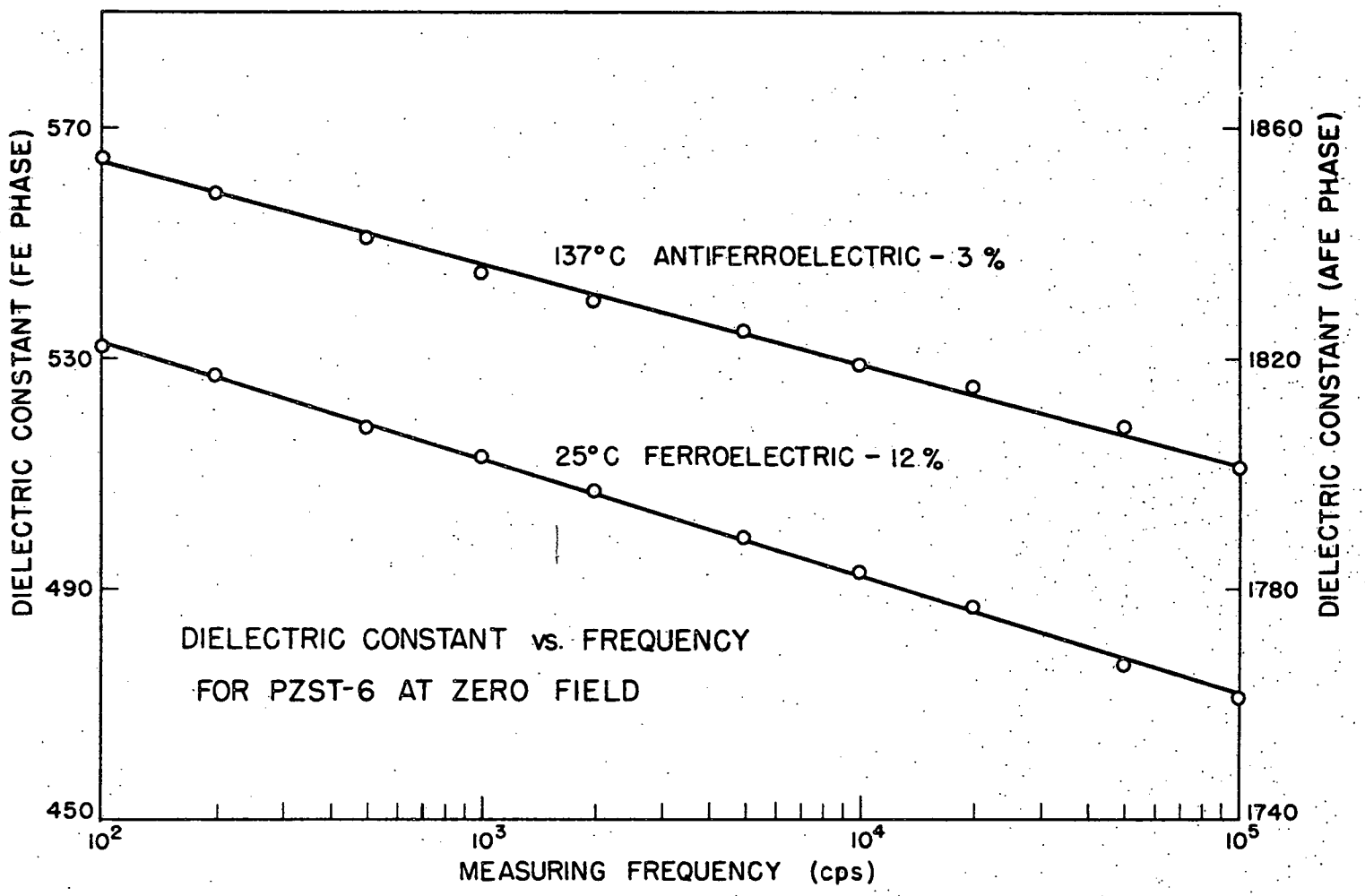

Figure 10. Typical Result of Dielectric Constant versus Measuring Frequency

calculate a relative percentage change for each set of data. This was done by taking the differences in the end point values of dielectric constant, dividing by the midpoint dielectric constant over the previously mentioned frequency range, and then converting this ratio to a percentage change. It must be understood that this calculated value is only meant to offer some comparison basis among the observed results. The percentage change for Figure 10 (ferroelectric curve) is approximately 12 per cent and this value is rather typical of the changes in the other ferroelectric materials tested. A more complete comparison will be offered later.

When the PZST-6 sample was heated above the ferroelectric-antiferroelectric transition temperature so that the sample was in the antiferroelectric phase the relative percentage change was reduced to around 3 per cent. The choice of a percentage change to depict results rather than the slopes of the curves is evident from Figure 10 where the slopes are nearly equal, the percentage changes differ by a factor of four.

At temperatures above the Curie point the dielectric constant no longer displayed a linear dependence upon log frequency. This is not of prime interest here and so no further mention will be made of this phenomenon.

The results of the dielectric constant versus frequency studies at room temperatures (23 to 26 $^{\circ}$C) and low measuring field strengths (less than 20 volts/cm) are illustrated in Figure 11. The relative percentage changes for each sample are given and range from 8 to 13 per cent for the three ferroelectric samples and 4 to 7 per cent for the two antiferroelectric samples.

Figure 12 is an equivalent conductance versus frequency plot for sample PZST-6 at various temperatures and low measuring field strengths.

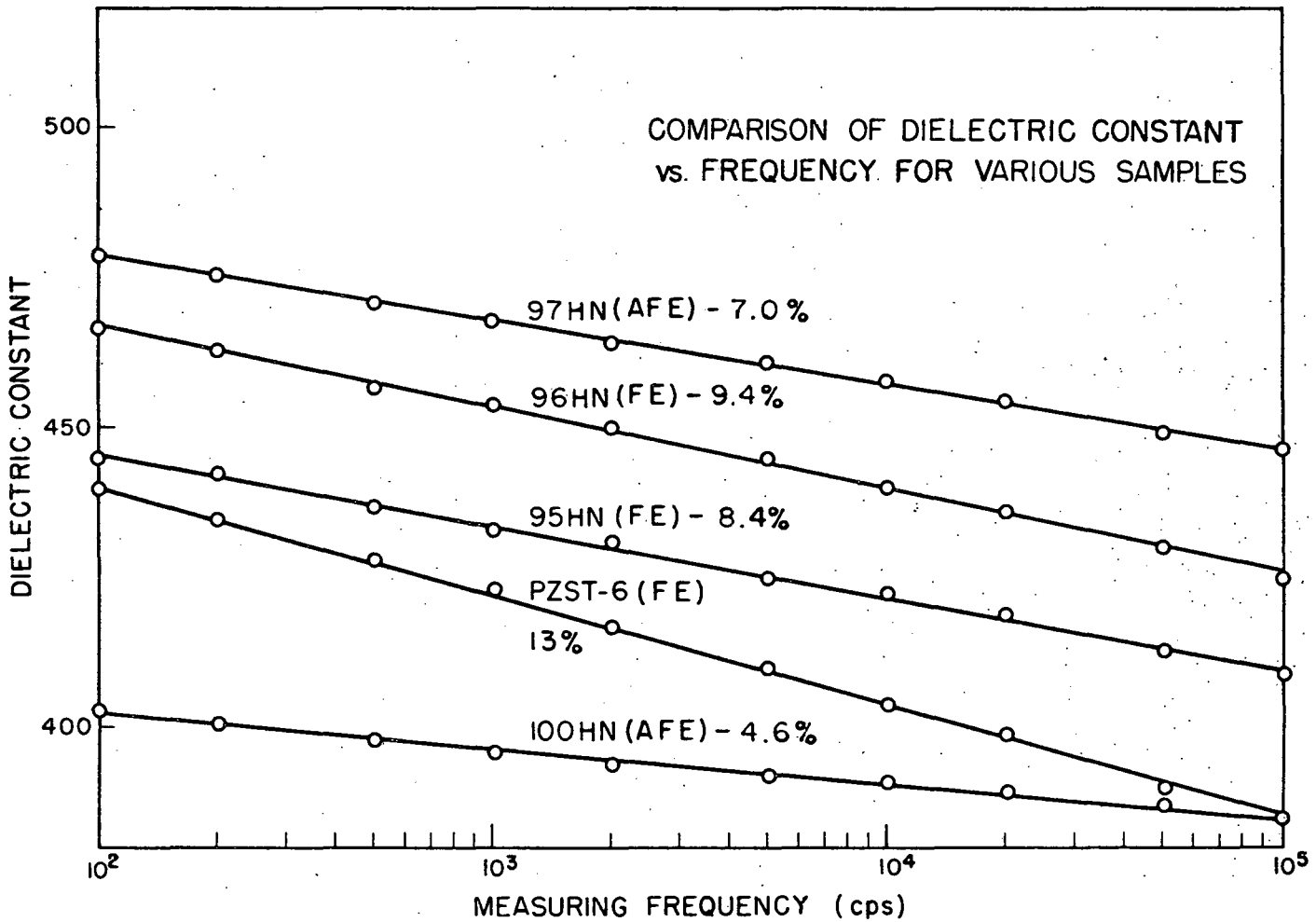

Figure 11. Results for Samples at Room Temperatures and Zero DC Field

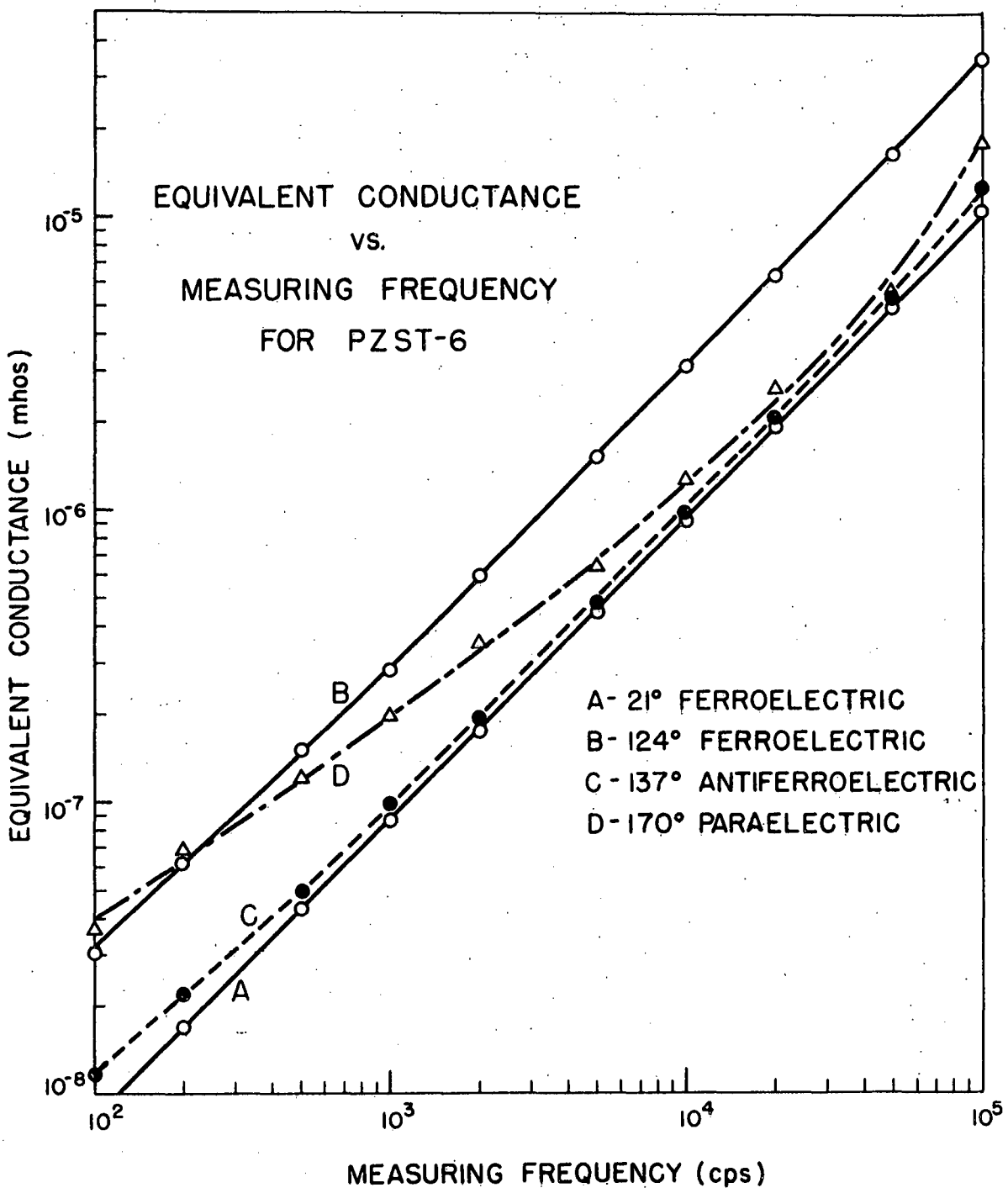

Figure 12. Typical Equivalent Conductance Curves at Zero DC Bias

The log-log plots A and B for the sample in the ferroelectric phase approximate straight lines with slopes of about one. The loss tangents for these curves show slight increases with increasing frequency. Plot C represents the sample in the antiferroelectric phase at a temperature of 137 ^{o}C. It lies below the ferroelectric plot at 124 ^{o}C with both the capacitance and the loss tangent in the antiferroelectric phase less than in the ferroelectric phase. In the antiferroelectric state the loss tangent is about one-half or one-third of that in the ferroelectric state (0.009 as compared to 0.025 at 10^2 cps). In the paraelectric phase (plot D at 170 ^{o}C) the loss tangent decreases from about 0.01 to 0.003 in the frequency range 10^2 to 5×10^4 cps and then increases abruptly to 0.045 at 10^5 cps.

If only two loss mechanisms are considered, namely hysteresis and ordinary Joule heating, it would appear from Figure 12 that the loss mechanism in the ferroelectric state could be attributed almost solely to hysteresis since a pure loss of this type would be representable on a log-log plot as a straight line with a slope of one. A loss due to frequency independent Joule heating alone, however, would be a line parallel to the abscissa in Figure 12.

The antiferroelectric equivalent conductance versus frequency curve displays a slight flattening at the lower frequencies. This suggests a relatively greater importance for Joule heating losses at low frequencies and, surprisingly, the continued presence of hysteresis losses at higher frequencies.

The results displayed in Figure 12 for sample PZST-6 are for the most part characteristic of the data obtained from the other samples. Later, mention will be made of a sample whose equivalent conductance versus frequency curves show a very pronounced flattening at higher

temperatures and low frequencies, perhaps offering some means of separating the total loss mechanism into its components.

In several cases measurements were made with the measuring field strengths near 50 volts/cm. The results shown in Figure 13 illustrate an enhanced dielectric constant, as compared to the low measuring field strength dielectric constant. This is true at the lower frequencies, but at higher frequencies the high and low measuring field strength results approach each other. For both samples shown in Figure 13 the samples were more lossy in the higher field strength case than in the low strength situation. At 10^2 cps, the loss tangent was 0.0255 as compared to 0.0237 for sample PZST-6. This will be discussed more fully later.

Bias Measurements

The results of the dc bias measurements are shown in Figures 14 and 15. Figure 14 depicts dielectric constant versus frequency with dc bias as a parameter. Curve A of Figure 14 shows the zero bias situation after the sample had been depoled by heating above the Curie point and slowly cooling in the absence of a bias field. This measurement was made with the power supply in the system and so a larger experimental error was possible than if the system had not been present. For this reason the linear portion of the curve has been extended in a straight line (dotted portion), rather than to the measured point, since previous measurements have revealed a completely linear log dependence upon frequency at zero bias. Curves B and C display a hook at the upper frequency end which appears to be the beginning of the resonance process discussed in the next section. The calculated slopes and percentage changes pertain only to the linear portions of the plots.

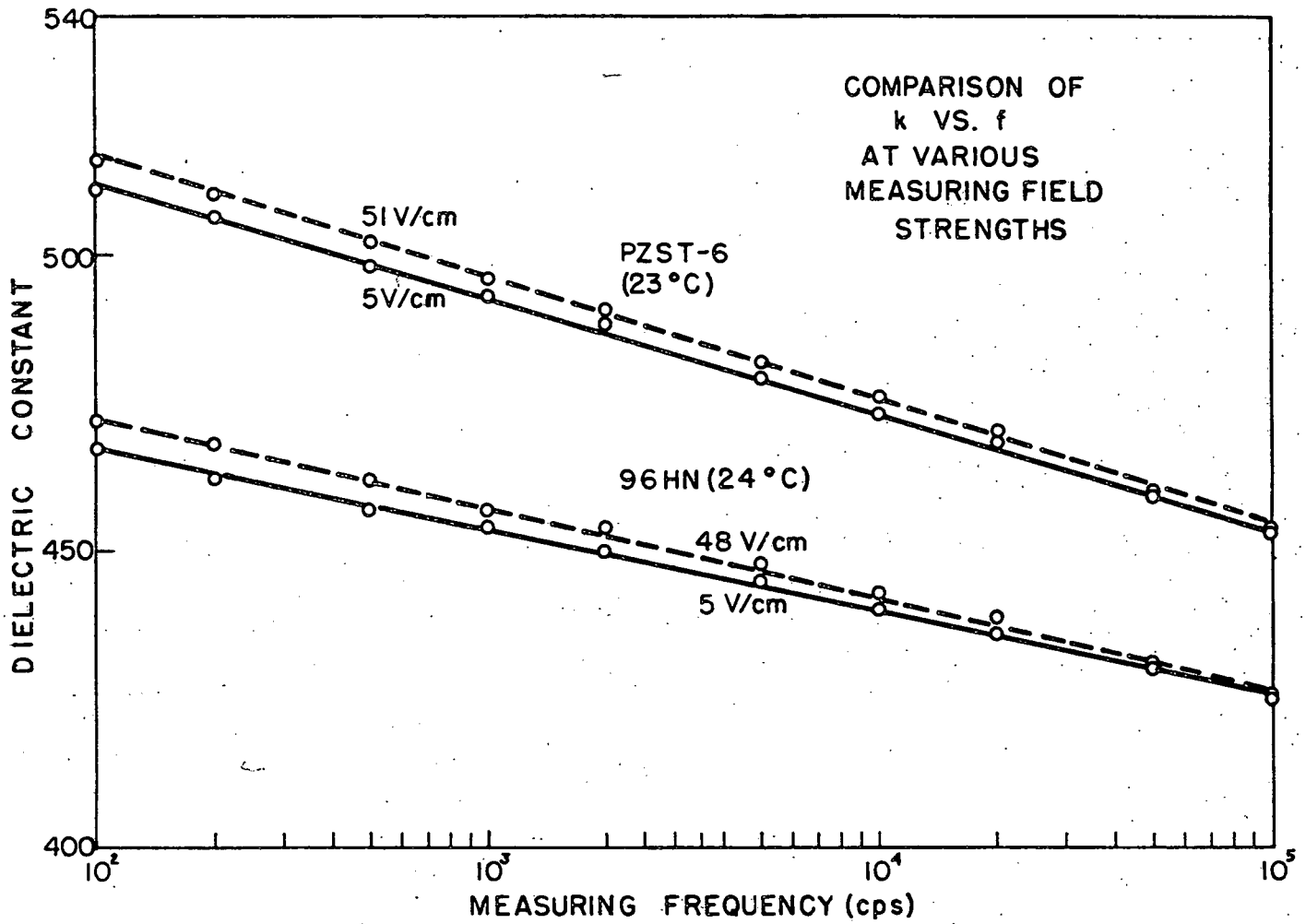

Figure 13. Results of Varying AC Measuring Field Strength with Zero DC Bias

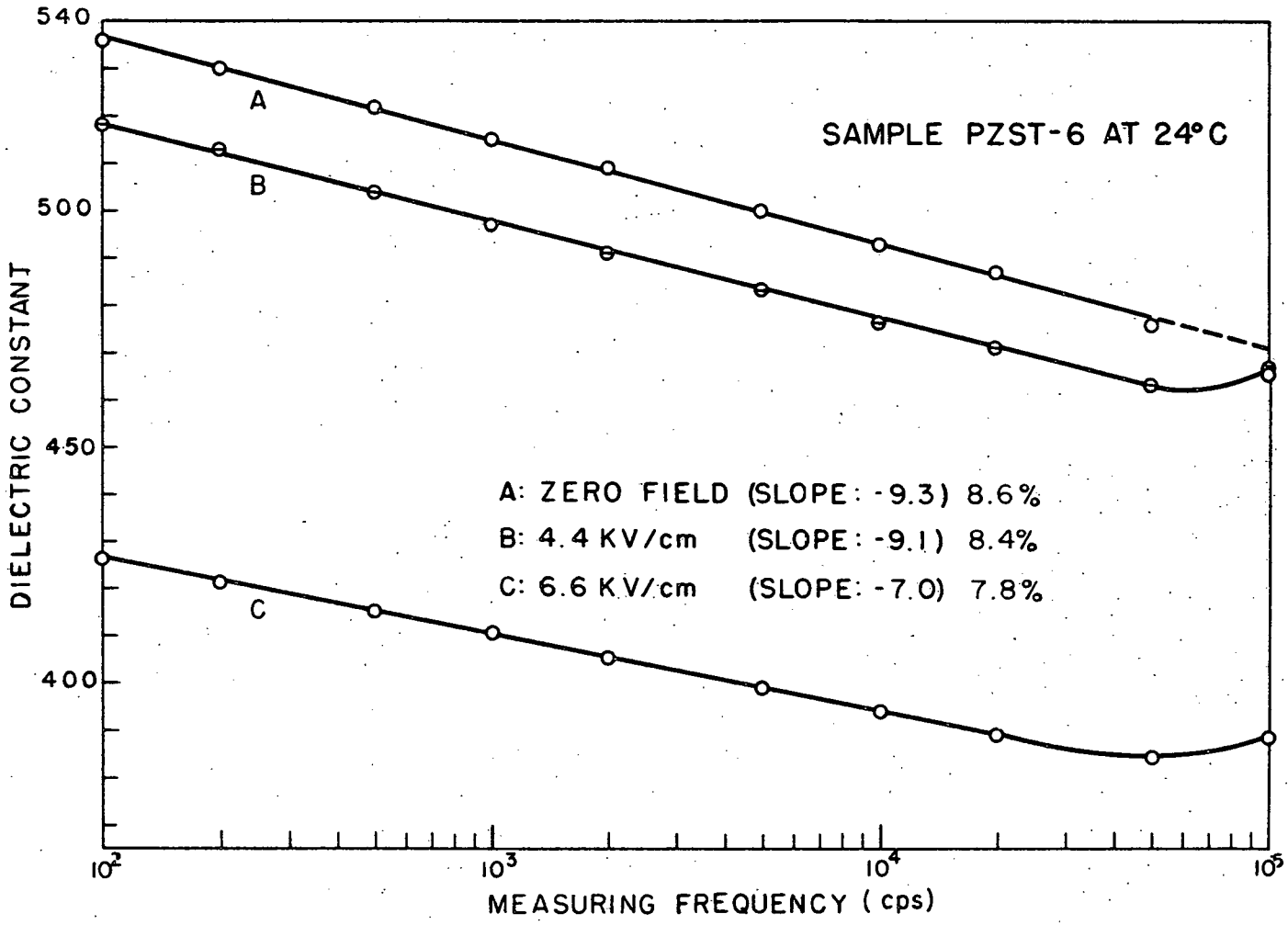

Figure 14. Typical Bias Measurement Results

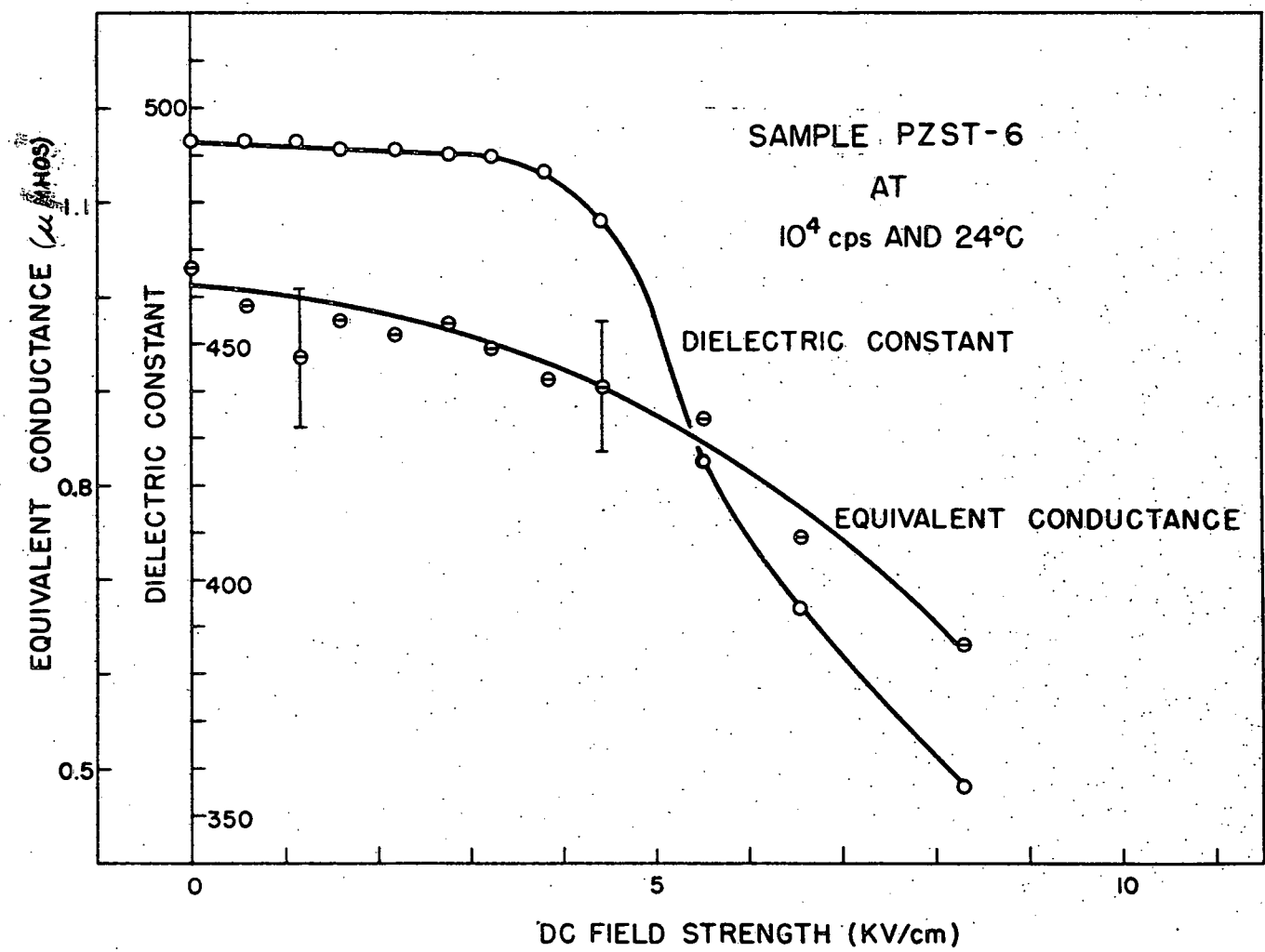

Figure 15. Dielectric Parameters as Functions of DC Field Strength

The fact that the high field strength curves lie below the zero field strength curve can be found upon consideration of Figure 15. The dielectric constant versus dc field strength curve shows an abrupt decrease above 4 kv/cm. This can be explained upon the basis of the hysteresis loop of Figure 1. Since $k \propto dP/dE$ the dielectric constant gives the slope of the hysteresis loop caused by the application of a dc field. The linear portion of the dielectric constant curve below 4 kv/cm of Figure 15 then corresponds to portion OF of Figure 1. The decrease in dielectric constant past 4 kv/cm indicates the decrease in slope of region FA of Figure 1. In the saturated region of the hysteresis loop the slope should eventually reach a constant value which would require another constant linear region in Figure 15 past 8 kv/cm. Readings at higher field strengths were not performed to avoid breakdown in the sample, but the curve of Figure 15 has gone through an inflection point and appears to be approaching a constant value.

The equivalent conductance curve of Figure 15 illustrates a general decreasing trend of losses with increasing field strength.

Poled Sample Measurements

The ferroelectric samples were poled by placing a voltage of 1500 to 2000 volts across them while at a temperature at least 30 degrees above their respective Curie points, and then allowing them to slowly cool with the bias remaining. This was done in hopes of detecting a piezoelectric resonance similar to that observed in polycrystalline barium titanate by Roberts (R1). The results are shown in Figures 16 and 17. The resonance peaks for both samples are quite sharp and well defined and both occur near 165 - 170 kcps. Using the resonance frequencies obtained from the graphs, the elastic compliance

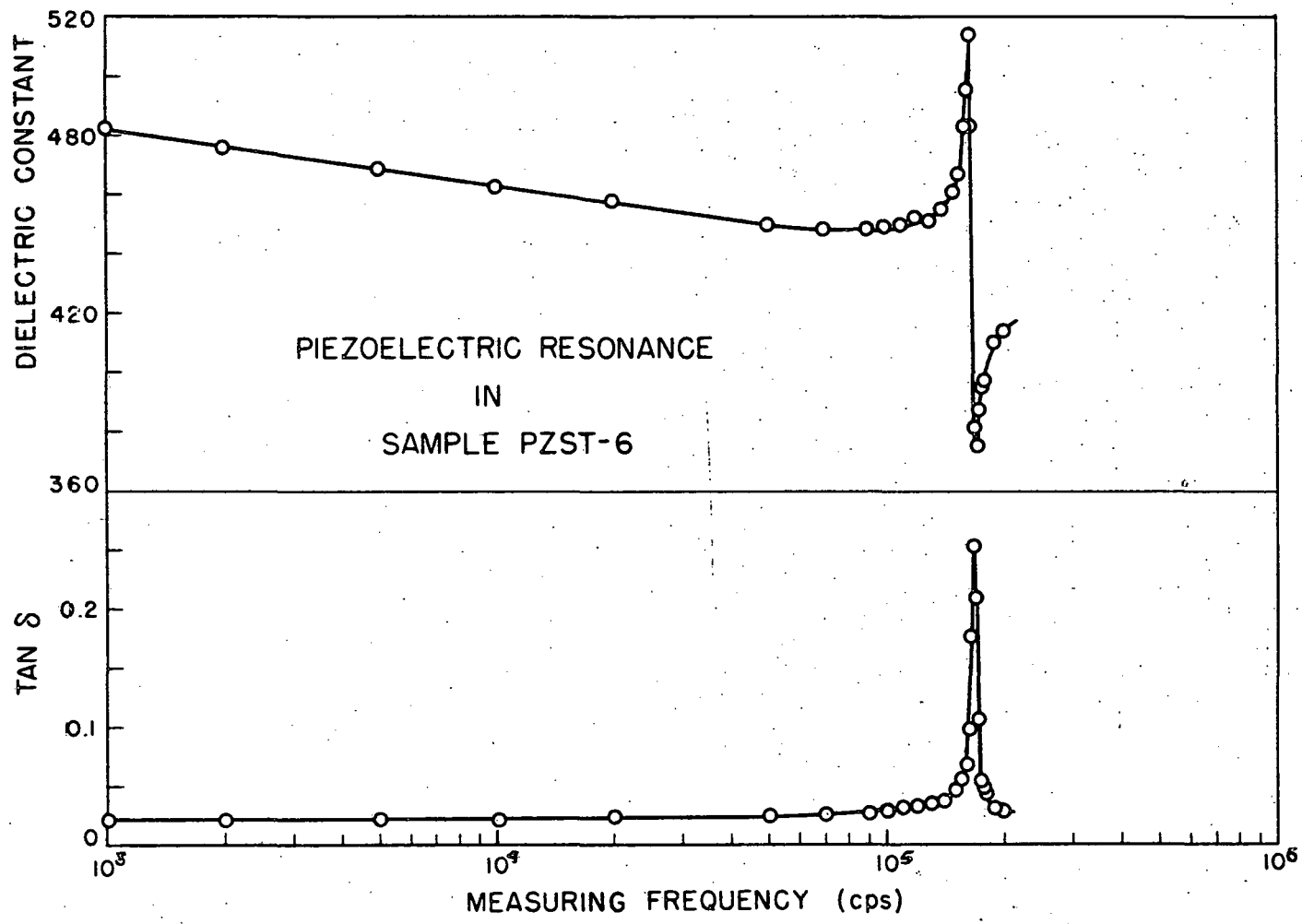

Figure 16. Resonance in PZST-6 at Room Temperature

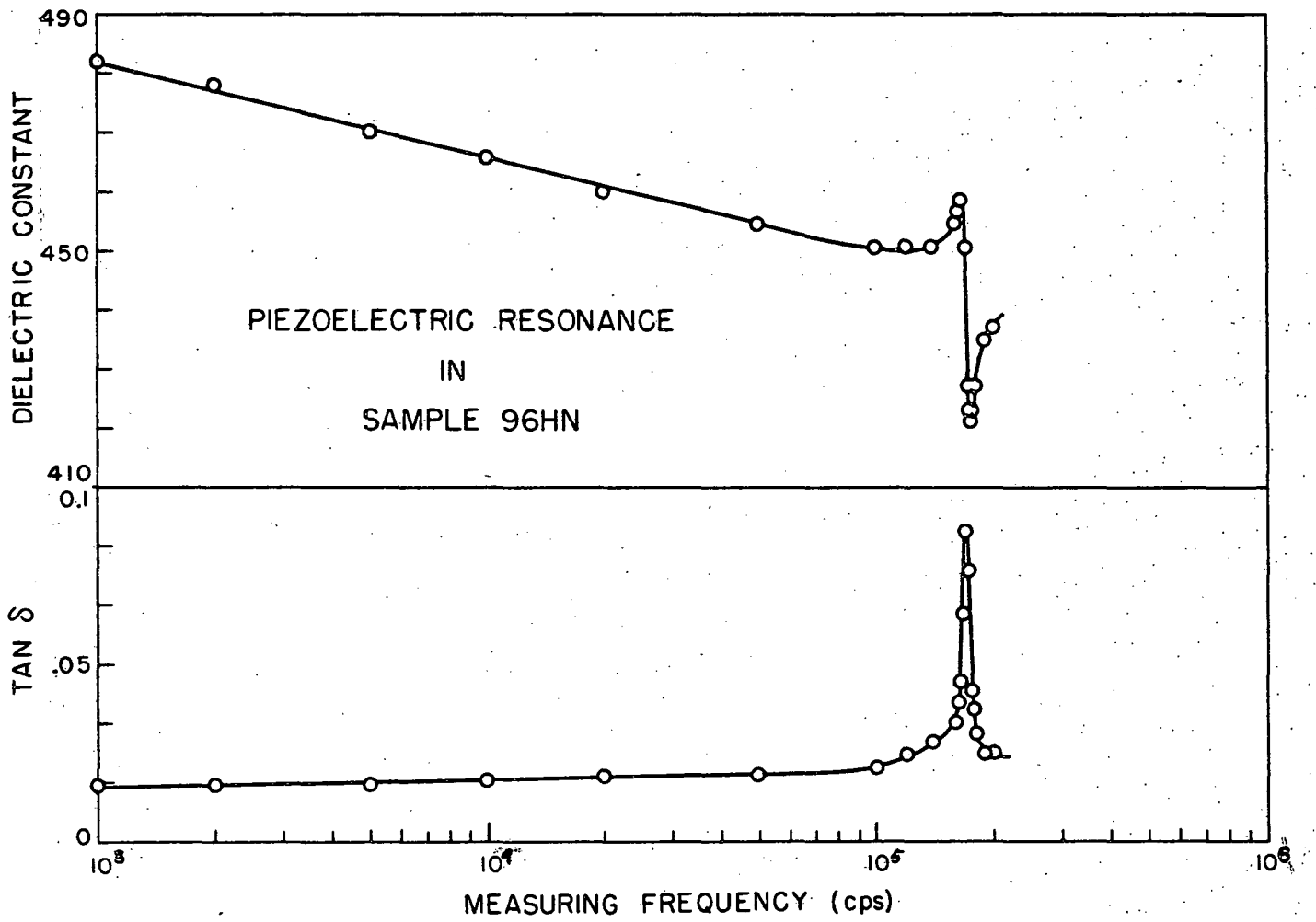

Figure 17. Resonance in 95 HN at Room Temperature

coefficients, S_{33}, for these materials are:

(PZST-6) $S_{33} = 3.71 \times 10^{-11}$ $cm^2/dyne$

(95 HN) $S_{33} = 1.38 \times 10^{-11}$ $cm^2/dyne$.

These values are calculated from the equation

$$S_{33} = \frac{1}{4(tF_r)^2\rho},$$

where t is sample thickness, ρ is density and F_r the resonant frequency.

The sample 96 HN also showed traces of a resonance, but it was weak compared to the other resonance peaks. Unfortunately the upper limit on the measuring frequency was 200 kcps so it could not be determined if other peaks were present as would be expected.

CHAPTER V

DISCUSSION AND CONCLUSIONS

It was first suggested that the observed decrease in dielectric constant with frequency could be due to some sort of Debye relaxation process. If this were true, the sample response could be represented in terms of equivalent circuit parameters. The simplest equivalent circuit of this nature is given in Figure 18, where C_o, C_1 and R are

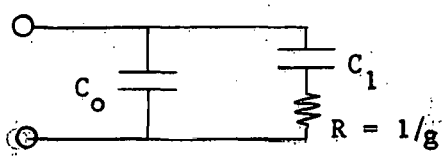

Figure 18. Relaxation Equivalent Circuit

constants. If the admittances of this circuit and that of a ferroelectric sample (Figure 4) are equated, one obtains the following relations

$$C_x = C_o + g^2C_1/(g^2 + \omega^2C_1^2)$$

$$G_x = gC_1^2\omega^2/(g^2 + \omega^2C_1^2).$$

These expressions yield a single relaxation time (the R-C branch of Figure 18), however, and since it proved impossible to fit the data to them, it became apparent that the experimental results could not be represented in terms of a single relaxation process.

Another standard equivalent circuit is that shown in Figure 19. This finds its primary utility in situations involving a resonance phenomenon. The result of equating admittances is

$$C_x = C_o + \frac{g^2 C_1 (1 - \omega^2 L C_1)}{g^2 (1 - \omega^2 L C_1)^2 + \omega^2 C_1^{\,2}}$$

$$G_x = \frac{\omega^2 g C_1^{\,2}}{g^2 (1 - \omega^2 L C_1)^2 + \omega^2 C_1^{\,2}} .$$

Inspection of the resonance expressions shows that they differ from those representing a relaxation process merely by the addition of the term in brackets and hence that it is often difficult to decide from experimental data which of the two types of processes is more prominent

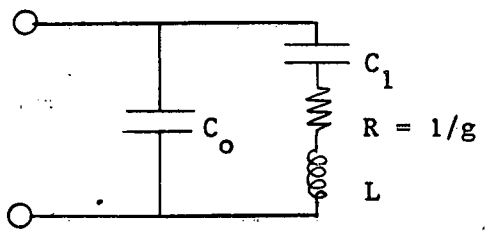

Figure 19. Resonance Equivalent Circuit

in a particular case.

This simple model also proved inadequate to fit the data at hand and it was deemed unprofitable to search for a more complicated equivalent circuit until such time as a clearer picture of the microscopic phenomena causing the dispersion is available.

In light of previous investigations, two of the more plausible physical explanations of the dielectric constant decrease with frequency lie in (1) a polarization switching due to domain wall motion, or (2) a relaxation due to interfacial polarization. The latter case, however, need not involve a nonferroelectric layer adjacent to the electrodes but could be associated with thin layers between grains in the ceramic.

Although the idea of an interfacial polarization has merit, the

observed decrease in dielectric constant is larger than that found by Gerson (G1) in a similar material and attributed by him to an interfacial polarization. The relative percentage changes of his results are roughly one-fifth to one-sixth of those observed in this work.

Consequently, an explanation of the dielectric constant decrease with frequency found in the present work will be sought in the mechanism of a polarization switching due to domain wall motion. The work of Landauer, Young and Drougard (L1) suggests that a dielectric constant measured during a switching process should display a dispersion with changing switching frequency. Based upon Merz's rate equation

$$\frac{dP}{dt} \propto \exp(-\text{const}/E),$$

they showed that the shape of the hysteresis loop was dependent upon the time allowed for the switching process. This implies that if switching is taking place and the hysteresis loop changes shape with changing frequency, the dielectric constant will also be dependent upon frequency since $k \propto dP/dE$. A simple check to show the nature of the dependence upon frequency of the dielectric constant was performed by taking the slopes (dP/dE) of the hysteresis loops illustrated by Landauer, Young and Drougard, and plotting them against a frequency parameter (found from the approximate rise rates associated with the curves). When this was done, the result was a log linear dependence of dielectric constant upon frequency over the frequency range employed in the present study.

These findings would lead one to believe that the dispersion observed in the present work can also be explained in terms of some nature of switching process. Generally polarization reversal is classified into three types: (1) nucleation of antiparallel domains, (2) forward domain wall motion, and (3) sideways domain wall motion. The

latter two cases have been previously mentioned in Chapter I. In light of a large number of observations, Jona and Shirane (J1) have concluded that the process of polarization reversal is governed mainly by domain wall motions. They point out in Chapter IV of their book that a 180° wall is not very likely to move as a unit parallel to itself, but perhaps sideways wall motion could effectively occur controlled by the nucleation of reversed domains at an existing 180° wall.

For these reasons it seems feasible to propose a model similar to that of Sannikov (S1) where a 180° wall is allowed to move sideways in the presence of an external field. (In the context of the following discussion it is to be emphasized that the term "external field" means the measuring field.) Consider Figure 20 which depicts two antiparallel domains existing in a single grain of the polycrystalline sample. According to Sannikov, a sinusoidal field applied parallel to the domain wall will cause it to oscillate with the frequency of the external field but perpendicular to the field direction. This is due to a pressure $p = -2P_oE$ exerted by the field on the wall, with P_o the static polarization in the uniform ferroelectric and E the applied field strength.

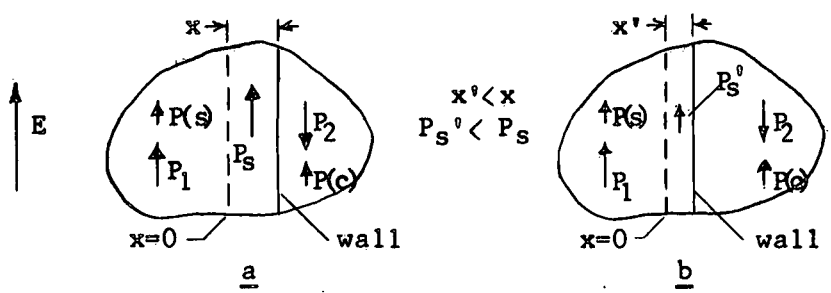

Figure 20. Domain Wall Motion Switching Model

In Figure 20-a, as the field increases in the direction shown, the wall moves to the right at the expense of the right hand domain. The result is an increase of polarization along the direction of the field.

This polarization is in addition to the increase in polarization caused by the "stretching" or "compression" of the individual dipoles labeled P(s) and P(c) respectively in the figure. It is this latter stretching that is normally considered in nonferroelectric materials and represents the situation where hysteresis is not observed. More simply, in the absence of any switching, the dielectric constant is measured solely due to this stretching or compression of individual electric dipoles.

Returning to the part of the polarization caused by the domain wall motion, it is then supposed that this polarization fluctuates with the frequency of the field, taking on both positive and negative values. In other words, with the application of a periodic field which has persisted for sufficient length of time, the total polarization must also be periodic in time. Generally, however, this polarization will not necessarily be in phase with E, but will show a phase shift $\emptyset$. Consider the expression

$$P = D - \epsilon_o E = (k^* - 1)\epsilon_o E,$$

with k* previously defined as

$$k^* = k' - jk''.$$

From these two expressions one obtains

$$P = (k' - 1)\epsilon_o E - jk''\epsilon_o E,$$

showing the total polarization is composed of a real and an imaginary part. The right hand term in the above expression represents a loss in that it is 90° out of phase with the external field. This can be depicted as in the vector diagram of Figure 21 where P_l and P_n are given by

$$P_l = jk''\epsilon_o E$$

$$P_n = (k' - 1)\epsilon_o E.$$

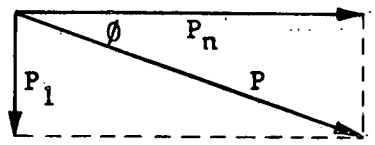

Figure 21. Vector Diagram Showing Components of Total Polarization

From the figure the tangent of the phase shift angle is apparently

$$\tan \emptyset = \frac{k''\epsilon_o E}{(k' - 1)\epsilon_o E} .$$

In Chapter III it was shown that

$$k'' = k' \tan \delta,$$

so

$$\tan \emptyset = \frac{k' \tan \delta}{k' - 1} .$$

But $k' \doteq k' - 1$, since k' is of the order of 500, and this results in

$$\tan \emptyset \doteq \tan \delta.$$

The loss part of the polarization P_1 is then representable as

$$P_1 = k'\epsilon_o E \tan \delta.$$

This out-of-phase component results in an elliptical Lissajous figure when plotted on a P-E diagram (Figure 22). The in-phase component of the total polarization, P_n, is represented in the figure as a straight line.

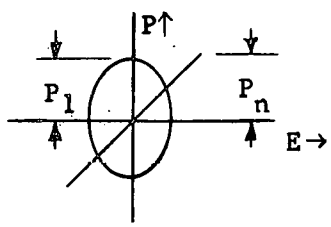

Figure 22. Polarization Components Plotted on a P-E Diagram

It should be pointed out that the component P_n does not merely

represent the in-phase component of the switching polarization but rather the sum of all in-phase components of polarization to stretching, compression, switching, etc. In like manner P_1 includes the total of out-of-phase parts resulting from all nature of losses. If all losses are considered negligible in comparison to domain wall motion loss, the magnitude of this particular loss can then be directly calculated from the area of the elliptical Lissajous loop.

At higher frequencies (Figure 20-b) it is supposed that the domain wall boundary cannot continue to move along as well with the rapidly changing field. This implies the effective distance the wall can move from its equilibrium position (at no external field) decreases with increasing frequency. Such an effect has been mentioned by Little (12). If the wall is displaced by a smaller amount (x') at higher frequencies, the result is a decrease in the total switching polarization from P_s to $P_s{}^0$, and ultimately a decrease in the dielectric constant. Although the total switching polarization decreases, the component of this polarization which represents a loss may increase. This arises from the fact that as the field oscillates faster and faster there should be a continuing increase in the loss angle. It was actually observed in the experimental work that the loss tangent showed a slight increase with increasing frequency. These suppositions are consistent with the results of Sannikov's theoretical treatment which leads to a complex susceptibility showing the same frequency trend.

It is unfortunate that the actual total polarization due to switching by domain wall motion cannot be obtained, for at best only the value of P_1 can be calculated. The total polarization P as shown in Figure 21 is related to its components by

$$P = (P_l^{\ 2} + P_n^{\ 2})^{\frac{1}{2}} .$$

Since there is no unique way to determine the fraction of P_n resulting from the assumed switching mechanism, the value of P_s is likewise unobtainable.

It has been mentioned that the loss is characterized by the area enclosed by the elliptical loop. This enables one to determine the various loop parameters from the conductance data. Again it is pointed out that interpretation of results from a microscopic point of view must take recognition of the fact that the experimental specimens were made up of randomly oriented domain regions and that consequently the values of the calculated dielectric parameters have true meaning only as being characteristic of the entire sample.

The power dissipation in a dielectric is normally calculable as

$$W = G_x V^2$$

with V the rms value of the applied external voltage. On the other hand the value of energy density lost per cycle must be

$$U = \pi P_l E_{max}$$

where now P_l represents only that portion of the total polarization which is out of phase with the field and E_{max} is the maximum value of the sinusoidal electric field strength. To find the power dissipation one multiplies this value by the sample volume and the frequency, or

$$W = UV_s f .$$

Combining these expressions one obtains a value for the appropriate loss component of the total polarization,

$$P_l = \frac{G_x V^2}{\pi f V_s E_{max}} .$$

For sample PZST-6 (V_s = 0.3456 cm^3) at room temperature , 10^2 cps

and with E_{max} = 14 volts/cm one finds

$$G_x = 8.5 \times 10^{-9} \text{ mhos}$$

and

$$W = G_x V^2 = 2.65 \times 10^{-8} \text{ watts/sample},$$

hence

$$P_1 = 1.7 \times 10^{-11} \text{ coul/cm}^2.$$

The calculated P_1 is the result, as previously described, of all loss mechanisms. For purposes of the following discussion, it will be assumed that the domain wall motion loss is the only one of major consequence and P_1, then, will be taken as a measure of the loss component of the switching polarization P_s. As such, it also serves as a lower limit value for P_s.

Using the value of P_1 calculated above it is possible to obtain the minimum portion of the sample contributing to the switching process. Consider a cubic unit cell with an edge length of 4.1×10^{-8} cm. This value is the approximate edge dimension of the unit cell in the paraelectric phase, but will suffice here. The unit cell volume is then found to be

$$V_c = 6.9 \times 10^{-23} \text{ cm}^3.$$

To reverse the polarization of the entire sample requires a coercive field of the order of 5 kv/cm with a spontaneous polarization of 2.5×10^{-5} coul/cm^2 (N1). Hence comparing the switching model polarization to the entire sample polarization, one can obtain a rough estimate for the fractional part F of the sample contributing to the switching process,

$$F = \frac{(P_1)_{model}}{(P_{sp})_{entire\ sample}}.$$

At 10^2 cps

$$F = 6.8 \times 10^{-7}.$$

From the sample volume and unit cell volume the total number of unit cells in the uniform sample is found to be 5.0×10^{21}, and hence roughly 10^{15} unit cells contribute to the switching process. This is something like one-millionth of the sample.

Let us recapitulate the bases upon which this conclusion has been reached. It was assumed that all losses were due to domain wall motion. Certainly some Joule heating losses are present but these should be negligible since the dc resistivity of PZST-6 is around 10^9 ohm-cm. Furthermore there still exists the possibility of loss associated with nonferroelectric regions in the sample and with the presence of general relaxation-type mechanisms common to all dielectric materials. The presence of any of these losses would result in the value of F being too large.

The use of only a component of the total switching polarization is not as illustrative as would be the use of the actual value P_s. However, since no unique method of calculating the part of P_n which is due to switching is possible, the value of P_s cannot be ascertained.

Although the calculation of the fractional part of the sample contributing to the switching process suffers from obvious weaknesses, the fact of prime importance is that the experimental results can be reasonably interpreted in terms of a model of this nature.

The switching model would be strengthened if a larger ac measuring field strength produced a larger dielectric constant. Such is indeed the situation at the lower frequencies as depicted in Figure 13. This should result from the added pressure on the domain wall causing a

larger value of P_s. A larger loss is also observed, again consistent with the view that the phase of the switching polarization differs from that of the field.

The results obtained from the dc bias measurements can also be incorporated into the model. At bias field strengths less than that required for sample saturation, the dielectric constant versus frequency results remain essentially unchanged. That is, the dependence of dielectric constant upon log frequency is still present as was illustrated in Figure 14. This does not necessarily contradict the model since it has been shown only a small number of unit cells (and hence domain walls) contribute to the switching process and the presence of the less-than-saturation dc field does not infer that all domain wall motion due to the ac field should cease.

At higher dc field strengths it is assumed that the majority of the sample has a polarization in the direction of the field. Ideally if the entire sample were poled in one direction, domain walls would not exist. Plot C of Figure 14 illustrates that the relative percentage change (and slope) has decreased at the higher dc field indicating a lesser amount of switching taking place. Since the equivalent conductance is a direct measure of the loss mechanism, the equivalent conductance curve of Figure 15 strengthens the idea that the switching mechanism decreases with increasing dc field strength as expected.

Up until now the model has been discussed mainly in terms of the loss component of the polarization. Recalling the equation expressing the dependence of the real part of the dielectric constant upon frequency

$$k^0 = k_i^0 + k_s^0[1 - a \ln(f/f_o)],$$

it is now easier to understand this behavior on the basis of the model. Because of its logarithmic nature, it seems reasonable that the term on the right, representing the frequency dependent part, can be interpreted as a contribution due to the domain wall motion. Mathematical verification of this point, however, is difficult since the real part of the dielectric constant is representative of the real part P_n of the total polarization and the part of P_n which is due to domain wall motion alone cannot be uniquely ascertained. Qualitatively this idea is consistent with the model which assures us that as the frequency increases (1) the domain wall motion loss angle increases and (2) the magnitude of P_s decreases. Both of these effects lead to a decrease of P_n (and hence of k^0).

Thus far no mention has been made of the antiferroelectric sample observations. However, comparing the results of k' versus f as depicted in Figure 11, there at first appears to be a basic inconsistency in that the antiferroelectric materials also obey an equation of the form

$$k^0 = k_i^0 + k_s^0[1 - a \ln(f/f_o)].$$

For sample 100 HN which is antiferroelectric at all temperatures, the room temperature values of the constants in this equation are:

$$k_i^0 = 367$$

$$k_s^0 = 48$$

$$a = 0.0543.$$

The use of k_s^0 to designate a dielectric contribution due to switching now appears as an unlikely situation, since none should occur in the antiferroelectric phase. An antipolar dipole array cannot display any dielectric hysteresis.

From examination of the slopes of the equivalent conductance curves, however, it appears as though a hysteresis type loss is present. In fact it is possible to calculate a value of P_1. For 100 HN at 10^2 cps and room temperatures one finds a value of

$$P_1 = 9.0 \times 10^{-12} \text{ coul/cm}^2.$$

This is about one-half the value found in the ferroelectric sample, but more significant is the fact that a polarization loss of this magnitude is still present. Thus assuming that the ferroelectric model and mathematical treatment are valid, it appears that perhaps a part of the antiferroelectric sample is switching. Since a purely antiferroelectric material cannot display domain wall motion, this implies that both ferroelectric and antiferroelectric phases exist in the polycrystalline material, with the latter phase more dominant. Such an implication is not as startling as it may first seem, for the free energies of the two phases are quite close and it is conceivable that a distribution of free energies may exist in the specimen. Further evidence along this line lies in the peculiar hysteresis loops that have been observed in other samples of the hafnate group near antiferroelectric-ferroelectric transition points (N1). These loops are the double hysteresis loops normally observed near the transition points superimposed upon a normal ferroelectric loop and hence suggesting the coexistence of both phases.

In retrospect, the proposal that both ferroelectric and antiferroelectric phases may coexist in these ceramic specimens is based essentially on the observed abnormal hysteresis loops and the agreement of the experimental results for the antiferroelectric samples with the model proposed for ferroelectric materials. The fact that the antiferroelectric changes have the same trend in reduced degree is provocative but must be interpreted with caution.

CHAPTER VI

AREAS FOR FURTHER STUDY

It is clear from the previous considerations that several obvious areas for further study exist as well as some areas which are not so obvious. A truly definitive experiment which could be performed to validate or possibly disprove the ideas presented here would be most desirable but it is still not at all evident what its nature should be.

Since the model given in this study is essentially that of Sannikov (S1), it would be worthwhile to judge whether or not the experimental results obtained for the ceramic samples could be fitted to his expression for susceptibility or to a modification of it. From the practical point of view it would also be of importance to fit the results to a more complex resonance equivalent circuit than that shown in Figure 19. This should afford a hint as to what modifications might be necessary in Sannikov's susceptibility expression in order to describe the behavior of polycrystalline materials like those employed here.

Extension of the frequency range to lower frequencies should show a further increase in the dielectric constant. Gerson's conclusion that no switching was present in his low frequency measurements was based upon the fact that the lead zirconate titanate sample without niobia added (to lower the coercive field), showed a larger change in dielectric constant over the frequency range than the sample with niobia. Since it would be expected that the sample with the low coercive field should provide a better situation for a switching

mechanism to take place, he decided that perhaps he was observing a phenomenon related to interfacial polarization. In the model proposed here, however, the coercive field is not considered since it is supposed that only a small portion of the sample actually partakes in the switching process. Thus it seems plausible that Gerson's results could be explained in terms of this model.

It would be interesting to extend the upper frequency range for several reasons. First, there should be a resonance at a higher frequency as predicted by Sannikov's theory, and secondly, a band of piezoelectric resonance peaks should follow the single peaks shown in Figures 16 and 17 for the poled ferroelectric samples.

A less obvious area for further study is an investigation of the possibility for a separation of loss mechanisms by use of the equivalent conductance versus frequency results. For most ferroelectric samples used here the hysteresis-type or switching losses are far more dominant than the Joule losses and the flattening in the low frequency range of the equivalent conductance curve was slightly detectable only in the antiferroelectric materials. However one polycrystalline sample supplied by Sandia Corporation (but not studied extensively in this work) showed interesting characteristics as depicted in Figure 23. The composition of this ceramic was $Pb(Hf_{0.8272}Zr_{0.1128}Ti_{0.06})O_3$ and it was ferroelectric under normal laboratory conditions. As the figure illustrates, with increasing temperatures the presence of Joule losses is more easily detectable, and in fact at the higher temperatures the Joule losses dominate.

Curves of this nature could provide a convenient means of separating the two sorts of loss mechanisms. Although other sorts of loss

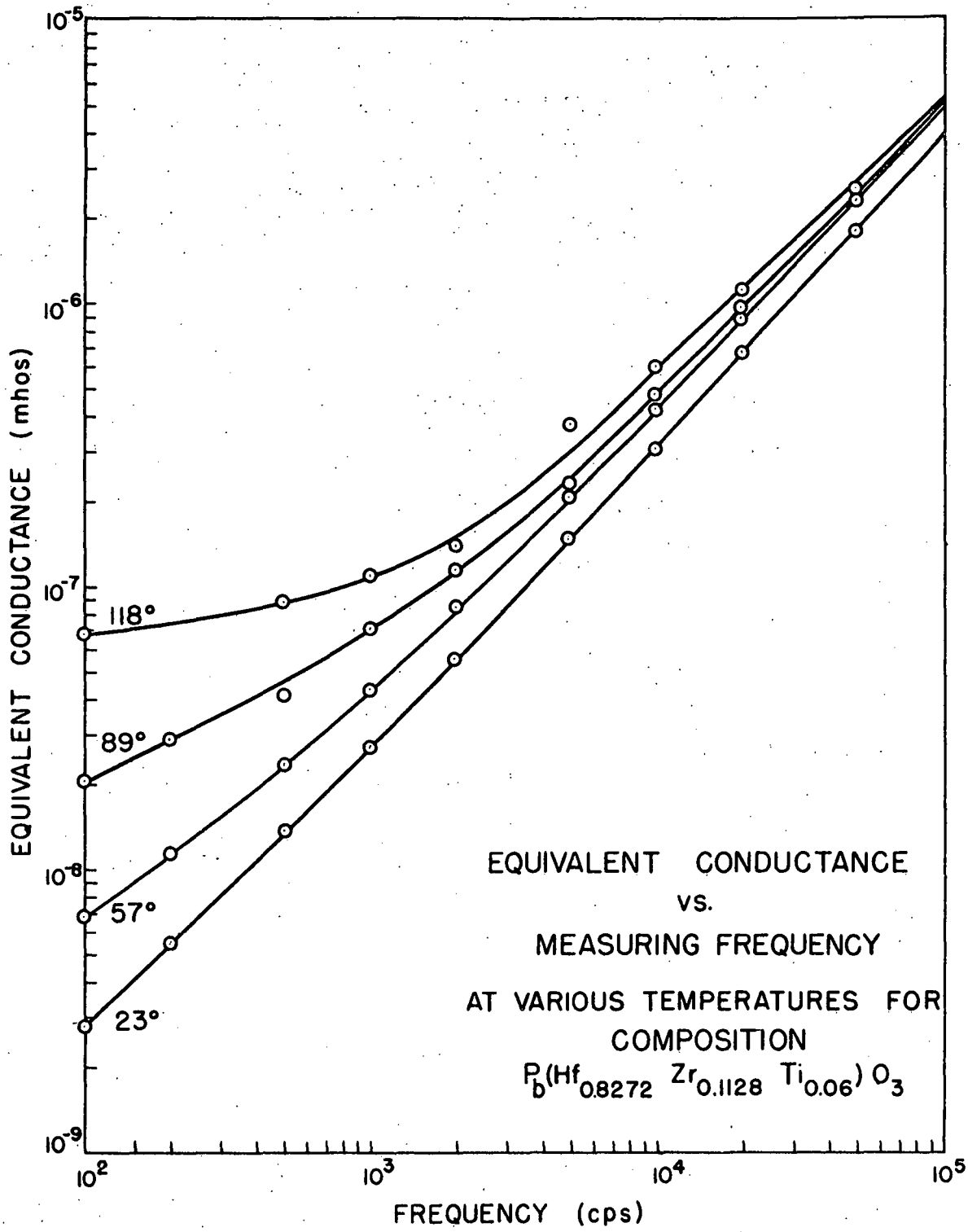

Figure 23. Equivalent Conductance Curves Showing the Presence of Joule Losses at High Temperatures

mechanisms are neglected (such as frictional losses encountered by rotating dipoles), this area surely merits further consideration.

BIBLIOGRAPHY

(B1) Berlincourt, D. and H. A. Krueger, J. Appl. Phys. 30, 1804 (1959).

(C1) Chynoweth, A. G., Phys. Rev. 110, 1316 (1958).

(D1) Drougard, M. E. and D. R. Young, Phys. Rev. 94, 1561 (1954).

(D2) Drougard, M. E., H. L. Funk, and D. R. Young, J. Appl. Phys. 25, 1166 (1954).

(D3) Drougard, M. E. and R. Landauer, J. Appl. Phys. 30, 1663 (1959).

(F1) Forsbergh, P. W., Jr., "Piezoelectricity, Electrostriction and Ferroelectricity," Handbuch der Physik 17, Berlin: Springer-Verlag (1956), pp. 264-392.

(F2) Fatuzzo, E., J. Appl. Phys. 33, 2588 (1962).

(G1) Gerson, R., J. Appl. Phys. 31, 1615 (1960).

(G2) Gerson, R., J. Appl. Phys. 31, 188 (1960).

(J1) Jona, F. and G. Shirane, Ferroelectric Crystals, New York: The Macmillan Company (1962).

(K1) Känzig, W., "Ferroelectrics and Antiferroelectrics," Solid State Physics, vol. 4, New York: Academic Press (1957), pp. 1-197.

(K2) Kittel, C., "Ferroelectric Crystals," Introduction to Solid State Physics, New York: John Wiley (1956), pp. 182-205.

(K3) Kittel, C., Phys. Rev. 83, 458 (1951).

(L1) Landauer, R., D. R. Young, and M. E. Drougard, J. Appl. Phys. 27, 752 (1956).

(L2) Little, E. A., Phys. Rev. 98, 978 (1955).

(M1) Megaw, H. D., Ferroelectricity in Crystals, London: Methuen (1957).

(M2) Merz, W. J., Phys. Rev. 95, 690 (1954).

(M3) Miller, R. C., Phys. Rev. 111, 736 (1958).

(M4) Miller, R. C. and A. Savage, Phys. Rev. 112, 755 (1958).

(M5) Miller, R. C. and A. Savage, Phys. Rev. 115, 1176 (1959).

(M6) Miller, R. C. and A. Savage, J. Appl. Phys. 31, 662 (1960).

(M7) Miller, R. C. and A. Savage, J. Appl. Phys. 31, 1546 (1960).

(M8) Merz, W. J., J. Appl. Phys. 27, 938 (1956).

(N1) Northrip, J. W., Ph.D. dissertation, Oklahoma State University, 1963 (Unpublished). Included as part of Final Report (1963), Sandia Corporation Purchase Order No. 16-8672.

(P1) Powles, J. G. and W. Jackson, Proc. Inst. Elec. Engrs. 96, (London) 383 (1949).

(R1) Roberts, S., Phys. Rev. 71, 890 (1947).

(S1) Sannikov, D. G., Soviet Physics JEPT 14, 98 (1962).

(V1) von Hippel, A. and W. B. Westphal, National Research Council Conference on Electrical Insulation, October (1948).